Università degli Studi di Ferrara

DOTTORATO DI RICERCA IN
"SCIENZE DELL'INGEGNERIA"

CICLO XXVII

COORDINATORE Prof. Stefano Trillo

Rheology of
Wood Polymer Composites

Settore Scientifico Disciplinare ING-IND/22

Dottorando
Ing. Valentina Mazzanti

Tutore
Ing. Francesco Mollica

Anni 2012/2014

“The cure for boredom is curiosity.
There is no cure for curiosity.”
- Dorothy Parker

TABLE OF CONTENTS

INTRODUCTION

Wood plastic composites (WPC) are materials composed of a matrix based on a thermoplastic polymer filled with natural fibers at different concentrations.

These materials existed since the early 1900's, they were re-born as a modern concept in Italy in the 1970's, and popularized in North America in the early 1990s. At the beginning of the 21st century they are spreading to India, Singapore, Malaysia, Japan and China [Clemons, 2002, Pritchard, 2004, Ashori 2008].

The birth of this market involved two industries that historically knew little about each other, having different expertise, aims and knowledge: forest and plastics industry. The forest industry has more experience in building products while the plastics industry has more expertise in processing and components. These markets had little in common and they processed materials differently and at different scales. The term "*extrudable wood*" has been used in a deliberate way to highlight the scope for producing fully finished wood – like products by mass production techniques [Pritchard 2004].

The perspective after the success of several WPC products has changed radically, in particular when the word "*sustainability*" has achieved increased importance. The opportunity to replace a portion of petroleum-based plastic with natural fibers, used recycled plastic and wood flour from waste, created the possibility of entering new markets [Markarian 2008, Cheung 2009, Zini 2011]. A further ecological advantage is to use natural fibers choosing from local waste production. Many types of natural fibers are being considered largely depending on local availability and economics; examples include rice husks in China, maple in Canada, agave in Mexico, fir in Italy etc. Thus, the WPC market is a dynamic and growing sector because the public generally regards products made from renewable raw material as environmentally friendly.

More than 1.5 million tons of wood plastic composites are now produced worldwide, with the majority manufactured in the U.S., as shown in Fig. 1. In the U.S., the market has been dominated by rail and decking products. In China and other parts of Asia, wood plastic composites are beginning to experience considerable growth along with a wider variety of product offerings including pallets, doors, and architectural items. In Europe WPC market is not fully developed, but is growing with small manufacturing industries focused in decking but with an emergent interest towards automotive [Markarian (2005), AccuVal Associates, Inc. (2015)].

The majority of the market is thus constituted by outdoor products such as decking, fencing, flooring and railings (Fig. 2). Windows and door profile manufacturers are another large industrial segment, but the second biggest sector is in automotive application, where other fibers may lose the competition against natural fibers. Automotive components made of plastics with plant fibers are currently being used by many manufacturers such as Audi, Opel, Fiat, Renault Ford, Mercedes Benz, BMW and Volvo [Bismarck 2006]

The reasons why WPCs are very promising and sustainable materials are to be found in the many advantages of natural fibers. Natural fiber composites offer specific properties with respect to conventional filled composites. Natural fibers are low cost, easy to obtain, have low density, biodegradable, non – abrasive for processing machine and show high filling levels capability.

WPC shows great technological advantages. It can be processed like a polymer using extrusion or injection molding techniques and can be worked in the same way of wood such as drilled, screwed or sawn. Moreover with respect to wood, it has a greater durability and requires less maintenance in particular in wet environments, while with respect to plastics the main advantages is a lower cost and a reduced environmental impact due to the presence of the natural fibers as filler.

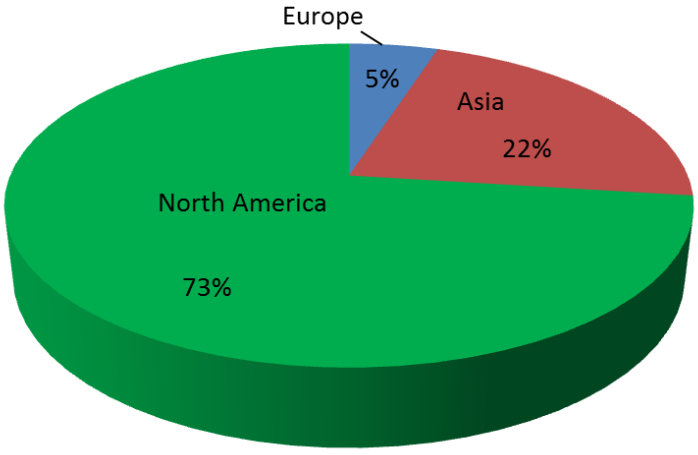

Fig. 1 – Global manufacturers of Wood Polymer Composites (WPC)

Fig. 2 - Some examples of WPC products (Photo: diytrade, yeskey, bombayharbour)

However, the presence of the fibers shows several drawbacks. The poor resistance at high temperature, the tendency to absorb moisture, the generally low strength and the chemical incompatibility with polymers reduce the potential of natural fillers and makes the processability of this material extremely challenging.
During processing, the way WPC behaves is the key for better understanding the phenomena that affect this material. In particular, in order to study the several problems during processing and improve its processability, it is essential to understand how the material flows varying temperature and concentration of filler.
The aim of this work is to investigate the influence of filler content and temperature on the rheological, mechanical and thermal properties of wood flour polypropylene composites (PP - WPC).
The classical way to characterize flow of materials is to use a rheometer. Testing WPCs at high temperatures and percentages of filler with oscillatory mode using off – line rheometer is quite challenging. The main reasons are a reduced linear viscoelastic region, high viscosity of the material and fibers degradation.
In this work a complete characterization of WPCs with different filler percentages (0 – 70%wt.) has been made. Rheological tests are performed at 170°C for the WPCs and in the 170 - 200°C range for neat polypropylene (PP). A single master curve is obtained using two shift factors that can be described by a modified Eilers model and a Williams - Landel - Ferry equation. This mastercurve, fitted with a Carreau – Yasuda model, can be useful for predicting the viscosity of WPCs at temperatures that are typically used during processing and for any percentage of filler. In order to validate the model, it is necessary to evaluate the flow curve of PP - WPC material at a temperature other than 170°C. This could not be done with classical instruments used for rheological characterization, mainly because the LVR was insufficient to obtain reliable results.
The viscosity of PP - WPC at higher temperature can be measured using an extruder with an instrumented in – line slit rheometer. This instrument is designed to be connected directly to the extruder and the measurement is performed using three pressure transducers along the die. With different slit heights, it is possible to correct for slip phenomena using the Mooney procedure.
The in line slit rheometer allows the determination of the flow characteristics of the material in a condition that is very similar to the

actual processing conditions and to compare the in line data with those off line.
The thesis is organized as follows:

- in Chapter I the Wood Polymer Composite (WPC) will be described. In particular its major constituents, its properties and drawbacks and processing issues will be discussed;
- in Chapter II some important concepts of non-Newtonian fluids and constitutive equations will be briefly introduced;
- in Chapter III the main techniques used to measure the rheological properties will be described: capillary rheometer, slit rheometer, parallel plate and cone and plate rheometers;
- in Chapter IV the extruder and some important issues about the classical modeling of extrusion will be presented;
- in Chapter V the complete characterization of the WPC focusing on the rheological behavior of the material will be presented. After this, a construction of a complete master curve as a function of the volume fraction of filler and the temperature of polymer will be proposed;
- in Chapter VI the instrumentation design of the in – line rheometer will be described. After this, the measurements realized during the extrusion process comparing to the off – line experimental measurements presented in Chapter V will be presented;
- in Chapter VII the results will be summarized and discussed

CHAPTER 1

WOOD POLYMER COMPOSITES

1.1 Wood polymer composites: a brief history

Wood Polymer Composites are a class of materials that contain wood (e.g. maple, pine), wood polymer (e.g. cellulose) or natural fiber (hemp, sisal, agave, rice) dispersed in a thermoplastic matrix (e.g. polypropylene, polyethylene).
This material appeared for the first time in 1960s as thermosetting molding compounds containing cellulose fiber as filler. Earliest attempts to make cellulose - filled thermoplastic compositions in the 1970s had serious difficulties. Cellulose fibers do not disperse easily throughout the plastic formulations during compounding and the finished products do not exhibit the desirable characteristics associated with fiber reinforced plastic composites. In the 1980s, more attention has been, directed to improving the mechanical and thermal properties. The problems of moisture and oxidation were recognized. In the 1990s attention has also been paid to improving the compatibility of the filler with the polymeric matrix by providing an interaction between the filler and the polymer. The innovation of using thermoplastic polymers and materials based on cellulose in the form of durable and easy to transport pellets was done in 2000s.

1.2 Polymer, wood or WPC?

WPC can be a convenient substitute for wood or plastics. The presence of the polymeric matrix imparts several advantages with respect to natural wood. WPC products can be manufactured in complex shapes easily and rapidly using forming techniques typical of plastics, such as extrusion and injection molding. For instance, WPC can be extruded as solid or hollow boards with an engineered design. At the same time, profiles can also be shaped using conventional woodworking tools like saw and drill. Coloring can be obtained quite easily through pigmentation, hence painting is not necessary, although possible. Moreover, thanks to the hydrophobic character of the polymer, WPC products require less maintenance than wood, especially in terms of a better durability in wet environment. Aesthetics and mechanical properties are not as good as natural wood, but if compared to other engineered wood products, such as medium density fiber board (MDF) or particleboard, WPC performs better [Bledszki 1998]. Lastly, WPC is recyclable like all thermoplastics: although it may be difficult to reprocess, Viksne and Rence and Shahi et al. have found that

the mechanical properties don't decay too much with the number of reprocessing cycles.

With respect to plastics the main advantages are low cost and reduced environmental impact due to the presence of the cheap natural fibers that can be obtained out of waste materials produced locally. In order to achieve maximum cost reduction and sustainability, WPCs should be made using recycled plastics [Yam 1990] and the filler quantity maximized to limit the usage of the more expensive polymer. This motivates the interest towards highly filled WPC. In fact, high percentage loadings (50%wt. or more) are commercially available, especially for extrusion grades WPC. Moreover, if compared to glass fibers and ceramic powders, natural fibers have lower density and are less abrasive: the composite is thus comparably lighter and the wear of processing machineries is reduced.

Nevertheless WPC has several drawbacks. First of all, the hydrophilic natural fibers are incompatible with the hydrophobic polymeric matrix: fiber - fiber interaction is preferred to fiber - matrix interaction, and this leads to agglomeration and reduced dispersion of the fibers. Macroscopically it results in mixing problems but also in lower mechanical properties due to the weak nature of the fiber - matrix interface.

Improving the mechanical behavior is an important research topic. Many papers deal with coupling agents (e.g. maleic anhydride modified polymers) to increase the adhesion between polymer and natural fibers [Raj 1991, Maldas 1991, Lu 2005, Zhang 2008, Gao 2008, Ichazo 2001,Bledzki 2003, Kumari 2007, Cui 2008, Tasdemir 2009, Ashori 2009, Ndiaye 2011, Adhikary 2011]: the mechanical properties generally increase with the amount of coupling agent up to a certain threshold value. The length and orientation of the fibers are parameters that play an important role in the mechanical performance, as noted by Migneault et al. and Beckermann and Pickering, with properties increasing with the fiber length. Also, activating the wood surface with chemical modification agents (silanes, alkali, isocyanate, ester, phenol formaldehyde resin) [Ichazo 2001, Xiong 2009, Kuruvilla 1996, Marcovich 2001, Maldas 1988, Das 1999, Tserki 2005] for decreasing fiber hydrophilicity has a positive effect on mechanical properties as well as reducing the filler - filler interaction (silica fillers) [Maldas 1988, Zhang 2012].

Another negative consequence of the natural fibers hydrophilicity is moisture absorption, which causes swelling and distortion as well as fiber pull out in the finite products, but also during processing there are absorption related problems, like water vapor cavities formation and the

consequent decay in the mechanical properties of the material. This effect is clearly more severe for high fiber content. In order to prevent these difficulties, it is necessary to dry the material before processing and, in the case of extrusion, to use a venting zone equipped extruder. Hesseinaei et al. describe a chemical way to obtain better performance with hemicellulose extraction. This method eliminates the most hydrophilic component, decreasing the water absorption.
The major limitation of the materials filled with natural fibers, though, is oxidative degradation during processing. Natural fibers are mainly composed of lignin, hemicellulose and cellulose. The starting degradation temperatures of these components are 110°C, 196°C and 255°C, respectively [Ramiah 1970, Bouafif 2009, Jeske 2012]. It is commonly assumed that the processing temperature should not exceed 200°C and this in turn reduces the choice of the polymers that can be used as matrix (usually polyolefins and polyvinylchloride). In any case, the processing window is narrow because it is limited not only by the thermal stability of the fibers but also by the melting temperature of the polymer.
If the material is processed at a temperature close to the melting temperature, the viscosity of the neat polymer can be considerably high and the presence of large quantities of filler increases the viscosity even further. Thus, WPC processing generally requires more power and the localized heating induced by viscous dissipation can worsen degradation problems. Therefore, although high natural fiber percentage is desirable in order to achieve sustainability and low material cost, processing may become a challenging task.
The following paragraphs will describe the generic properties of polymeric matrix, ligno-cellulosic fibers and additives used during compounding. Afterwards the most important properties and the most significant problems of this material will be listed.

1.3 Compositions of WPC: polymer and natural filler

Many types of polymers can be used for the fabrication of WPC, but the main consideration which has to be taken into account is the operating temperature. Due to the limitations imposed by the processing of wood (not to exceed 200 °C), only polymers which can be processed at temperatures lower than 200°C can be used.
Both thermosets and thermoplastics are attractive as matrix materials for WPC but the second ones offer many advantages, such as low processing cost, ease of molding complex parts and reprocessability.

The main types of thermoplastics used for the fabrication of WPCs are

- high density polypropylene
- low density polypropylene
- polyvinyl chloride
- polypropylene
- polystyrene

Polypropylene was chosen in this study as the polymeric matrix for WPC.

1.4 Polypropylene

In 1954 G. Natta, following the work of K. Ziegler found that some "Ziegler – type" catalysts allowed to produce high molecular weight polymers from propylene. Using different form of the catalysts, Natta was able to produce different types of polypropylenes. The isotactic form was similar to high density polyethylene but with higher softening point, rigidity and hardness. The polypropylene business grew rapidly, isotactic polypropylene was marketed by Montecatini (Ferrara) as Moplen in 1957 [Brydson, 1999].

1.4.1 Structure and properties

Polypropylene (PP) is a thermoplastic polymer produced by polymerization of propylene (Fig. 1.1). With respect to polyethylene (PE) $(-C_2H_4-)_n$, the difference is the presence of a methyl group attached to alternate carbon atoms on the chain backbone.

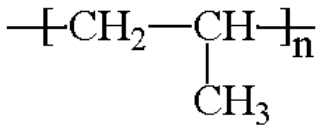

Fig. 1.1 - Chemical structure of polypropylene

The presence of this group makes polypropylene a vinyl polymer. The methyl group gives many properties to the polymer, such as a higher melting point. The most significant influence of the methyl group is that it can lead to products of different tacticity, ranging from completely isotactic and syndiotactic structures to atactic molecules. The tacticity is the stereochemical arrangement of the units in the main chain of a polymer. The isotactic form is the most regular with all the methyl groups located on one side of the molecule. The structure does not crystallize in a planar zigzag form but in a helix and this justifies the otherwise surprising

lower density of PP with respect to PE. Commercial polypropylene are usually 90 – 95% isotactic although atactic and syndiotactic structures may be present either as complete molecules or as blocks of varying length in chains of isotactic molecules. Whereas the atactic polymer is an amorphous somewhat rubbery material of little value, the isotactic polymer is stiff, highly crystalline and with a high melting point. Within the range of commercial polymers, the greater the amount of isotactic material, the greater is crystallinity, softening point, stiffness, tensile strength, modulus and hardness.
Another characteristic that influences the properties of PP is the molecular weight. However this influence is not univocal. An increase in molecular weight leads to an increase in melt viscosity and impact strength but it also leads to a lower tensile strength, hardness stiffness and softening point; this because a high molecular weight polymer does not crystallize as easily as a lower molecular weight material and it is the differences in the degree of crystallization which affects the bulk properties.
Also, the morphological structure influences the properties of PP. The properties of the polymer depend on the size and type of crystal structure formed and in turn are influenced by the relative rates of nucleation to crystal growth. It is possible to control the properties by varying the rate of cooling and by the incorporation of nucleating agents
A limit of polypropylene is a glass transition which occurs at about 0 ° C with the effect that the polymer becomes brittle at this temperature. In Tab. 1.1 some properties of a standard isotactic PP are presented.

Tab. 1.1 – Some properties of a isotactic PP

Properties	**Isotactic PP**
Density (g/cm_3)	0.9
Elastic modulus (MPa)	16.5
Impact strength (-23°C) (kJ/m^2)	16
Opacity (%)	85
Crystallinity (%)	40 - 60
Melt temperature (°C)	163

Comparing isotactic PP to PE, the main differences are: a lower density, a lower specific heat, a higher softening point, better mechanical properties and a higher brittle point. PP is more susceptible to oxidation but is not subject to environmental stress cracking and the permeability to liquids

and gases is lower. About the melt flow properties, PP is more non – Newtonian and more sensitive to temperature than PE.

1.4.2 Additives

Commercial grades of PP can be compounded with several additives. Of these, the most relevant are: fillers, pigments, ultraviolet absorbers, antioxidant and nucleating agents.
Though it is less common than in PE, fillers that are mostly used with PP are talc, calcium carbonate and glass fibers. Talc improves stiffness and heat deformation resistance, calcium carbonate improves impact strength, brighter color, thermal stability, fatigue strength and reduces stiffness. Tensile strength is markedly reduced with both fillers. Glass fibers are used to improve strength and rigidity. Substantial enhancements are, however, only realized after a coupling reaction takes place between organofunctional silanes deposed on the glass fiber and reactive groups introduced into the PP molecule.
The choice of the pigment must be made suitably because the high processing temperatures and the lower resistance to oxidation require rather more care.
PP is liable to chain degradation from exposure to heat and UV radiation such as that present in sunlight. Oxidation usually occurs at the tertiary carbon atom present in every repeat unit. A free radical is formed and then reacts further with oxygen, followed by chain scission to yield aldehydes and carboxylic acids. In external applications, it shows up as a network of fine cracks and crazes that become deeper and more severe with time of exposure. To improve the resistance to ultraviolet light carbon black is often useful as a light screen.
Antioxidants, such as phenol alkane type, are necessary components of all PP compounds to ensure the stability of the compound.

1.4.3 Polypropylene copolymers

The characteristics of PP can be largely modified by copolymerization. There are three general types of polypropylene: homopolymer (PP – H), block copolymer (PP – B) and random copolymer (PP - R).
Homopolymers are more crystalline, have a well-defined melting temperature between 161 – 165 °C, soften at 155°C and have a rather narrow molecular weight distribution. Copolymers typically contain some amount of ethylene comonomer and are subdivided to random and block copolymers. Their melting points are in a range of 140 – 155 °C.

Randomly polymerized ethylene monomer added to polypropylene homopolymer decreases the polymer crystallinity, lowers melting point and modulus and makes the polymer more transparent.
Block copolymers are made up of blocks of different polymerized monomers, in particular "diblock copolymer" if it contains two different chemical blocks, "triblocks" id it contains three etc.
Ordinarily, PP-copolymers are random. In a block copolymer, the monomeric units of propylene are segregated from those of the second monomer. An example, propylene-ethylene block copolymer shows an adequate stiffness, a high crystallinity and a better impact strength, particularly a low-temperature impact strength, due to the lower glass transition temperature of the ethylene-propylene interface [Chiu 1998].
Ethylene-propylene rubber or EPDM added to polypropylene homopolymer increases its low temperature impact strength. Also reactive blend (PP – I) with methyl methacrylate or styrene are available and have the following advantages: low density, high weather resistance, reduced shrinkage and deformation during processing.

1.4.4 Applications

Polypropylene homopolymers and copolymers have found applications where good appearance, low-density, sterilisability, environmental stress cracking resistance and good heat resistance are important.
Many plastic items for medical or laboratory use can be made of PP because it can resist the heat in an autoclave. Food containers made from it will not melt in the dishwasher, and do not melt during industrial hot filling processes.
One further particularly useful property of this polymer is the excellent resistance of thin sections to continued bending. This has led to the introduction of PP for boxes, cases in which the hinge is an integral part of the functionality. The special copolymer grades with their higher impact strength and lower brittle point have absorbed a large part of this market.

1.5 Wood

Wood is a hard, porous and fibrous structural natural material found in the stems and roots of trees and other plants. It has been used for thousands years for both fuel and as a construction material. Wood is a heterogeneous, hygroscopic, cellular and anisotropic material. In Fig. 1.2 a schematic structure is presented. It is an organic material, a natural composite of cellulose fibers, which are strong in tension, embedded in a matrix of lignin which resists compression. It is composed of cells, and the cell walls are composed of micro-fibrils of cellulose and hemicellulose impregnated with lignin [Kim 2010].

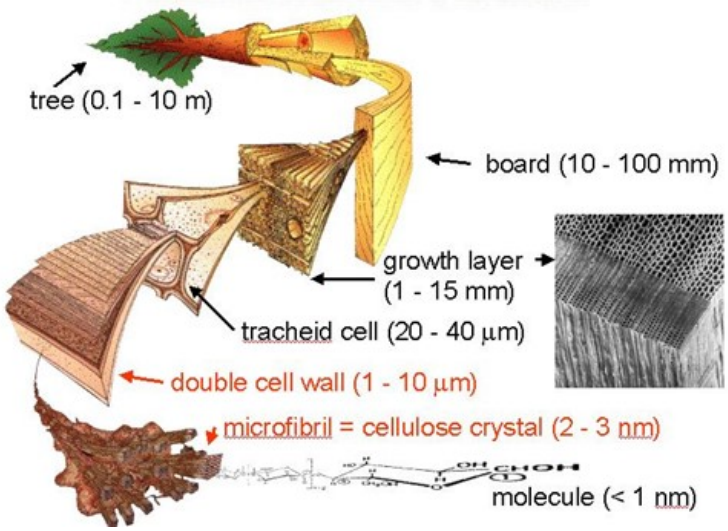

Fig. 1.2 - Hierarchic softwood structure

As a general classification, wood types are grouped into softwood and hardwood. To define them botanically, softwoods are those woods that come from gymnosperms(mostly conifers), and hardwoods are woods that come from angiosperms (flowering plants) The structure of a typical softwood is relatively simple. The axial or vertical system is composed mostly of axial tracheids, and the radial or horizontal system is the rays, which are composed mostly of ray parenchyma cells. The structure of a typical hardwood is much more complicated than that of a softwood. The axial system is composed of fibrous elements of various kinds, vessel

elements in various sizes and arrangements, and axial parenchyma in various patterns [Wiedenhoeft 2010].

In Fig. 1.3 a cross section of a trunk is shown that reveals different parts of the stem. The outer layer of a tree is bark which can be subdivided into the outer dead bark and inner living bark. Close to the inner bark there is the vascular cambium which is the growth layer of wood. The inner parts of the stem consists of dead cells in the sapwood and in the heartwood.

Heartwood is a result of a naturally occurring chemical transformation that makes it more resistant to decay. The heartwood formation occurs spontaneously and when the formation is complete, the heartwood is dead. In the living tree, sapwood is responsible not only for conduction of sap but also for storage and synthesis of biochemicals. Sapwood is the younger, outermost wood and its principal functions are to conduct water from the roots to the leaves and to store up and give back according to the season the reserves prepared in the leaves.

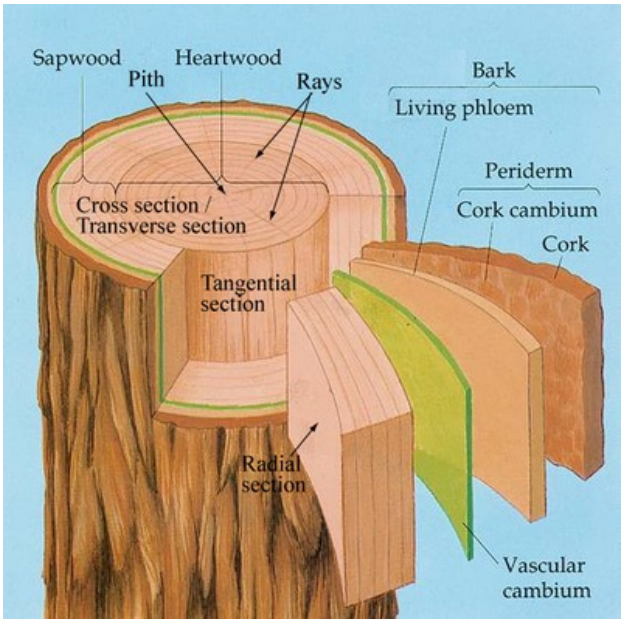

Fig. 1.3 – Radial and tangential structure of the wood

At the molecular level wood fiber is formed of natural polymers like cellulose, hemicellulose, lignin, pectin and low percentage of inorganic compounds and other extractives. In Tab. 1.2 are reported the mean percentages of dry weight of wood for each component.

Tab. 1.2 – Percentage of dry weight of wood of each component

Component	Percentage of dry weight
Cellulose	40 – 50 %
Hemicellulose	15 – 35 %
Lignin	20 - 40 %
Extractives	5 %

1.5.1 Cellulose

Cellulose $(C_6H_{10}O_5)_n$ is the most abundant organic polymer on earth. It is a polysaccharide consisting of a linear chain of several hundred to many thousands of β(1→4) glycosidic bonds linked D-glucose units (Fig. 1.4).
It is synthesized in plants, trees and grass as their most important structural component. Due to the linear nature of cellulose, it is capable of forming strong inter and intra – molecular bonds and aggregated bundles of molecules. This aggregates have different names such as fibrils, microfibrils etc. Natural cellulose has two different unit cells: I_α and I_β. Cellulose produced by bacteria and algae is enriched in I_α while cellulose of higher plants consists mainly of I_β. I_β is thermodynamically more stable, thus providing higher thermal resistance and higher strength.
The chain length or degree of polymerization, defines the properties of cellulose. The number of glucose units that make up one polymer molecule depends on the origin of the cellulose. For example, cellulose from wood pulp has typical chain lengths between 300 and 1700 units, cotton and other plant fibers have chain lengths ranging from 800 to 10,000 units.
The oxidative degradation of cellulose starts at 255°C, this makes it more resistant to high temperatures respect to the other components of the wood fiber.

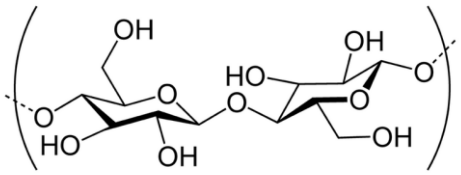

Fig. 1.4 – Cellulose structure

1.5.2 Hemicellulose

Hemicelluloses (Fig. 1.5) are a group of heterogeneous biopolymers such as mannose, arabinose, xylose, galactose and glucose that have a have a structural role in the fiber walls. Some acidic sugars like galacturonic and glucoronic acids are also present in hemicellulose polymers. The hemicellulose chains play the role of amorphous soft filler, wrapping cellulose regions. The strength and the hardness of wood depends on the percentage of these monomers. The common degree of polymerization is in the range of 200 – 300. Hemicellulose oxidative degradation starts at 196°C.

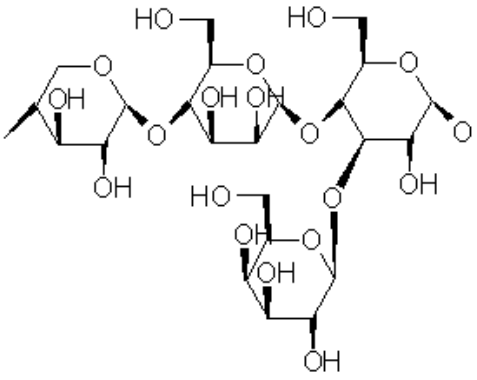

Fig. 1.5 – Hemicellulose structure

1.5.3 Lignin

Lignin (Fig. 1.6) is a complex heterogeneous 3 – D polymer of aromatic alcohols known as monolignols (p – coumaryl alcohol, coniferyl alcohol and sinapyl alcohol). It is the most abundant biopolymer after cellulose. The composition of lignin varies from species to species. Lignin fills the

spaces in the cell wall between cellulose and hemicellulose components, limits the penetration of water into the wood cell and makes the wood compact . It is relatively hydrophobic and protects wood against bacterial infections. Lignin has the lowest resistance to oxidative degradation, which begins at 110 °C.

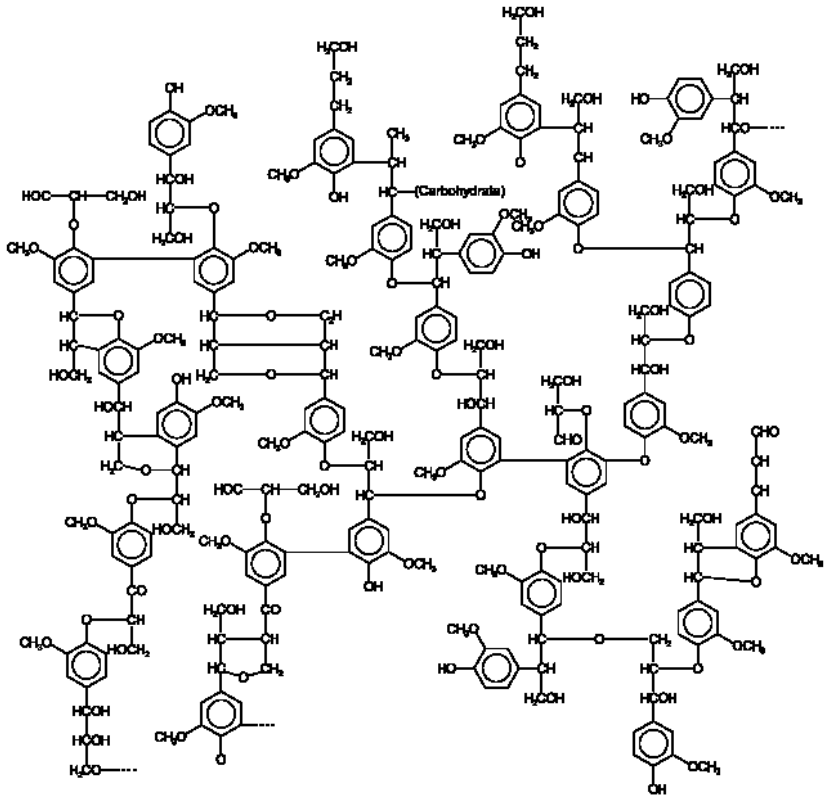

Fig. 1.6 – Lignin structure

1.5.4 Extractives

Besides the three principal components, that have just been discussed, plants contain non - structural components such as terpenes, pinenes, tannins etc. They contribute to wood odor and can diffuse to the wood surface during drying and can have some antimicrobial properties.

1.6 Natural fiber

Natural fiber have a complex layered structure (Fig. 1.7) consisting of two layer of thin primary wall covered by a cuticle that are the first layers deposited during cell growth encircling a secondary wall. This secondary wall is made of three layers. The thickness of the middle layer determines the ultimate mechanical properties of the fiber. The middle layer is complex and consists of helically wound cellular microfibrils typically of 10 – 30 nm long) from cellulose chain molecules (30 – 100 cellulose molecules). Between the secondary wall and the lumen there is an amorphous matrix. This matrix is very complex and consists of hemicellulose, lignin and pectin. The hemicellulose molecules act as cementing matrix between cellulose microfibrils forming a complex cellulose – hemicellulose network which is the main structural component of the fiber cell. The hydrophobic lignin and pectin components act as coupling agents and increase the stiffness of this cellulose – hemicellulose component.
There are many different type of natural fibers used in WPC: wood flour, sawdust, rice hulls and long fibers.

1.7 Typical WPCs fillers

1.7.1 Wood flour

Wood flour is finely pulverized wood that has a consistency fairly equal to sand or sawdust. Wood flour that is typically used in WPCs has mesh size of about 40 (400 μm). Most wood flour manufacturers are able to create batches of wood flour that have the same consistency throughout. All high quality wood flour is made from hardwoods because of its durability and strength. Very low grade wood flour is occasionally made from sapless softwoods such as pine or fir. Increasing the particles size decrease the mold shrinkage and increases the flexural modulus. Bulk density is around 1.3 – 1.4 g/cm^3. The aspect ratio (length to thickness) is typically around 3:1 or 5:1. Wood flour decomposes above 190 °C due to the presence of hemicellulose and lignin.

1.7.2 Sawdust

Sawdust is essentially the same thing as wood flour except it is formed as a product of wood sawing. Usually the particles are 30 – 400 μm larger. The great advantage of the sawdust is the lower cost.

1.7.3 Rice Hulls

Rice hulls are the hard protecting coverings of grains of rice and are by-products of rice mills, where lighter rice hulls are separated from heavy husked rice through aspiration.
Chemically, rice hulls are close to wood and contain the same principal components. However, rice hulls lignin significantly differs from lignin in wood in that rice hulls are much more resistant to microbial degradation and more resistant to moisture penetration.

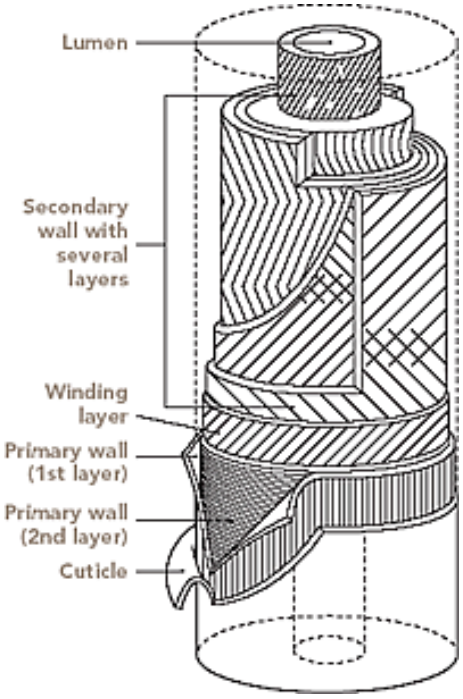

Fig 1.7 – General structure of natural fiber

1.7.4 Long fibers

In nature, there are many kinds of long natural fibers such as bast (flax, hemp, jute, kenaf etc.), leaf fibers (sisal, pineapple, oil palm etc.), seed fibers (cotton) and fruit fibers (coconut). Long natural fibers are considered as excellent reinforcing fillers for WPCs. As drawback of long

fiber as a filler, high moisture uptake and swelling are often considered. Also, it is difficult to uniformly mix long cellulose fiber with molten plastic. Besides. Long cellulose fiber of a good quality costs much more than rice hulls and wood flour.

1.8 Additives

The world filler market for plastics is dominated by carbon black and calcium carbonate. However, only few wood plastic composites use mineral filler. The most important additives used in WPCs compounds are:

- coupling agents;
- lubricants;
- flame retardants.

1.8.1 Coupling agents

WPCs based on polyolefins are commonly a blend of a hydrophobic polymer and hydrophilic wood. Hence, the adhesion between them is poor and the polymer – wood filler interface extremely weak and fails to transfer stresses between the two phases when loaded. In fact, natural fibers have a strong tendency to form aggregates.
In order to improve these two issues it is necessary to:

- distribute the filler in the polymeric matrix as uniformly as possible;
- create an interface linking coupling wood fibers and plastic.

A proper coupling agent should contain two functional domains, one capable to forming entanglements with polymeric matrix and the other capable to strongly interact with the filler through covalent bonds, ionic interactions or hydrogen bonds. These links increase the interface adhesion between matrix and filler.
The coupling agents can be subdivided into

- maleated polyolefin which can interact with inorganic fillers with hydrogen bonds or ionic interactions;
- alkali treatment;
- bifunctional oligomers or polymers which can interact with ion – pair bond;
- silanes grafted onto polymers that interact with covalent bonds;
- acrylic – modified polytetrafluoroethylene (PTFE).

1.8.2 Maleated polyolefins

Maleated polyolefins are the most widely used coupling agents. They contain two functional groups: one polyolefin (typically HDPE or PP), which is able to form entanglements with the polymer matrix and the second group, maleic anhydride, which is able to build strong links (hydrogen or ionic bonds) with cellulose fiber. Maleated polyolefins are used at 1 – 5% by weight in WPC formulation. In this percentage, the coupling agent could increase flexural and tensile Young's modulus up to 20 – 40 % and flexural and tensile strength up to 100 – 160 % [Klyosov].
It should be taken into account that maleated polyolefin can slowly react with moisture during storage. As a result, chemical reactivity of the coupling agent decreases.
Coupling agent also increases the density of WPCs because it decreases water absorption.

1.8.3 Alkali treatment

Alkaline treatment is one of the oldest, inexpensive and most widely used treatments on natural fibers. It is efficient for removing surface impurities but it can also remove the majority of lignin, wax and oils covering the surface of the fibers. Alkali treatment also removes hemicellulose from the natural fibers surface, making the interfibrillar region less dense, rigid and more easy to rearrange along the direction of stress. However alkali treatment causes a decrease in tensile strength and Young's modulus of fibers due to extensive damage if treatment is too long or concentration is too high. Thus the choice of optimum concentration and treatment time is fundamental to obtain good properties. Generally the treatment consists in 5 – 9% NaOH solution for 30 – 45 minutes.

1.8.4 Lubricants

A lubricant is a substance introduced to reduce friction between surfaces in mutual contact and also reduce the heat generated when the surfaces move. Thus, it is a common practice to introduce lubricants during polymer processing. This effect can help also WPCs processing, mainly because it is particularly sensitive to oxidative degradation produced by temperature. Introducing a lubricant, the viscous friction that produces heat can be reduced. There are two types of lubricants: surface and bulk. Surface lubricants have a low solubility, thus they migrate to the surface where they can create a layer between the material and the process

machine reducing friction between the surfaces. Bulk lubricants remain within the material reducing the viscous friction during the process.
As soon as the maleated coupling agents were introduced, it was noticed that their effect often significantly depends on lubricants employed in the system. In particularly the most conflicting effect was observed between maleated polyolefins and metal stearate lubricants. Compared with a nonmetal lubricant, the presence of zinc stearate decreases both strength and stiffness. This antagonist effect could be explained because the maleic acid, formed from grafted maleic anhydride during the compounding in the presence of moisture, reacts with zinc stearate. This reaction is thermodynamically favorable compared to the coupling of the maleated polymer to cellulose fiber and removes the coupling agent from WPC.

1.8.5 Flame retardants

Flame retardants are compounds added to manufactured materials and surface finishes and coatings that inhibit, suppress, or delay the production of flames to prevent the spread of fire.
Flame retardants for WPCs can be subdivided into four principal groups according to their physical action:

- inert fillers;
- water releasing and cooling;
- halogen (gas) forming and flame poisoning;
- protective layer forming.

The inert fillers (calcium carbonate, talc, clay) serve as passive flame retardants, reducing heat generation and removing the supply for flame propagation but they do not change the ignition point. The water releasing (alumina trihydrate, magnesium hydroxide) acts as heat sinks and prevent oxygen to get to flammable compounds. The halogen forming act by isolating the flammable material from oxygen and removing free radicals in the gas phase by reducing the heat generation. The protective layer when heated produces a solid form that shields it from releasing or flammable gases feeding flames.

1.9 Processing

The manufacture of thermoplastic WPC is usually a two – step process. The raw materials are first mixed together in a process called compounding and the compounded material is then formed into a product. Compounding is the feeding and dispersing of fillers and additives in the

molten polymers. Many options are available for compounding but frequently a twin screw extruder is used and the material is formed into pellets. The compounded material can then be shaped into a finished product by extrusion or injection molding.

1.10 Mechanical properties of WPC

The properties of WPC depend on a number of parameters such as volume fraction of the fiber, fiber aspect ratio, fiber – matrix adhesion, stress transfer at the interface and orientation. Both matrix and fiber properties are important in improving mechanical properties of the composites. The tensile strength is more sensitive to the matrix properties, while the modulus is more dependent on the fiber properties. Though the mechanical properties of WPC are lower than wood, it is possible to improve the tensile strength with a strong interface, low stress concentration and fiber orientation. A good fiber wetting in the matrix phase and a high fiber aspect ratio are necessary to improve the tensile modulus.

1.11 Typical problems of WPC

1.11.1 Oxidative degradation

Natural fibers are a complex mixture of organic materials and as a result, a temperature increase leads to a variety of physical and chemical changes. The starting degradation temperatures of lignin, hemicellulose and cellulose are 110°C, 196°C and 255°C, respectively. Thus, the main components subject to this problem are lignin and hemicellulose. Oxidative degradation of natural fibers in WPCs makes this material really complex to be processed and to characterize.

Oxidative degradation could be the cause of a premature mechanical failure, change the properties of the material, weaken the bonds between natural fibers and polymeric matrix. The damage appears inside and on the surface of WPC. The material becomes darker and layers of material can be easily removed. The damage in the bulk appears because typically WPCs are porous. The pores are formed by steam or volatile organic compounds during extrusion. WPCs become partially foamed and the pores are open and connected to each other, forming cavities. Oxygen flows through these pores and oxidizes, at elevated temperatures, the material from inside. Also water, which is always present in natural filled composite, serves as a catalyst for the oxidation when it evaporates within pores.

For improving thermal stability, attempts have been made to coat the fibers and/or to graft the fibers with monomers. Grafting is possible since lignin can react with the monomers [Nabi Saheb (1999)]. Mohanty et al al. have reported that grafting of acrylonitrile on jute improved the thermal stability from 170 up to 280 °C. Sabaa has also reported for acrylonitrile – grafted sisal fibers a lowering rate of degradation.

1.11.2 Hydrophilicity

In WPCs, natural fibers are embedded in a polymeric matrix. This makes the material less susceptible to moisture uptake than wood but not completely inert. When the content of natural fibers is greater than 40% by weight, there are enough cellulose particles to form extended and contacting chains, along which water and humidity could penetrate into the bulk of the material. The consequences of this phenomenon are loss of dimensional stability, swelling, pull out on surface material, a decrease of strength and mechanical properties in general, deterioration of the product and low resistance to thermal cycles.
The most commonly used methods to reduce this problem are to dry natural fibers prior to process and to use a venting zone in the extruder to improve the compaction by reducing the pores and remove the gases that are formed during the extrusion.

CHAPTER 2

NON NEWTONIAN FLUIDS

2.1 Introduction

The fluid state of a material starts when forces between molecules are large enough that the molecules remain in close proximity but too small to force the molecules to remain in a fixed position Morrison 2013]. When forces act on a fluid, it moves and deforms, the subject of fluid mechanics is to explain how this occurs.

2.2 Simple shearing

Fig. 2.1 shows an incompressible fluid between two parallel plates, separated by a distance d. Assuming that the plates are very large, with an area A such that edge effects may be ignored, and that the lower plate is fixed, at the top plate, a tangential force F is applied, thus the plate moves with a constant speed v in the x direction.

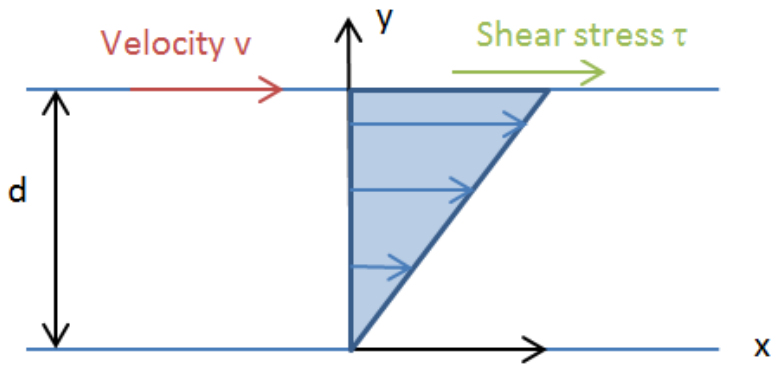

Fig. 2.1 – Simple shearing

In one dimension, the shear stress to which the fluid is subject is written as

$$\tau = \frac{F}{A} \tag{2.1}$$

The shear stress causes a flow and a velocity profile. The velocity distribution is

$$v_x = \frac{v}{d} y \tag{2.2}$$

The velocity profile close to the top plate is maximum and decreases linearly down to the zero value in contact with the stationary plate.
The shear rate for a fluid flowing between two parallel plates is defined as the rate at which a progressive shearing deformation is applied. For this particular type of flow is defined as

$$\dot{\gamma} = \frac{dv}{dy} = \frac{v}{d} \tag{2.3}$$

The ratio between the tangential stress and the shear rate is the viscosity

$$\eta = \frac{\tau}{\dot{\gamma}} \tag{2.4}$$

The viscosity of a system is determined by how molecules constituting the system interact.

2.3 Constitutive equations

A constitutive equation is defined as an equation that relates the stress on some material to the motion of that material. This analytical relationship allows to determine a priori the viscosity of a fluid for a given value of shear stress or shear rate.

2.4 Newtonian fluid

The Newtonian constitutive equation is the simplest equation used for viscous fluids and it is at the basis of all fluid mechanics. In general, Newtonian equation accurately describes the behavior of low molecular weight fluids and even high polymers at very slow deformation[Tanner 1985]. In Newtonian fluids, the viscosity is the coefficient of proportionality between the shear rate and shear stress. The graphical representation of the shear stress versus shear rate is called "*flow curve*". For a Newtonian fluid this diagram is obviously a straight line with a constant slope. In this type of fluids, the viscosity depends only on the temperature and pressure of the fluid.

2.5 Non Newtonian fluids

When the fluid behavior deviates from the Newtonian behavior it is called Non – Newtonian.
Many fluids with complex structure behave in different way and are not described by the constitutive equation appropriate for Newtonian fluids. The principal deviations of non-Newtonian fluids are:

- shear rate dependent viscosity;
- normal stress effects in steady flows;
- presence of yield stress;
- transient responses in un steady shear flows (stress relaxation, creep);
- other phenomena (swelling of extrudates, vortex in the inlet flow, melt fracture and solid – like behavior of polymeric liquids subjected to high velocity impact).

In this chapter only the first and third deviations from Newtonian behavior will be discussed. Fluids with shear rate dependent viscosity are called "Generalized Newtonian fluids". For this type of fluids a possible model is given by

$$\dot{\gamma} = \frac{dv}{dy} = f(\tau) \tag{2.5}$$

This equation implies that the shear rate at any point in the fluid is a function of the shear stress at that point. Such fluids may be termed generalized Newtonian fluids.
In terms of shear stress Eq. 2.4 can be rewritten as

$$\tau = \eta(\dot{\gamma})\dot{\gamma} \tag{2.6}$$

in terms, the constitutive equation for a non-Newtonian fluid is written as that of the Newtonian fluid, but the viscosity is not constant but it is a function of shear rate.
These fluids are subdivided into three distinct types depending on the nature of the function. These types are

- Pseudo-plastic or shear- thinning fluids;
- Dilatant or shear- thickening fluids
- Bingham plastics.

And typical flow curves for these fluids are shown in Fig. 2.2.

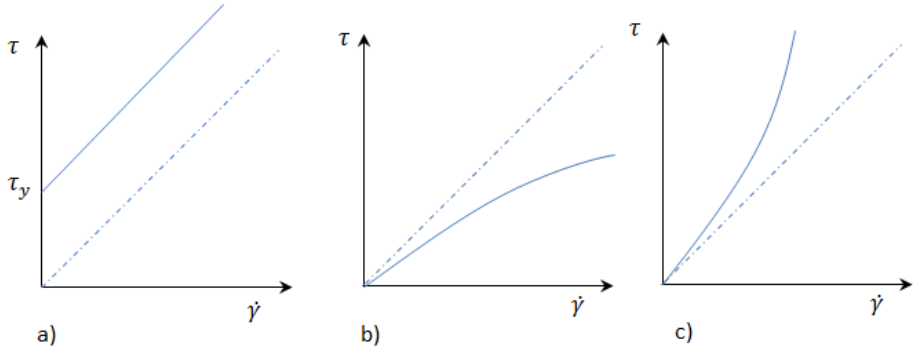

Fig. 2.2 – Shear stress versus shear rate for a) Bingham fluid b) Pseudo-plastic fluid and c) Dilatant fluid. Dotted line show a Newtonian fluid.

2.5.1 Pseudo-plastic or shear- thinning fluids

Pseudo – plastic fluids show a typical flow curve characterized by a nonlinear behavior. In particular, the curve indicates that the ratio of shear stress to the shear rate decreases progressively with shear rate.
Two common explanations are given for pseudoplastic behavior: alignment and desolvation. Asymmetric particles extensively entangled and/or oriented at rest, under shear, become oriented and points of entanglement reduced. This alignment and reduction of entanglement could produce a decrease of viscosity. At very high shear rates orientation become complete and, in this range of value, a constant viscosity could be observed. In case o desolvation, highly solvated particles may be present. With an increase of shear rate, solvated layers may be shared away, resulting in decreased interaction of the particles and consequently a reduction in the viscosity occurs.

2.5.2 Dilatant or shear- thickening fluids

Dilatant fluids show a viscosity that increases with the shear rate. This type of behavior is historically discussed in connection with concentrated suspensions of solids. When this suspensions are at rest, the relative amount of space left between the particles is at a minimum and the liquid is only sufficient to fill the voids. When the material is sheared at low rates, the liquid lubricates the motion of the particles and the stresses are reduced. At higher shear rates the dense packing of the particles is broken up and the material expands slightly. This new structure "*dilated*" does

not have enough liquid to lubricate the motion of the particles and the applied stresses have to be much greater. Dilatant fluids are less common than pseudoplastic fluids.

2.5.3 Bingham plastics

Many materials appear to show an yield stress. In them no detectable flow arises until the local stresses exceed a critical value. A Bingham plastic is characterized by a flow curve which is a straight line having an intercept τ_y on the shear stress axis. The yield stress τ_y, is the magnitude of the stress which must be exceeded before flow starts. At $\tau \leq \tau_y$ the material is substantially solid. The analytical equation for a Bingham plastic ($\dot{\gamma} \geq 0$) is written as

$$\tau - \tau_y = \eta_P \dot{\gamma};\ \tau > \tau_y \qquad (2.7)$$
$$\dot{\gamma} = 0;\ |\tau| \leq \tau_y$$

where η_P, the plastic viscosity is the slope of the flow curve.
The physical explanation of an idealized Bingham plastic is usually explained in terms of an internal structure. The fluid at rest contains a three – dimensional structure of sufficient rigidity to resist any stress less than the yield stress. If this stress τ_y is exceeded the structure breaks and the system behaves as a Newtonian fluid. If the stress falls below τ_y the structure is reformed.

2.6 Power law model

The "power law" is the most widely relation used to characterize generalized Newtonian fluids. Also known as the Ostwald–de Waele model [Scott 1939] this simple mathematical relationship describes the behavior of both, shear – thinning and shear thickening fluids. The flow curve is written as

$$\tau = m\,|\dot{\gamma}|^{n-1}\dot{\gamma} \qquad (2.8)$$

where m and n for the particular fluid are constants.
n is defined as power law index and is a measure of the degree of non-Newtonian behavior, a greater distance from unity corresponds to a more pronounced non – Newtonian properties. A Newtonian fluid is a power law fluid with a power law index of 1, where the shear stress is directly proportional to the shear rate. It is important to remember that the

equation written in the form of Eq. 2.8 is valid only for simple shearing flow.
If the power law index is less than 1 the fluid is pseudoplastic while if n is greater than 1 the fluid is dilatant. m is a measure of the consistency of the fluid. The higher is the m value, the more viscous is the fluid. The viscosity for a power law fluid is expressed in terms of m and n as

$$\eta = m\,|\dot{\gamma}|^{n-1} \tag{2.9}$$

The power law is widely used and this is due to its simplicity and in the polymers processing range it is a good approximation of the viscosity versus shear rate, but it shows some drawbacks. One of the disadvantages of the power law is that it fails to describe the low shear rate region. If n is less than one, the power law predicts that the effective viscosity would decrease with increasing shear rate indefinitely, requiring a fluid with infinite viscosity at rest and zero viscosity as the shear rate approaches infinity, but a real fluid has both a minimum and a maximum effective viscosity that depend on the physical chemistry at the molecular level. There are a number of other models that better describe the entire flow behavior of shear-dependent fluids.

2.7 Carreau model

Carreau fluid [Carreau 1997] is a type of generalized Newtonian fluid where viscosity η depends upon the shear rate by the following equation

$$\frac{\boldsymbol{\eta} - \boldsymbol{\eta}_{\infty}}{\boldsymbol{\eta_0} - \boldsymbol{\eta}_{\infty}} = \frac{\mathbf{1}}{(\mathbf{1} + (\boldsymbol{\lambda}\,\dot{\boldsymbol{\gamma}})^{\mathbf{2}})^{\frac{\mathbf{1}-\boldsymbol{n}}{\mathbf{2}}}} \tag{2.10}$$

where η_0 is the viscosity at zero shear rate, η_∞ is the viscosity at infinite shear rate, λ is the relaxation time and n is the pseudoplastic index. The Carreau model combines all the power law region and the two Newtonian regions of the complete curve. The zero – shear viscosity captures the low shear rate plateau, the infinite shear rate captures the high shear rate plateau, the relaxation time determines the value of shear rate at which the low shear rate plateau ends and the n index determines the law the slope of decreasing portion curve.
A slightly better fit can be obtained by replacing 2 by c, a shape factor, in Eq. 2.10, giving rise to the Carreau - Yasuda model. The shape factor

determines the shape of the transition between the upper plateau and the rapidly increasing portion of the curve.

2.8 Cross model

The Cross model [Cross 1965] is a type of generalized Newtonian fluid, with four constants model, whose viscosity depends upon the shear rate according to the following equation

$$\frac{\boldsymbol{\eta} - \boldsymbol{\eta}_\infty}{\boldsymbol{\eta_0} - \boldsymbol{\eta}_\infty} = \frac{\mathbf{1}}{\mathbf{1} + (\boldsymbol{K}\,\dot{\boldsymbol{\gamma}})^{\mathbf{1-n}}} \tag{2.11}$$

where K is a time parameter. Typically $\eta_0 \gg \eta_\infty$ so when $\dot{\gamma}$ is very small, $\boldsymbol{\eta}$ goes to $\boldsymbol{\eta_0}$. At intermediate $\dot{\gamma}$ the Cross model has the power law region

$$\boldsymbol{\eta} - \boldsymbol{\eta}_\infty \cong \boldsymbol{\eta_0} - \boldsymbol{\eta}_\infty\, \boldsymbol{m}\, |\dot{\boldsymbol{\gamma}}|^{\boldsymbol{n-1}} \tag{2.12}$$

where $m = K^{n-1}$, or for $\eta \gg \eta_\infty$

$$\eta = \eta_0 m\, |\dot{\gamma}|^{n-1} \tag{2.13}$$

At very high shear rates the right side of Eq. (2.12) becomes very small and η goes to the high shear rate Newtonian limit η_∞.

2.9 Herschel Bulkley model

The Herschel Bulkley [Herschel Bulkley 1926] equation combines the Bingham and the power law models. The Herschel–Bulkley fluid is a generalized model of a non-Newtonian fluid. Three parameters characterize this relationship: the consistency m, the power law index n, and the yield tress τ_y. The consistency is a simple constant of proportionality, while the flow index measures the degree to which the fluid is shear-thinning or shear-thickening. Finally, the yield stress quantifies the amount of stress that the fluid may experience before it yields and begins to flow.
The analytical equation for Herschel Bulkley model is written as

$$\tau - \tau_y = m\, |\dot{\gamma}|^{n-1}\dot{\gamma};\ \tau > \tau_y \tag{2.14}$$

$$\dot{\gamma} = 0;\ |\tau| \le \tau_y$$

2.10 Temperature and pressure dependence of viscosity

The temperature dependence of viscosity can often be important as its shear rate dependence [Tanner 1985]. For all fluids, viscosity decreases with increasing temperature and decreasing pressure.
A relation that is valid over a wider temperature range is an Arrhenius-type equation

$$\eta = A\, e^{-E_\eta/RT} \tag{2.15}$$

where T is temperature, R is the molar gas constant and A is aa constant and $E_{\boldsymbol{\eta}}$ is an activation energy for viscous flow so that the mobility of fluid molecules is a temperature-activated process. This equation is derived from the hypothesis that small molecules move by jumping into unoccupied sites or holes. Polymer also obey this equation at temperatures above glass transition. With polymers, viscosity could be governed by jumps of chain segments.
An equation that describes the viscosity at temperature T in terms of viscosity at some reference temperature is the Williams – Landel – Ferry (WLF) equation. This equation is written as

$$\frac{\boldsymbol{\eta}}{\boldsymbol{\eta_r}} = -\frac{\boldsymbol{C_1(T-T_r)}}{\boldsymbol{C_2+T-T_r}} \tag{2.16}$$

in which C_1 and C_2 are constants, $\boldsymbol{T_r}$ is the reference temperature and $\boldsymbol{\eta_r}$ is the viscosity corresponding to the reference temperature.
The WLF temperature dependence forms the basis for horizontal shifting of linear viscoelastic properties to the so – called *time-temperature superimposition*.

CHAPTER 3

RHEOLOGY AND RHEOMETRY

3.1 Introduction

Rheology is defined as the study of the flow of materials under deformation. The principal concepts of this field are related with: geometrical aspects of the flow, force balance, stresses and interchanges with special relations (constitutive relations) that serve to link motion and forces to complete the description of the flow process and are specific to a material.
Rheometry is a set of standard techniques that are used to measure the rheological properties of the material experimentally. A rheometer is an instrument that measures stress and deformation history on a material for which the constitutive relation is not known and can be used to determine the material functions [Macosko 1994].
The basic principle of rheometry is to perform experiments where the flow characteristics such as the shear stress distribution and the velocity profile are known in advance and can be imposed. Under these conditions, it is possible to obtain a flow curve, that is the variation of shear stress as a function of shear rate, from measurements of quantities, such as torque and rotational velocity.
To perform a rheological test, a sample gets mounted into the rheometer and subjected to a well-defined stress or strain history.
In strain-controlled experiments, strain or strain rate is prescribed and stress response gets recorded. Instead, stress-controlled instruments prescribe the stress and record the strain. Typically, rheometers are designed for both mode of operation. Therefore an experiment is a simultaneous measurement of two quantities: dynamics and kinematics. In order to connect these two quantities a mathematical equation is necessary. The equation of a rheometer is obtainable by solving the equations of motion for the particular flow geometry of the apparatus.
The analytical procedure is the following:

- a balance of momentum in a control volume;
- in the balance a constitutive law is introduced;
- the resulting equation is integrated with the appropriate boundary conditions. The result is a relationship between two quantities: dynamics and kinematics.

3.2 Capillary rheometer

The first measurement of viscosity was done by Hagen (1839) and Poiseuille (1840) using a small straight tube or capillary to measure the viscosity of water.
A capillary rheometer is a pressure-driven flow that consists in a cylindrical reservoir where at the end a capillary die is placed. A transducer is located above the capillary die entrance. The barrel is filled with polymer with a series of subsequent loads. After melting and upon reaching test temperature, a piston is driven down the reservoir by an electrical motor at known velocity. Several piston velocities are set before starting the test. During measurement, the pressure drop through the capillary is measured at each velocity. These procedures allow to have a sweep of processing rate.
A schematic diagram of a single capillary rheometer is shown in Fig. 3.1.

The pressure measurement, when the system is in steady state, can be acquired at each velocity value. After the acquisition, the test is advanced to the next value of velocity. Temperature of the rheometer barrel is maintained by separately controlled barrel heaters. The procedure involves the manual compression of the polymer with several sequences of melting and compression.
Calculations involves some assumptions:

- the flow is fully developed, isothermal and steady;
- the fluid is incompressible;
- no velocity in r and θ directions;
- the viscosity is independent of pressure;
- the fluid velocity is zero at the wall.

With these assumptions, the equation of motion in axial flow direction in cylindrical coordinates reduces to

$$0 = \frac{-\delta P}{\delta x} + \frac{1}{r}\frac{\delta(r\tau_{rx})}{\delta r} \tag{3.1}$$

$\delta P/\delta x$ should be constant for fully developed incompressible flow, thus by integration, it is possible to obtain the shear stress distribution.
The shear stress in a fully developed capillary flow grows linearly with the distance from the centre of the capillary (r = 0) to its maximum value (r = R), the wall shear stress τ_w being expressed as

$$\tau_w = \frac{\Delta P\, R}{2\, L} \tag{3.2}$$

where R is the radios and $\Delta P/L$ is the pressure drop over the capillary per unit length.

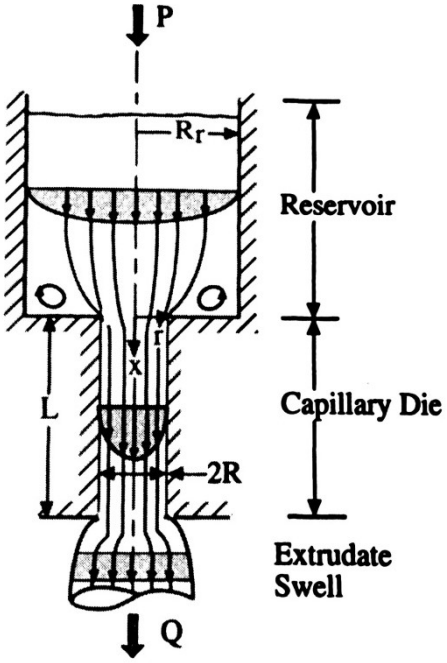

Fig 3.1 - Schematic representation of a single bore capillary rheometer [Macosko 1994]

The volumetric flow rate Q in the barrel can be calculated as

$$Q = \pi {R_b}^2 V \tag{3.3}$$

where R_b is the barrel radius and V is the velocity of the piston.
Difficulties in this measure arise because neither the shear stress, τ_w, nor the shear rate, $\dot{\gamma}_a$, are measured directly. Their values are extracted from the pressure readings and the superimposed volume flow rate.
The shear rate in fully developed capillary flow grows sharply with increasing distance from the centre of the capillary. The shear rate distribution is expressed with the following equation

$$\dot{\gamma}_a = \frac{4\,Q}{\pi\,R^3} \tag{3.4}$$

Capillary rheometers are designed for characterizing polymer melts at high shear rates, typically in a range between 10 - 10.000 s^{-1}. The range of measurable shear stress and shear rate is dependent upon the equipment used. The shear rate values are dependent by piston velocity and as a result by the volumetric flow. High shear rates can be reached easily in polymer processing (extrusion, injection molding). For this reason, usually capillary tests are performed in order to know the behaviour of the material during processing. Excessive heat generation due to viscous dissipation [Winter, 1977], flow instabilities [Ramamurthy, 1986], or wall slip [Mooney, 1931] determine the upper limit of such high shear rate with capillary rheometers and require particular attention.
The measures with the capillary rheometer are affected by some uncertainties. The principal sources are end effects, slip at die wall and non-parabolic velocity profile.

3.2.1 Bagley correction

In general, in a capillary rheometer the total pressure is given by the sum of the pressure drop along the capillary and in the entrance region (Fig 3.2). The latter cannot be neglected and in some cases it is even higher than the former. Thus, end effects must be corrected in order to obtain significant measurements.
In Fig. 3.3 the axial pressure variation ΔP in the capillary die including entrance and exit zone is plotted. The total pressure is

$$\Delta \boldsymbol{P} = \Delta \boldsymbol{P_{Ent}} + \Delta \boldsymbol{P_{Cap}} + \Delta \boldsymbol{P_{Exit}} = \Delta \boldsymbol{P_{End}} + \Delta \boldsymbol{P_{Cap}} \tag{3.5}$$

where ΔP_{Cap} is the pressure drop over the length of the capillary where the flow is fully developed, and $\Delta P_{End} = = \Delta P_{Ent} + \Delta P_{Exit}$ is the excess pressure drop due to the entrance and exit flows. The additional exit pressure drop is comparatively small and usually negligible.
Bagley has suggested the following method for calculating the entrance pressure ΔP_{Ent}. The measurements are repeated using at least three capillaries with the same die radii but different length. The pressure drop ΔP versus the ratio of die length to diameter L/D for a constant apparent shear rate $\dot{\gamma}_a$ gives a straight line with a positive intercept. The linear regression is used to find the intercept on the pressure axis, which represents the pressure drop at the zero distance from the entrance ΔP_{Ent} (Fig. 3.4).

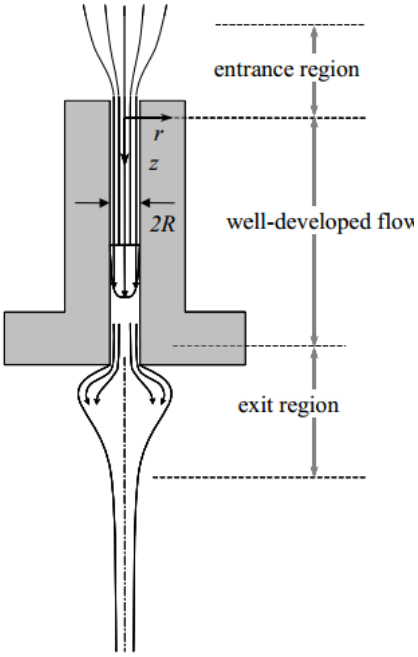

Fig. 3.2 – Schematic representation of the capillary regions

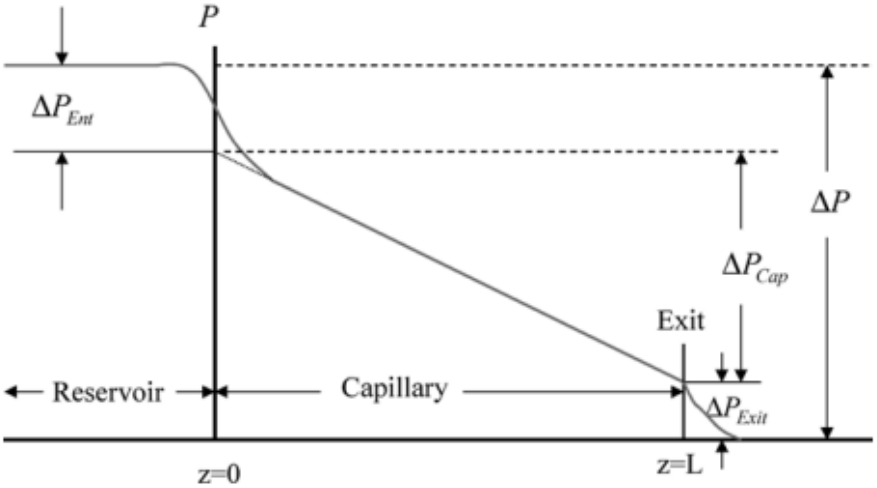

Fig. 3.3 - Schematic diagram of the effect of the pressure drop in a capillary

The results from this procedure are presented in terms of the Bagley correction defined as

$$\boldsymbol{n_b = \frac{\Delta P_{Ent}}{2\,\tau_w}} \tag{3.6}$$

where τ_w is the wall shear stress in the die for fully developed flow.
In a capillary die of radius R and length L, the true shear stress, τ_w can be related to the Bagley correction, n_b and overall pressure drop ΔP as

$$\boldsymbol{\tau_w = \frac{\Delta P}{2\left(\frac{L}{R} + n_b\right)}} \tag{3.7}$$

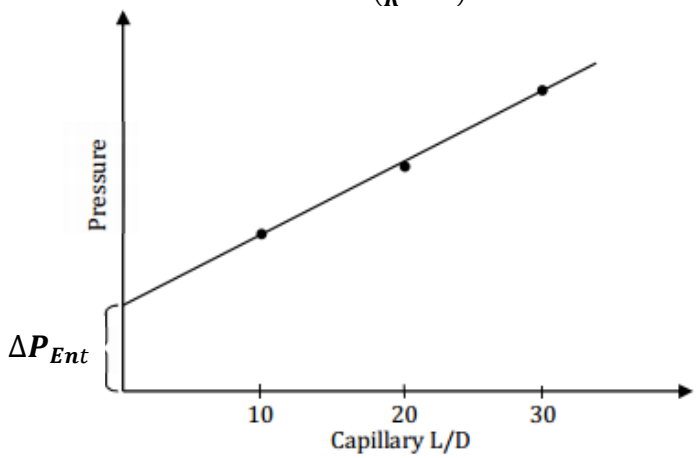

Fig 3.4 Bagley plot example with pressure as a function of the L/D ratio.at one measured shear rate.

3.2.2 Mooney procedure

In capillary rheometry one of the first assumptions is that the velocity at the wall is equal to zero i.e. the melt adheres to the wall. However it is well known that sometimes wall slip occurs. The result of this phenomenon is to reduce the shear rate near the wall.
By 1929, rheologists were actively considering slip. An indirect method of measurement has been developed by Mooney.
In general, the discharge from a tube of radius R is

$$Q = 2\pi \int_0^R vr\, dr \tag{3.8}$$

where v is the axial velocity of the fluid. Integrating Eq. 3.8 by parts, if slip does not vanish at the wall, the flow rate becomes

$$Q = \pi v(R)R^2 - \pi \int_0^R r^2 \frac{dv}{dr} dr \tag{3.9}$$

or, with $q = Q/\pi R^2$ and $\varphi = 1/\ \eta(\tau)$

$$q = v(R)R - {\tau_w}^{-3} \int_0^{\tau_w} \tau^3\ \varphi(\tau) d\tau \tag{3.10}$$

where $v(R)$ is the slip velocity v_s. Clearly slip increases the discharge. Following Mooney, it is assumed that v_s is a function of τ_w. Then the Eq. 3.10 becomes

$$q = v_s + {\tau_w}^{-3} \int_0^{\tau_w} \tau^3\ \varphi(\tau) d\tau \tag{3.11}$$

Using different die diameters is possible to measure the shear rate at a specific shear stress. If the plot apparent shear rate versus 1/R at constant shear stress gives a horizontal line, no slip occurs. If the curve is linear with a positive slope, the slip velocity can be calculated from the slope, according to the Mooney procedure. The flow rate is a sum of two components: shear and slip

$$Q = \frac{\pi R^2 \dot{\gamma}}{4} + \pi R^2 v_s \tag{3.12}$$

and the equation of the apparent shear rate results

$$\dot{\gamma}_a^{slip} = \frac{4Q}{\pi R^3} = \dot{\gamma}_a^{No\ slip} + \frac{4v_s}{R} \tag{3.13}$$

where v_s is the slip velocity.
Tadmor lists several possibilities concerning slip:

- the presence of a solid wall may alter the concentration of solute near the wall, thereby inducing a low viscosity layer and apparent slip. In this case, the solvent does not slip at the wall;
- in a molten polymer, the wall will alter the configuration space available to molecules near the wall, even if slip does not occur, thereby altering the material behaviour next to the wall;
- slip may occur, separately from or in addition to the reasons listed above (e.g. presence of lubricants).

3.2.3 Rabinowitsch correction

When flowing in tubes, Newtonian fluids display a parabolic velocity profile. Non – Newtonian fluids, on the other hand, are often characterized by a velocity profile which is not parabolic, but rather more similar to plug flow (Fig. 3.5).

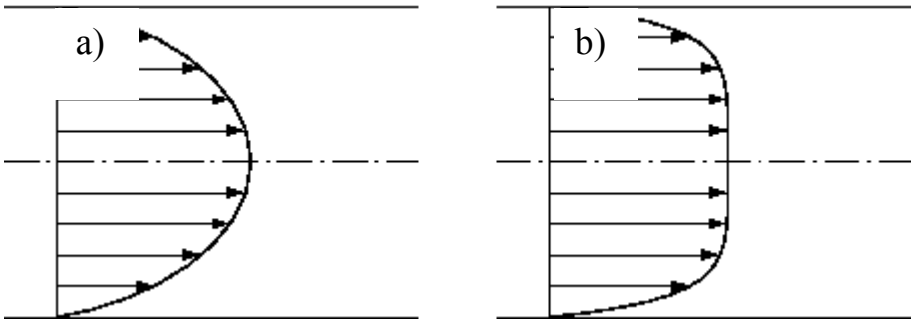

Fig. 3.5 - a) Parabolic velocity profile and b) plug flow velocity profile

Rabinowitsch published a correction to obtain the shear rate in such a case, i.e. for an arbitrary fluid. The correction is carried out by plotting log wall shear stress versus log apparent shear rate. If the curve is a straight line, the slope obtained is the power-law index and the real shear rate is expressed as

$$\dot{\gamma} = \left(\frac{3n' + 1}{4n'}\right)\dot{\gamma}_a \tag{3.14}$$

where n' = n and is the power law index.
If the log shear stress versus log apparent shear rate is not a straight line, the n' index at each shear rate is obtained by numerical derivation as the slope of the apparent shear rate as a function of wall shear stress on a log – log plot

$$n' = \left(\frac{d \log \tau_w}{d \log \dot{\gamma}_{wa}}\right) \tag{3.15}$$

Viscosity corrected for entrance pressure drop, slip and the non – Newtonian flow profile is expressed as

$$\eta = \frac{\tau_w}{\dot{\gamma}_w} = \frac{R\,\Delta P}{2L} \frac{1}{(\frac{3n'+1}{4n'})\left[\dot{\gamma}_a - \frac{4v_s}{R}\right]} \tag{3.16}$$

3.3 Slit rheometer

Capillary rheometers can be modified readily to force liquid through a thin rectangular channel or slit to measure the rheological properties of the material in pressure – driven flow. A schematic representation of a slit capillary rheometer is shown in Fig. 3.6.
The main advantage is that the flat geometry of the wall makes it possible to directly measure the pressure in the slit where the flow is fully developed. A non – linear pressure profile with slit geometry is possible, thus a minimum of three pressure transducers for accurate results are required.
The polymer flows into the slit thus there are no pressure drops due to changes in the flow cross section in areas near or between the location of the transducer. For this reasons the slit die does not require the entrance effect correction (i.e. the Bagley correction).

Knowing the pressure gradient along the longitudinal length axis the shear stress and shear viscosity can be obtained. The shear stress grows linearly with the distance from the centre of the slit to its maximum value at the wall. The shear stress τ_w on the wall is expressed as

$$\tau_w = \frac{h}{2}\frac{\Delta P}{L} \tag{3.17}$$

where *L* is the length of the capillary, *h* is heights of the slit and the $\Delta P = p1 - p2 = p2 - p3$ if the pressure profile is linear.
It is possible to assume that the slit is infinitely wide and to ignore the edge effect with a good accuracy if the width is long more than 10 times the height [Wales at al. 1965, Han 1971]. For w/h<10 the wall shear stress should be corrected as [Macosko]

$$\tau_w = \frac{h}{2(1+\frac{h}{w})}\frac{\Delta P}{L} \tag{3.18}$$

The apparent shear rate $\dot{\gamma}_a$ in a rectangular slit is

$$\dot{\gamma}_a = \frac{6Q}{wh^2} \tag{3.19}$$

where *w* is the width of the slit.

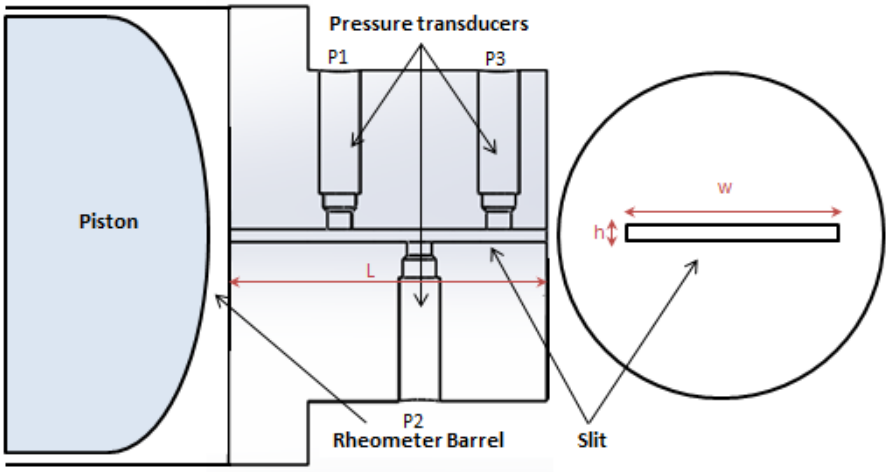

Fig 3.6 Schematic representation of a slit capillary rheometer

3.3.1 Mooney procedure

If the shear stress versus apparent shear rate curves do not superpose for different slit heights than the fluid slips at the wall. Using the Mooney procedure it is possible to determine the slip velocity also for the slit geometry. Plotting $\dot{\gamma}_a$ against 1/h for the same wall shear stress τ_w, the slip velocity is calculated from the slope of these curves according to

$$\dot{\gamma}_a^{slip} = \frac{6v_s}{h} + \dot{\gamma}_a^{No\ slip} \tag{3.20}$$

3.3.2 Rabinowitsch correction

The procedure is analogous to what was described for capillary rheometry. If the behaviour of the fluid is non – Newtonian, the Rabinowitsch correction for the slit rheometer is expressed as

$$\dot{\gamma} = \frac{6Q}{wh^2}\left(\frac{2n'+1}{3n'}\right) \tag{3.21}$$

where

$$n' = \left(\frac{d \log \boldsymbol{\tau_w}}{d \log \dot{\gamma}_a}\right) \tag{3.22}$$

If fluid has a power law behaviour $n = n'$.
The shear viscosity corrected for entrance pressure drop, slip and the non – Newtonian flow profile is then:

$$\eta = \frac{\tau_w}{\dot{\gamma}_w} = \frac{h\,\Delta P}{2L} \frac{1}{\left(\frac{2n'+1}{3n'}\right)\left[\dot{\gamma}_a - \frac{2v_s}{h}\right]} \tag{3.23}$$

3.4 Comparison between capillary rheometer and slit rheometer

While the use of capillary rheometer to determine the rheological properties of filled and unfilled materials is well developed, the application of slit die rheometer is more limited. The principal advantage of capillary rheometry is the well-developed analysis of the simple flow behavior. On the other hand a significant disadvantage is the fact that reservoir curvature prevents flush mounting of the pressure transducer. In fact, the curvature of the cylinder produces a gap between the edge of the transducer and the die wall. This small gap introduces a source of uncertainty during the measurement because it creates a disturbance in the shear flow around the hole. This uncertainty is called "pressure hole effect" (Walters, 1975). This problem is not present in the slit die if the transducer is perfectly flat with respect to the flow and any possible "hole effect" is eliminated. Another important disadvantage is the effect of pressure drop that converges into the capillary entrance and the importance to perform the Bagley correction.
When the capillary rheometer is used to determine the rheological properties of WPC melts, a variety of other problems can be encountered. The influence of such flow disturbances is suspect because, small gap in dies tend to produce inclusions that grow with time as the thermally sensitive natural fibers degrade. Another aspect to take into account when testing these materials is the particle size of the wood filler. This constraint limits the analysis to small particle sizing. In addition, since wood fibers are anisometric (aspect ratio of ~10), the constrained flow of restrictive capillary dies produce oriented material structures.

3.5 Cone – plate and parallel plate rheometer

Mooney and Ewart (1934) appear to have been the first to suggest the cone and plate geometry for viscosity measurements. Today the method

of rheometry more widely used for polymer melts is rotational rheometry, in particular using sliding plates. Cone – plate and parallel plate rheometry are commonly used to measure the viscometric functions of the polymer melts.
In this method, two parallel plates, or a cone and a plate, are fixed with melt occupying the space in between them. These types of rheometer can be used to generate drag flow. One plate is rotated and the other is kept stationary, inducing a shear flow within the melt dependent upon rotation speed and gap width. Torque is measured in the opposite plate and from this value shear stress can be calculated. In strain rate controlled mode, deformation rate is set and the torque value is measured while in the stress controlled mode the torque is the set value and the value of the deformation measured. Usually the rheometer could operate in both modes. The tests can be run in step – strain mode with a shear rate profile from low rate to high and vice versa.
Rotational rheometers have an accurate temperature control in isothermal tests using an oven. The presence of the oven makes it possible to use nitrogen to carry out the test in a controlled atmosphere. Only a very small amount of sample is necessary to perform the measurements.

3.6 Cone and plate rheometer

The cone – plate geometry (Fig. 3.7) is one of most common geometry for measuring rheological properties at small deformation rate.
The bottom part of geometry is e plate and the upper part has a conical profile with a truncated tip. The polymer melt flows in the gap formed by rotating cone, with angle φ, and stationary plate. The gap in the measurement position is defined by the imaginary cone tip witch would touch the lower plate.
The cone and plate rheometer has the important property of a uniform shear rate along the radius at every point of the rheometer.
The simplifying assumptions are

- Steady, laminar, isothermal flow
- Negligible body forces
- $\beta <$ 0.10 rad
- Spherical liquid boundary

then the equations of motion reduce to

$$\rho \frac{{v_\theta}^2}{r} = \frac{1}{r^2}\frac{\delta(r^2\tau_{rr})}{\delta r} - \frac{\tau_{\theta\theta} + \tau_{\phi\phi}}{r} \tag{3.24}$$

$$0 = \frac{1}{r sin\theta}\frac{\delta(\tau_{\theta\theta} sin\theta)}{\delta\theta} - \frac{cot\ \theta\ \tau_{\theta\theta}}{r} \tag{3.25}$$

$$0 = \frac{1}{r}\frac{\delta\tau_{\theta\phi}}{\delta\theta} + 2\frac{cot\ \theta\ \tau_{\theta\phi}}{r} \tag{3.26}$$

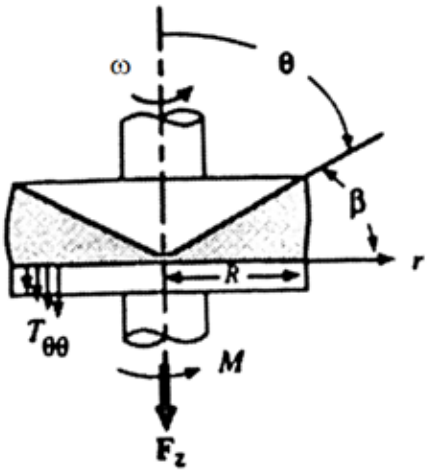

Fig. 3.7 Schematic representation of a cone on plate rheometer [Makosco 1994].

Assuming that the cone rotates at ω angular velocity, the shear rate at a given radius r is then the linear velocity of the cone there $r\omega_0$, divided by the gap width $r\beta$, so the shear rate is

$$\dot{\gamma} = \frac{\omega}{\beta} \tag{3.27}$$

If the fluid fills the gap out to the radius R, the moment M exerted on slip surfaces out to this radius must be the same for each surface, since there is no angular acceleration and is equal to

$$M = 2\pi\int_0^R \dot{\gamma}\,\eta(rcos\beta)^{\,2}dr \tag{3.28}$$

Thus, measurement of the moment required to turn the cone gives practically a direct reading of shear stress expressed as

$$\tau = \frac{3M}{2\pi R^3} \tag{3.29}$$

thus the viscosity is

$$\eta = \frac{3M\beta}{2\pi R^3 \omega} \tag{3.30}$$

3.7 Parallel plate rheometer

In a plate - plate geometry (Fig. 3.8), the simplifying assumptions are

- Steady, laminar, isothermal flow
- Negligible body forces
- Cylindrical edge;

then the equations of motion reduce to

$$0 = \frac{\delta \tau_{\theta z}}{\delta z} \tag{3.31}$$

$$0 = \frac{\delta \tau_{zz}}{\delta z} \tag{3.32}$$

$$-\rho \frac{{v_\theta}^2}{r} = \frac{1}{r}\frac{\delta (r\tau_{rr})}{\delta r} - \frac{\tau_{\theta\theta}}{r} \tag{3.33}$$

In viscometry, this type of rheometer is the only completely controllable flow that is used.
The equation for the shear rate is determined by angular velocity ω, the height between the plates h and the radius r as

$$\dot{\gamma} = \frac{\omega r}{h} \tag{3.34}$$

In the equation it is possible to observe that in the case of plate – plate the shear rate is dependent on the radius, indeed the maximum shear rate is for r = R. At any given shear rate centrifugal force can be made arbitrarily small by decreasing the angular velocity and the gap width in the same proportion. Thus the inertial effects can be made negligible.
If the fluid is in contact with the plates, then the moment required to turn the rotating disc is

$$M = 2\pi \int_0^R \dot{\gamma}\, \eta r^{\,2} dr \tag{3.35}$$

The equation for maximum shear stress is

$$\tau_{max} = \frac{2M}{\pi R^3} \tag{3.36}$$

where M is torque.

The Newtonian analysis provides the equation of the plate - plate rheometer as

$$\eta = \frac{2Mh}{\pi R^4 \omega} \tag{3.37}$$

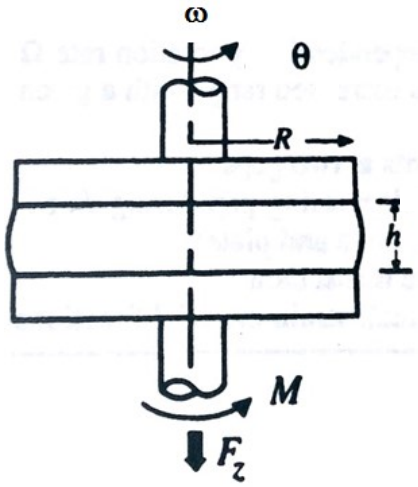

Fig. 3.8 Schematic representation of a plate on plate rheometer [Makosko 1994]

3.7.1 Mooney procedure

Using the Mooney procedure it could be possible to determine the slip velocity also for the parallel plate geometry. Plotting $\dot{\gamma}_a$versus 1/h for each τ_w, the slip velocity is calculated from the slope of these curves according to

$$\dot{\gamma}_a^{slip} = \frac{2\omega R}{h} + \dot{\gamma}_a^{No\ slip} \tag{3.38}$$

3.7.2 Rabinowitsch correction

Due to a non-uniform shear rate it is impossible to determine the viscosity for a non-Newtonian fluid without an appropriate correction.
In particular for a power law fluid the maximum shear stress as a function of torque M is

$$\tau_{max}^{PL} = \frac{M(3+n)}{\pi R^3} = \tau_{max}^{N} \frac{(n+3)}{4} \tag{3.39}$$

where n is the power law index and τ_{max}^{N}.is shear stress for a Newtonian fluid.
The parallel plate equation for a power law fluid is expressed as

$$\eta = \frac{M(n+3)}{2\,\pi R^3 \omega} \tag{3.40}$$

Extending the correction for any generalized Newtonian fluid. the maximum shear stress as function of torque M is

$$\tau_{max}^{NG} = \frac{\tau_{max}^{N}}{4}\left[3 + \frac{d(log\frac{M}{2\,\pi R^3})}{d(log\dot{\gamma}_{\max})}\right] \tag{3.41}$$

3.8 Oscillatory Rheometry

Rheometers of the parallel plate and cone-and-plate geometry often have the capability to perform small amplitude oscillatory shear tests.
The parallel plate rheometer (Fig 3.9) can be used in dynamic oscillatory mode to measure linear viscoelastic properties. These tests involve the application of a sinusoidal displacement to the upper plate or cone of the rheometer.
The resulting stress can be resolved into components that are in phase with the input (elastic response) and out of phase with the input (viscous response).
This technique is valid if displacement applied to the sample are small and measurements are made in the linear viscoelastic region (LVR).

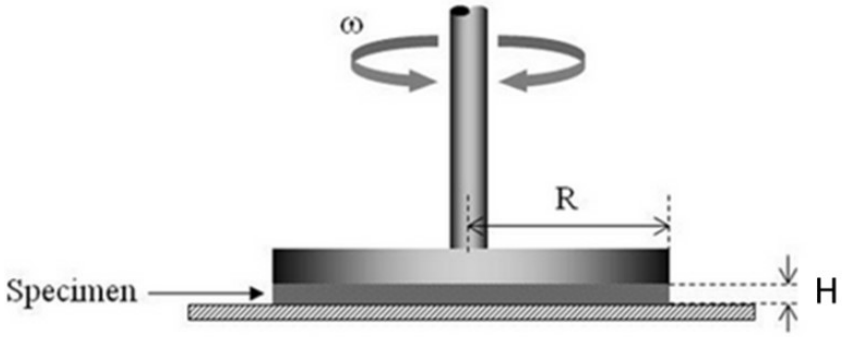

Fig. 3.9 Schematic representation of a plate on plate rheometer during oscillation test

In fact in case of small displacements the shear rate can be expressed as

$$\dot{\gamma} = \frac{dv_x}{dy} = \frac{d\gamma}{dt} \tag{3.42}$$

The equation of the displacement is expressed as

$$\gamma_{max} = \gamma_0 sen(\omega t) \text{ with } \gamma_0 = u_0/H \tag{3.43}$$

where ω is the frequency, H is the gap between plate and u_0 is the displacement.

The equation of the shear rate is

$$\dot{\gamma} = \frac{u_0 \omega cos(\omega t)}{H} \tag{3.44}$$

and

$$\tau = \tau_0 \, sin(\omega t + \delta) \tag{3.45}$$

where τ_0 is the stress and δ is the phase angle shift.

From the equation of shear stress it is possible to define storage modulus G' and loss modulus G'' as

$$G' = \frac{\tau_0}{u_0/H} \cos\delta \tag{3.46}$$

$$G'' = \frac{\tau_0}{u_0/H} \sin\delta \tag{3.47}$$

The oscillatory measurement procedure consists of two steps: strain sweep and frequency sweep tests.

During the strain sweep test, it is possible to determine the linear viscoelastic region (LVR) of the material. The sample is subjected to a small amplitude oscillatory strain sweep. In the early stages of the test, the strain is sufficiently low to preserve structure and G′ and G′′ are constant but as the test progresses the applied strain causes the disruption of structure and a decrease in elasticity (phase angle rises) and decrease in rigidity (complex modulus). The linearity is assured in the part of the test in which the moduli are constant.

Oscillatory frequency sweeps allow us to probe and identify the nature of the structuring mechanisms present in a fluid. The sample is exposed to small-deformation oscillations at fixed strain (in LVR region) covering a range of frequencies to assess the structural response. In Fig. 3.10 the input values (γ_0, ω)and the output values (τ_0, δ) during oscillation test are presented.

3.9 Cox – Mertz rule

Using the rheometer in oscillatory mode the viscosity is obtained using an empirical relationship called Cox-Merz "rule". This rule has been found to be of great use in rheology. This rule states that the shear rate dependence of the steady state viscosity η is equal to the frequency dependence of the linear viscoelastic complex viscosity η*, where the complex viscosity is expressed as

$$\eta * = \sqrt{\left(\frac{G'}{\omega}\right)^2 + \left(\frac{G''}{\omega}\right)^2} \tag{3.48}$$

If applied correctly, the Cox-Merz rule can be important in polymer rheology, and there are several circumstances in which it may be used. For many polymeric systems the steady state viscosity is difficult to measure at high shear rates, because of sample fracture, secondary flows and so forth.

It is important during the application of the rule to ensure that the appropriate values for η ($\dot{\gamma}$) and η*(ω) are used. For example, in both cases steady state values are required, and any transient effects due to flow or oscillation, start-up or inertia must not be present.

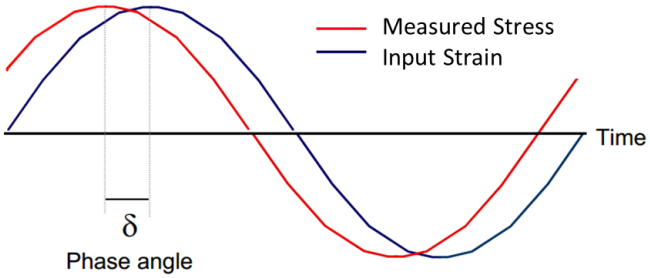

Fig. 3.10 – Input strain wave (γ_0, ω) and measured stress wave (τ_0, δ) during a oscillation test

CHAPTER 4

THE EXTRUSION PROCESS

4.1 Introduction

In polymer processing, the extruder is one of the most versatile machineries. An extruder is a screw pump fed by a solid thermoplastic polymer that allows to obtain a constant section of semi-finished products forcing the material through a die.
The extruder can be fed through one or more hoppers. From the hopper the material, usually in the form of pellets, is pumped into the forming cylinder called *barrel*. The material is pushed forward inside the barrel where there is a screw with a variable section that homogenizes, melts and pressurizes the material. Using an electric motor and a reducer, the screw is driven. The die has the function of giving the final shape to the product. On the surface of the barrel there are heating elements used to control the temperature together with fans and thermocouples.
In the simplest case, the extruder is divided into three main areas: the solids conveying zone, the melting zone and the metering or fluid transport zone. Sometimes an additional zone, called delay zone, is also present and occurs between the solids conveying zone and the melting zone.
In the solids conveying zone, the section of the screw is uniform, in the melting zone the section increases linearly and in the metering zone the screw section is again constant, but larger than in the solids conveying zone (Fig. 4.1).
The extrusion process is complex to control and model and this is due to the presence of different physical phenomena that need to be studied separately, without forgetting the connection to each other.
The main processing variables are: the screw rotation speed and the barrel temperature profile. The main geometric variables are: the screw diameter D, the screw length L, the ratio L / D and the compression ratio that is the ratio between the screw height of the transport fluid zone and the screw height of the end of the conveying zone.

4.2 Literature review

In the literature, several works about the simulation of the extrusion process are available. Z. Tadmor and C. G. Gogos (1979) make a review

of all studies previously published and provide a useful tool for the study of the extrusion process. The starting point of these studies has been the development of an experimental analysis, performed for the first time since Maddock (1959) and Street (1961), and subsequently refined by Tadmor (1972, 1970, 1966). This experimental analysis has been carried out by stopping an extruder in steady state, with a rapid cooling of the barrel and the screw, freezing the polymer in the channel. After the cooling, it has been possible to reconstruct what happened for the entire screw length. Small traces of colored polymers, used as tracers, has been used to better interpret this type of experiments and to differentiate the portion of the molten material from the solid.

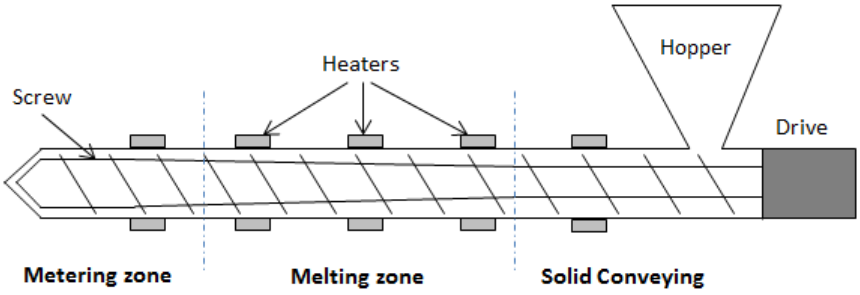

Fig. 4.1 - Schematic structure of the different zones of the extruder

In this way, the process of extrusion of many polymers has been analyzed [Tadmor 1971], and important information on the physical phenomena has been obtained, in particular on the mechanisms of polymer melting.
In the scientific literature, the mathematical treatment of phenomena that occur in each zone is also studied. In particular, four reference models for the individual zones are available: Darnell and Mol (1956) for the conveying zone, Kacir and Tadmor (1972) for the delay zone, Tadmor (1966), for the melting zone and Rauwendaal (1985) for the metering zone.
Each of these models examines the physical phenomena that occur in the individual zones, and use a number of simplifying assumptions that allow a plausible mathematical treatment.

4.3 Conveying zone

Before the beginning of plasticization in the conveying zone, solid raw material in the form of grains or powder is mixed. The screw height is constant and the length of this zone is such as to ensure a correct rate of

feed forward. The model [Darnell Moll and (1956)] allows to determine the pressure profile of the zone with the aim to balance the process variables (flow rate, screw velocity, pressure).
For modeling it is necessary to assume that:

- the material is elastic and can have an internal pressure;
- the contact between the solid and the parts of the extruder is elastic;
- the coefficient of friction between the plastic and the metal surface is independent of pressure;
- there is no shear stress within the portion of solid considered;
- the barrel is supposed to be rotating, while the screw is supposed to be fixed;
- the width of the threads is negligible;
- the distance between the threads and the barrel is negligible;
- the weight of the polymer and the screw is negligible.

Inside the extruder, the solid particulate is dragged along the channel formed by the helical screw and the barrel. The friction between the particles and the walls, during forming, is the driving force for transportation. A rigorous analysis of the phenomenon is difficult and this is due to the complexity of the process (the rise in temperature caused by friction and by external heating, the viscoelastic response of particulate, etc.).
To study the displacement of the flow in a straight channel with constant cross section, a column of particulate solid of length L compressed between two walls is considered (Fig 4.2). The left wall applies a force F_0 on the solid and it is opposed to a force F_L applied to the right side thus the friction force on the channel walls is opposed to the resulting force.
It is assumed that:

- the solids are compacted, in motion or in a state of incipient slip on the wall;
- the axial and radial tension varies only with the axial distance;
- the relationship between the radial and axial tension is a constant (K) that is independent of the position;
- the friction coefficient is constant and independent of compaction;
- the effects of temperature are neglected.

Solving the balance of the forces in x - direction one obtains the following expression

$$F_x = F_0 e^{\frac{-f_i K C x}{A}} \tag{4.1}$$

where F_X is the axial force, f_i is the static coefficient of friction between the material and the walls, K is the ratio between the radial and axial forces, C is the generalized circumference that represents the perimeter of the area of friction and A is the cross-sectional area on which the force F_X acts.
If in the same scheme a movable upper wall is considered, it is necessary to add a new component of friction for forces balance. This new component is the dynamic friction coefficient.
In Fig. 4.3 the dynamic friction coefficient fw_1 between the material and the upper wall and the static friction coefficient fw_2 between the material and the lower wall are shown.

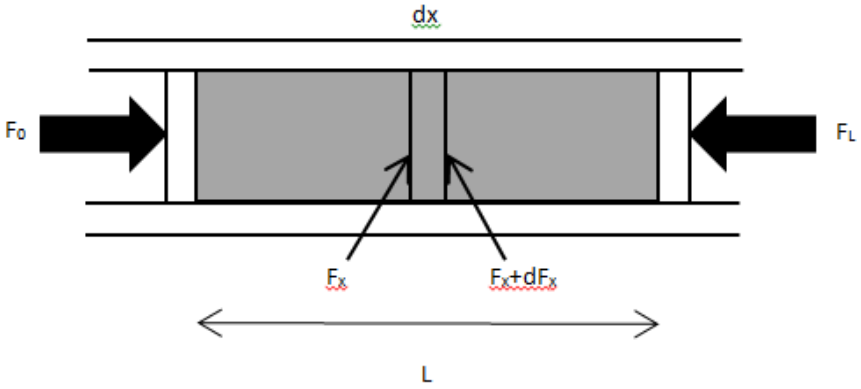

Fig. 4.2 - Column of solid particulate in a channel with constant cross section.

Fig. 4.3 – Forces balances on a differential element of solids.
Thus, it is possible to write the relationship between the forces of the left and right side of the channel as

$$\frac{F_L}{F_0} = \exp\left[\left(C_1 f_{w1} - C_2 f_{w2}\right)\frac{KL}{A}\right] \tag{4.2}$$

where C_1 is the portion of the wet perimeter on the movable wall and C_2 on the lower wall.

If the movable wall becomes an upper endless wall that moves with an angle θ (angle of the threads), the friction force exerted on the solid by the movement of the wall remains the same.
At steady state, the solid has a relative velocity determined as the difference between the axial velocity with which the particulate solid is pushed V_{pl} and the tangential velocity of the surface on the barrel V_b , respectively

$$V_{pl} = \frac{G}{\rho_b \left[\frac{\pi}{4}\left(D_b^{\,2} - D_s^{\,2}\right) - \frac{eH}{sen\bar{\theta}} \right]} \tag{4.3}$$

$$V_b = \pi N D_b \tag{4.4}$$

where G is mass flow rate, D_b diameter of the barrel, D_s diameter of the screw, and e is the thickness of the threads , H the depth of the channel, $\bar{\theta}$ the angle of the threads , ρ_b is density and N is screw velocity. In Fig. 4.4 it is possible to observe the velocity components where ϕ is the angle between the direction of motion of the force exerted by the moving plate on the solid and the direction of motion of the moving plate.

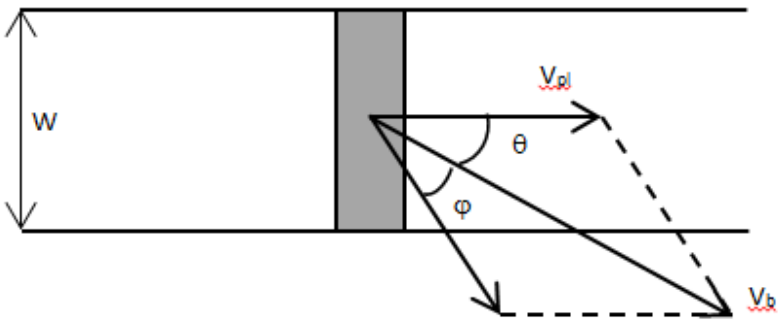

Fig. 4.4 - Diagram of speed in the extrusion channel
After integration, the down channel force balance results as

$$\frac{F_x}{F_0} = \exp\left\{ \left[C_1 f_{w1} \cos\left(\vartheta + \phi\right) - C_2 f_{w2} \right] \frac{Kx}{A} \right\} \tag{4.5}$$

The ratio between the forces becomes a function of the flow rate through the angle ϕ. It is possible to know the amount of output pressure that can be generated for a given flow rate.
The balance of forces in the barrel can be expressed in terms of coefficients of friction, geometry and pressure increase. In particular, eight forces are applied to a solid element inside the channel: the friction with the barrel, the force generated by the upstream and downstream of the solid, the pressure acting on the passive and active threads, the friction forces with the active and passive threads and the friction with the screw. From the balance of forces it is possible to determine the output pressure P_2.

$$M = 2\frac{H}{W_b}\frac{f_s}{f_b}sen\theta_b\left(K_s + \frac{\overline{D}}{D_b}\cot\overline{\theta}\right) + \frac{W_s}{W_b}\frac{f_s}{f_b}sen\theta_b\left(K_s + \frac{D_s}{D_b}\cot\theta_s\right) + \quad (4.7)$$
$$+\frac{\overline{W}}{W_b}\frac{H}{Z_b}\frac{1}{f_b}sen\theta_b\left(K_s + \frac{\overline{D}}{D_b}\cot\overline{\theta}\right)\ln\frac{P_2}{P_1}$$

where W is the width channel, Zb is the "unwound" distance in the conveying zone, $\overline{D}$ is the diameter of the barrel, θ_b is the angle at the base of the threads , θ_b is the angle at the top of the threads , f_s is the friction coefficient on the screw, f_b is the friction coefficient on the barrel, P_1 is the pressure at the base of the hopper and P_2 is the output pressure.

4.4 Delay zone

The delay zone begins at the end of the solids conveying zone where the material, in contact with the barrel, melts and creates a thin layer of molten film and the fusion mechanism is not yet steady. Kacir and Tadmor (1972) have developed a theoretical model that allows to estimate the thickness of the molten film, the pressure profile and the flow rate of the fluid at the beginning of the melting zone. By comparing the experimental values with the theoretical model they established a criterion for estimating the length of this zone and the thickness of the fluid film as a function of the length of the compression zone and the height of leakage between the threads and the barrel.

$$L_D = 0.2L_C \quad (4.8)$$

where L_D is the "unwound" length in the area of delay and L_C is the length of the compression zone that is

$$L_c = g\frac{\pi D}{\cos\phi} \tag{4.9}$$

where g is the turn number, ϕ is the angle of threads , and D is the diameter of the barrel and

$$\delta_d = 5c \tag{4.10}$$

where δ_d is the thickness of the molten film and c is the leakage between barrel and top of the threads .
Once the molten film thickness is known, it is possible to estimate the flow of fluid that is formed in the delay area as

$$Q_d = \frac{1}{2}W\delta_d V_{bz} \tag{4.11}$$

where W is the channel width and V_{bz} is the speed of the barrel along the z direction.

4.5 Melting zone

In the melting zone, the solid material gradually melts. This zone is characterized by a section of the channel that decreases linearly. The model, developed by Z. Tadmor (1966), aims at defining the equations that are necessary to determine the length of the melting zone. This length is a parameter that depends on the physical properties of the polymer and the operating conditions during extrusion. In fact, the melting of the material in the channel does not occur all at once. Between two subsequent screw threads a solid and a liquid portion are in fact simultaneously present. The material, still solid towards the thread is pushed and melting takes places in a liquid film close to the barrel and subsequently in the fluid bed. Melting takes place via two phenomena involving, respectively, the fluid and solid. The solid portion contributes to melting with the dissipated heat by compression. This heat is caused by the increase in the section of the screw. The liquid contributes with the heat dissipation due to viscous action.
Let us consider a slit of a homogeneous and isotropic material of width W pushed against a heated wall that is moved at a velocity Vb with a direction orthogonal to the solid. The thin film of molten material which is

formed between the plate and the wall is removed continuously (Fig. 4.5). The problem is two-dimensional and velocity and temperature profiles are only a function of x and y, because the dimension z is supposed to be infinite. The thickness of the molten film, for $x \cong 0$, is small and then increases along the x coordinate. The profile of the molten film δ (x) is the unknown function.
The heat is conducted from the heated wall at a constant temperature T_0 towards the solid-melt interface which is at a temperature T_m. The solid is perfectly rigid, incompressible and moves towards the interface without rotation. The amount of molten material at the interface is independent of x because the speed of the solid is independent from that coordinate and it is assumed to be constant.
The assumptions of the model are:

- thermo physical properties are constant;
- incompressible fluid;
- condition of adherence to the walls;
- steady flow;
- gravity forces negligible;
- laminar flow;
- thickness of the thin film δ«W and H;
- the viscosity of the fluid follows a power law;
- the temperature follows an Arrhenius model.

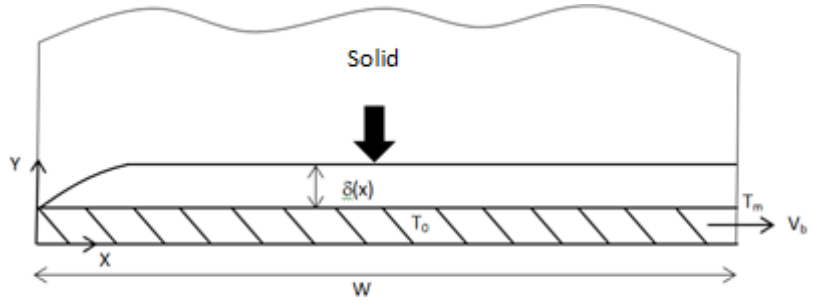

Fig. 4.5 - Representation of the molten polymer slab on a heated surface.

The equation of continuity is expressed as

$$\frac{\partial v_x}{\partial x} + \frac{\partial v_y}{\partial y} = 0 \tag{4.12}$$

and the momentum equation as

$$\frac{\partial P}{\partial x} + \frac{\partial \tau_{yx}}{\partial y} = 0 \tag{4.13}$$

assuming a pure drag flow in the film, the momentum equation reduces to

$$\frac{\partial \tau_{yx}}{\partial y} = 0 \tag{4.14}$$

expressing the shear stress in terms of the shear rate yields

$$\frac{\partial}{\partial y}\left[e^{-a(T-T_m)} \left(\frac{-\partial v_x}{\partial y} \right)^n \right] = 0 \tag{4.15}$$

integrating the shear rate with respect to y

$$-\frac{\partial v_x}{\partial y} = C_1 e^{a(T-T_m)/n} \tag{4.16}$$

the energy equation in the fluid film is written as

$$\rho_m c_m \left(v_x \frac{\partial T}{\partial x} + v_y \frac{\partial T}{\partial y} \right) = K_m \frac{\partial^2 T}{\partial y^2} - \tau_{xy} \frac{\partial v_x}{\partial y} \tag{4.17}$$

where ρ_m, c_m , K_m are the thermal properties of the polymer melt.
The boundary conditions in the film are

$$\begin{aligned} T(0) &= T_0 \qquad \mathrm{T}(\delta)=\mathrm{T}_m \\ v_x(0) &= V_0 \qquad v_x(\delta) = 0 \\ v_y(0) &= 0 \end{aligned} \tag{4.18}$$

The velocity $v_y(\delta)$ at any position x is determined by the rate of melting at the interface and it is obtained by the following balance

$$k_m \left(-\frac{\partial T}{\partial y} \right)_{y=\delta} = \rho_m \left[-v_y(\delta)\lambda \right] + k_s \left(-\frac{\partial T_s}{\partial y} \right)_{y=\delta} \tag{4.19}$$

where the first term corresponds to the heat flux conducted into the interface from the film, the second is the rate of melting at the interface and the third term is the heat flow conducted out from the interface, where λ is the heat of fusion, Ks is the thermal conductivity and T_s is the solid temperature.
The energy equation in the solid bed is reduced to

$$\rho_s c_s v_{sy} \frac{\partial T_s}{\partial y} = K_s \frac{\partial^2 T_s}{\partial y^2} \tag{4.20}$$

where ρs, cs, Ks are the solid bed thermal properties.
Equation 4.20 can be solved with the following boundary conditions

$$T(\infty) = T_{s0} \qquad \mathrm{T}_s(\delta)=\mathrm{T}_m \tag{4.21}$$

obtaining the temperature profile as

$$T = T_{s0} + (\mathrm{T}_m - T_{s0}) \exp \left[\frac{v_{sy}(y-\delta)}{\alpha_s} \right] \tag{4.22}$$

with $\rho_m v_y(\delta) = v_{sy}\rho_s$ the rate of heat conduction out of the interface is

$$-k_s\left(\frac{\partial T_s}{\partial y}\right)_{y=\delta} = -\left(T_m - T_{s0}\right) v_y(\delta)\rho_m C_s \tag{4.23}$$

Thus (4.19) can be written as

$$k_m\left(\frac{\partial T}{\partial y}\right)_{y=\delta} = \rho_m v_y(\delta)\lambda^* \tag{4.24}$$

where

$$\lambda^* = \lambda + C_s(T_m - T_{so}) \tag{4.25}$$

where λ^* è is the total heat energy required to bring the solid from an initial temperature T_{so} to T_m and to melt it.
Using dimensionless variables

$$\Theta = \frac{T - T_m}{T_0 - T_m} \tag{4.26}$$

$$\xi = \frac{x}{W} \quad \text{e} \quad \eta = \frac{y}{\delta} \tag{4.27}$$

$$u_x = \frac{v_x}{V_0} \quad \text{e} \quad \text{u}_y = \frac{v_y}{V_0(\delta_0 / W)} \tag{4.28}$$

the dimensionless boundary conditions are

$$\begin{aligned} &\Theta(0) = 1 \qquad \Theta(1) = 0 \\ &u_x(0) = 0 \qquad u_x(1) = 0 \\ &u_y(0) = 0 \end{aligned} \tag{4.29}$$

The melting condition at the interface (4.24) reduces to

$$\frac{k_m(T_0 - T_m)W}{\lambda^* \rho_m V_0 \delta_0^2}\left(\frac{\partial \Theta}{\partial \eta}\right)_{\eta=1} = \frac{\delta}{\delta_0} u_y(1) \tag{4.30}$$

Maintaining the dimensionless group to the order 1 it is possible to write the δ_0 value as

$$\delta_0 = \left(\frac{k_m(T_0 - T_m)W}{\lambda^* \rho_m V_0}\right)^{1/2} \tag{4.31}$$

the continuity equation in dimensionless form becomes

$$\frac{\partial u_x}{\partial \xi} - \eta \frac{\dot{\epsilon}}{\delta} \frac{\partial u_x}{\partial \eta} + \frac{v_0}{\delta} \frac{\partial u_y}{\partial \eta} = 0 \tag{4.32}$$

with $\dot{\epsilon}$ [illegible] ξ, and the dimensionless form of the equation of motion is

$$\frac{\partial}{\partial \eta}\left[e^{b\Theta}\left(-\frac{\partial u_x}{\partial \eta}\right)^n\right] = 0 \tag{4.33}$$

with $b = -a(T_0 - T_m)$.

Finally the equation of energy using δ_0 is

$$M^{-1}\left[u_x \frac{\partial \Theta}{\partial \xi} - u_x \frac{\dot{\epsilon}}{\delta} \eta \frac{\partial}{\partial \eta} + u_y \frac{\delta_0}{\delta} \frac{\partial \Theta}{\partial \eta}\right] = \left(\frac{\delta_0}{\delta}\right)^2 \frac{\partial^2 \Theta}{\partial \eta^2} + Br\left(\frac{\delta_0}{\delta}\right)^{n+1} e^{b\Theta}\left(-\frac{\partial u_x}{\partial \eta}\right)^{n+1} \tag{4.34}$$

where M represents the ratio of heat energy needed to melt the polymer as compared to that needed to heat the melt to T_0, b is a dimensionless parameter that is related to the temperature dependence of the viscosity over the temperature range considered and Br is a modified Brinkman number.

In summary, the system has four equations (4.30), (4.32), (4.33), (4.34) and four unknown variables: Θ, δ, ux and uy.
Both shear rate and temperature dependence of viscosity strongly affect the melting rate. Their effect can be estimated by neglecting convection and assuming the viscous dissipation low enough that the viscosity across the film can be determined by a linear temperature profile

$$\Theta = 1 - \eta \tag{4.35}$$

the equation of motion (4.37), reduces to

$$\frac{\partial}{\partial \eta}\left[e^{b[1-\eta]}\left(-\frac{\partial u_x}{\partial \eta} \right)^n \right] = 0 \tag{4.36}$$

obtaining from Eq. 4.36 the velocity profile

$$u_x(\eta) = \frac{e^{b'\eta} - e^{b'}}{1 - e^{b'}} \tag{4.37}$$

where

$$b' = \frac{b}{n} = -\frac{a(T_0 - T_m)}{n} \tag{4.38}$$

The energy equation 4.33 reduces to

$$\frac{\partial^2 \Theta}{\partial \eta^2} + Br\left(\frac{\delta_0}{\delta} \right)^{n-1} e^{b(1-\eta)}\left(-\frac{\partial u_x}{\partial \eta} \right)^{n+1} = 0 \tag{4.39}$$

Substituting (4.37) into (4.39) and integrating the temperature profile yields

$$\Theta = 1 - \eta + Br\left(\frac{\delta_0}{\delta}\right)^{n-1}\left(\frac{b'}{1-e^{-b'}}\right)\left(\frac{b'-1+e^{-b'}}{b'^2}\right) \tag{4.40}$$

by solving the balance Eq. 4.33 for $u_y(1)$ after obtaining from $\left(\partial\Theta/\partial\eta\right)_{\eta=1}$

$$u_y(1) = -\left(\frac{\delta_0}{\delta}\right)\left[1 - \eta + Br\left(\frac{\delta_0}{\delta}\right)^{n-1}\left(\frac{b'}{1-e^{-b'}}\right)\left(\frac{b'-1+e^{-b'}}{b'^2}\right)\right] \tag{4.41}$$

Finally, integrating the equation of continuity 4.32 with $\partial u_x / \partial \xi = 0$ and $\partial u_x / \partial \eta$ from Eq. 4.37 yields

$$u_y(1) = \frac{\dot{c}}{\delta_0}\left(\frac{\quad -1)e^{-b'}}{b'(1-e^{-b'})}\right) \tag{4.42}$$

Combining Eq. 4.41 and Eq. 4.42 results in a differential equation for δ

$$\delta\frac{d\delta}{d\xi} = \frac{-\delta_0^{\,2}\left[1 + Br\left(\frac{\delta_0}{\delta}\right)^{n-1}\left(\frac{b'}{1-e^{-b'}}\right)^{n+1}\left(\frac{b'-1+e^{-b'}}{b'^2}\right)\right]}{\left(\frac{1+(b'-1)e^{b'}}{b'(1-e^{b'})}\right)} \tag{4.43}$$

The rate of melting is given by

$$w_L(x) = \rho_m V_0 \delta \int_0^1 u_x d\eta \tag{4.44}$$

The mean temperature of the film

$$\bar{\Theta} = \frac{\int_0^1 u_x \Theta d\eta}{\int_0^1 u_x d\eta} \tag{4.45}$$

is obtained by substituting Eq. 4.37 and Eq. 4.40 into Eq. 4.45

$$\bar{\Theta} = \frac{b'/2 - 1/b' + (1 + 1/b')e^{-b'}}{b' - 1 + e^{-b'}} \tag{4.46}$$

In the model, the solid bed profile is an important parameter. The product of solid bed profile with the height, the velocity and the solid bed density allows to obtain the local mass flow rate. Furthermore subtracting the solid bed size from the total channel width it is possible to obtain the width of the fluid bed, which increases along the z coordinate.
The transport mechanism, in this region, is caused by the viscous resistance on the surface of the barrel caused by the shear applied to the molten film and the screw threads friction.
The film thickness increases with the increasing height of the channel until a constant value.
It is assumed:

- steady state condition;
- melting occurs only near the barrel surface where there is a drag induced by a removal mechanism of the fluid film;
- the solid bed is homogeneous, non-deformable and continuous;
- constant solid bed velocity;
- constant thermoplastic properties;
- separation interface between the solid bed and the film melted and this interface is at melting point;
- solid bed size depends on the velocity of the interface of fusion between the solid bed and molten film.

Considering a differential element perpendicular to the solid-melt, the velocity solid bed is V_{SZ} and the component in the melt is V_{SY}. The barrel moves at velocity Vb and the cross channel components are V_{BZ} and V_{BX}. The relative velocity between the barrel and the solid bed is

$$V_j = V_b - V_{sz} \tag{4.47}$$

the solid bed width is obtained by a mass balance

$$\rho_s V_{sz}(H-\delta)X\,|_z - \rho_s V_{sz}(H-\delta)X\,|_{z+\Delta z} = w_L(z)\Delta z \tag{4.48}$$

which for $\Delta z \to 0$ neglecting the change in film thickness in the down channel direction

$$-\frac{d(HX)}{dz} = \frac{w_L(z)}{\rho_s V_{sz}} \tag{4.49}$$

where X is the solid bed thickness and H is the height of the channel. The rate of melting per unit width is

$$w_L(z) = \frac{\rho_m V_{bx}\delta(x)}{2} \tag{4.50}$$

and the solid bed velocity at the beginning of the melting zone is

$$V_{sz} = \frac{G}{\rho_s HW} \tag{4.51}$$

where G is the mass flow rate, ρ_s is the density of the solid, H and W are respectively the height and width of the channel at the beginning of the melting zone. Assuming that the channel height decreases linearly

$$H = H_0 - Az \tag{4.52}$$

from Eq. 4.49 the differential equation becomes

$$\frac{dX}{dz} = \left(AX - \frac{\rho_m V_{bx}\delta(x)}{2\rho_s V_{sz}} \right) / \left(H_0 - A(z - z_0) \right) \tag{4.53}$$

where z_0 is the final length of the constant cross section zone and with the slope of the melting zone equal to

$$A = \frac{H_0 - H_f}{nD / sen\phi} \tag{4.54}$$

where H_0 and H_f are the initial and final heights of the melting zone, n is the screw turns in the melting zone, D is the diameter barrel and ϕ is the thread angle.
Equations 4.42 and 4.52 form the basis for the resolution of the model to obtain the solid bed thickness as a function of the z coordinate following an iterative procedure.

4.5.1 Pressure profile in melting and metering zone

Considering an infinitesimal element in the interface between liquid and solid, the volume flow Q_{VI} is determined by the following balance of masses

$$\rho_l Q_{Vl}\,|_{z+dz} - \rho_l Q_{Vl}\,|_z = w_L(z)dz \tag{4.55}$$

from which

$$dQ_{Vl} = \frac{w_L(z)}{\rho_l} dz \tag{4.56}$$

where $W_L(z)$ is the flow rate of molten material that enters the system through the phase change.
The relationship between flow rate and pressure gradient becomes evident and explains the volume flow out of the extruder

$$Q_{Vl} = Q_{Vdrag} + Q_{Vpress} \tag{4.57}$$

where

$$Q_{Vdrag} = \frac{V_{bz}((W - X(z))H(z)}{2} \tag{4.58}$$

and

$$Q_{Vpress} = \frac{((W - X(z))H^3(z)}{12\mu}\left(-\frac{dP}{dz}\right) \tag{4.59}$$

from Eq. 4.57, 4.58 and 4.59 the pressure gradient is

$$\frac{dP}{dz} = \frac{6\mu}{H^2(z)}\left(V_{bz} - \frac{2Q_{Vl}}{(W - X(z))H(z)}\right) \tag{4.60}$$

where both the channel height H and the fluid bed thickness depend on the coordinate z.
Equations 4.56 and 4.60 allow to obtain the flow rate and the pressure gradient as a function of the z coordinate using the Euler method.

4.6 Metering zone

In the metering zone the polymer is completely molten and the screw section is constant. The function of this zone is to homogenize the polymer melt.

4.6.1 Drag flow

Considering the motion of a fluid between two parallel plates with the top plate that moves at a speed V_d (Fig. 4.6), it is possible to study an infinitesimal element at a distance dy from the fixed plate.

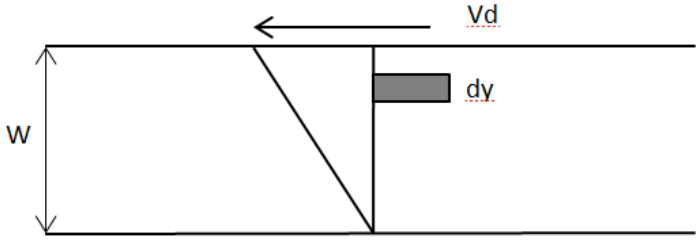

Fig. 4.6 – Drag flow between parallel plates

The flow rate of the infinitesimal element is

$$dQ = WVdy \tag{4.61}$$

where W is the channel width and V the velocity gradient. Assuming a linear gradient of velocity

$$V = \frac{V_d y}{H} \tag{4.62}$$

substituting Eq. 4.61 into Eq. 4.62 and integrating, the flow rate is expressed as

$$Q_d = \frac{1}{2} W H V_d \tag{4.63}$$

applying these equations to the extruder(Fig. 4.7), H is the depth of the channel, W is the distance between the threads and N are the round per minute of the screw.

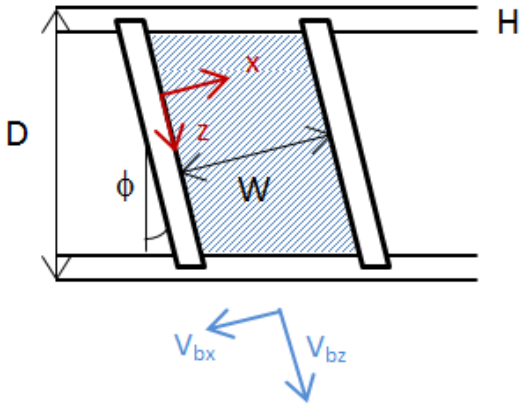

Fig. 4.7 - Drag flow inside the extruder

The motion is expressed as

$$V_d = \pi D N \cos\phi \tag{4.64}$$

and

$$W = (\pi D \tan\phi - e)\cos\phi \tag{4.65}$$

substituting Eq. 4.65 into Eq. 4.63 the flow rate is expressed as

$$Q_d = \frac{1}{2}\pi^2 D^2 N sen\phi \cos\phi H \tag{4.66}$$

4.6.2 Pressure flow

Whereas an infinitesimal element of fluid in a channel bound by parallel plates, the forces acting on the element are (Fig. 4.8)

$$F_1 = (P + \frac{\partial P}{\partial z} dz)2y \tag{4.67}$$

$$F_2 = P2y \tag{4.68}$$

$$F_3 = \tau dz \tag{4.69}$$

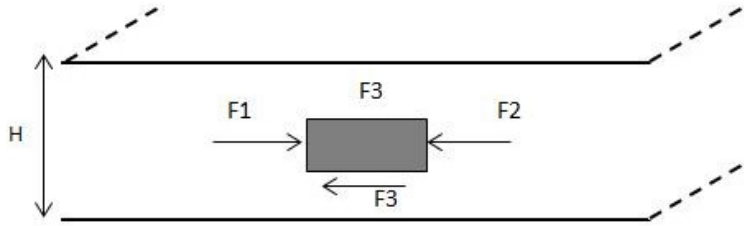

Fig. 4.8 - Forces acting on a fluid element subject to pressure gradient

From the forces equilibrium, the shear stress τ is:

$$\tau = y\frac{\partial P}{\partial z} \tag{4.70}$$

if a Newtonian behavior is assumed, the shear stress is

$$\eta\frac{\partial V}{\partial y} = y\frac{\partial P}{\partial z} \tag{4.71}$$

Integrating Eq. 4.71 the velocity profile is

$$V = \frac{1}{\eta}\frac{dP}{dz}\left(\frac{y^2}{2} - \frac{H^2}{8}\right) \tag{4.72}$$

substituting (4.72) into (4.71), integrating in y and using the geometry of the extruder, the flow rate is related to the pressure gradient by

$$Q_P = \frac{\pi D H^3 \sin^2 \phi}{12\eta}\left(\frac{dP}{dl}\right) \tag{4.73}$$

From the difference between drag and pressure gradient it is possible to obtain the net capacity of the extruder as

$$Q = \frac{1}{2}\pi^2 D^2 N H sen\theta \cos\theta - \left(\frac{\pi D^3 \, sen^2\theta \Delta P}{12\eta l}\right) \tag{4.74}$$

where, η is the viscosity and l is the axial length of the extruder.

CHAPTER 5

CHARACTERIZATION OF WPC

5.1 Introduction

In this chapter the influence of filler content and temperature on the rheological, mechanical and thermal properties of wood flour polypropylene composites (WPCs) will be investigate.
In order to gain a better control on the many processing variables it is necessary to characterize the material from the rheological point of view. The number of papers dedicated to the rheological characterization of natural fiber filled composites is increasing, and this testifies the interest towards these materials. If polyethylene (high density polyethylene or HDPE) is used as matrix, thermal stability is a less critical issue due to the melting temperature (about 135°C) that is much lower than natural fiber degradation. Many authors, in fact, have studied the rheological properties of HDPE - based WPC, even with a high percentage of filler. Li and Wolcott (2005) and Carrino et al. (2011) have studied the shear flow of HDPE - based WPC using capillary rheometry with a particular attention to wall slip phenomena and surface tearing. Hristov et al. [Hristov 2006, Huang 2009] have also used capillary rheometry measurements with extrudate distortions evaluations, in conjunction with rotational rheometry performed in oscillatory mode. Other authors [Xiong 2009, Huang 2009, Godard 2009] have characterized the viscosity of HDPE - based WPC with the rotational rheometer varying the filler concentration. In particular, Godard et al. (2009) obtained a mastercurve valid for a wide range of filler concentrations (0%wt. - 60%wt.) and fitted it using a Carreau – Yasuda model. The curve of the shift factor as a function of concentration was fitted with a Krieger – Dougherty equation, which is one of the most widely used models for concentrated suspensions.
Polypropylene (PP) has a melting temperature that is higher than polyethylene by 30°C at least. The processability range is thus only about 20°C wide (180°C - 200°C), and this makes processing particularly difficult at high fiber volume fractions. Nevertheless, the mechanical properties of PP - based WPC are generally higher than HDPE - based ones, as can be seen by comparing the main results of papers dealing with HDPE - based WPC [Raj 1991, Lu 2005, Xiong 2009, Hugot 2008, Hugot 2009, Soury 2012,] with those dealing with PP - based WPC [Schirp

2010, Leu 2012, Tasdemir 2009, Polec 2010]. In particular, Englund et al. (2011) make a comparison between the mechanical properties of various polymer matrix WPCs and find that among PP, PVC and HDPE, PP - based ones offer a good compromise between adequate strength and stiffness and good ductility.

The ease of degradation of PP – based WPC (from now on PP-WPC) may prevent from getting a good quality product, but can also invalidate the results of material characterization, since the material may be kept at high temperatures in the presence of oxygen for long times. Such a drawback, in principle, can be solved by reducing the testing temperatures and performing tests in controlled atmosphere or in vacuum. Capillary viscometry can be used in this way, but it is well known that measurements on wood filled materials are affected by extensive wall slip [Carrino 2011, Le Mogne 2013, Li 2004, Li 2006, Wolcott 2006] and other flow instabilities [Hristov 2006, Hristov 2007] that may render the experimental procedures more difficult. Moreover, highly filled materials display too high a viscosity for capillary flow. Another possibility is to characterize the material in oscillatory mode, thus obtaining the flow curve using the Cox – Merz rule but one must ensure that the material be loaded within the linear viscoelasticity range (LVR). This is difficult, because the testing temperature must be anyway sufficiently low and it is known that at high filler contents the LVR size is reduced [Hristov 2007]. It is thus clear that characterizing this material at the usual processing temperatures may be very difficult.

Perhaps for this reason rheological properties of PP-WPC have been measured only in a few papers, usually with moderate filler content. Maiti et al. [Maiti 2004] have studied the shear flow of i-PP - wood fiber composites at 220°C using capillary rheometry, with a fiber concentration between 0 – 32.2 vol %. Marcovich et al. (2004) have investigated the behavior of PP-WPC (0 – 50%wt. wood content) at 200°C with a parallel plate rheometer in oscillatory mode. The dynamic moduli were scaled with respect to the filler content with horizontal shift factors obtaining a single master curve, that has been modeled using a generalized Maxwell model. Azizi and Ghasemi (2009) have investigated the properties of PP-WPC at 190°C using a parallel plate rheometer relating the complex viscosity to wood and coupling agent content (0 – 60%wt. and 0 – 4% respectively). Soury et al. (2012) have studied PP-WPC at three different wood contents (50 – 60 – 70%wt.) and at two temperatures (175 - 195°C) using a rotational rheometer generating a large body of interesting experimental

data, but fail to show their results in a clear graphical format**.** Ares et al. (2010) have investigated the effect of recycled PP on the rheological properties of PP-WPC at 200°C with a 0 – 30%wt. wood filler content. Other authors, like Gonzàles - Sànchez et al. (2011) and Le Moigne et al. (2013) have studied PP based composites with different type of filler other than wood i.e. kraft pulp and molten flax, respectively.
In this chapter, the characterization of PP-WPC in oscillatory mode in nitrogen atmosphere and at low temperature (170°C) will be described, in order to gain reliability of the measured quantities. The flow curves at higher temperatures, that are more useful for processing, will be estimated by mathematical modeling, using a master-curve obtained from measurements on WPCs at various fiber volume fractions (0%, 30%, 50% and 70% wt.) and on neat PP at various temperatures (170°C, 180°C, 190°C and 200°C).
The rheological characterization will be completed with capillary viscometer measurements. Static and dynamic mechanical properties will also be measured to verify the quality of the final product, while thermal measurements, using differential scanning calorimetry, are convenient for assessing degradation during characterization and for obtaining information on the material.

5.2 Material

Commercial wood-flour polypropylene composites (WPC) have been purchased from PlasticWOOD S.r.l., Mazzantica di Oppeano (VR), Italy. The materials used for the study contain 30, 50, and 70% natural fibers in mass from white fir. The 30% wt. (commercial name PP 30 S) and the 70% wt. (commercial name PP CO 68/BZ) have been acquired from the producer as compounds, while the 50% wt. has been obtained by processing the two commercial compounds in equal weight percentage, as described below. The producer has also supplied the neat polypropylene (PP) used as the matrix of the composites. The bulk density, as declared by the producer, is 909 kg/m^3 for neat PP, 1067 kg/m^3 for the 30% wt. WPC and 1183 kg/m^3 for the 70% wt. WPC. The bulk density for the 50% wt. (1125 kg/m^3) is the average of the two commercial compounds. In Tab. 5.1 length, diameter and L/D ratio of the fibers are listed.

5.3 Samples preparation

Neat PP, 30% wt. and 70% wt. WPC samples are produced either from pellets directly or from extruded profiles, while 50% wt. WPC samples are

obtained only from extruded profiles by mixing 30% wt. and 70% wt. in equal percentages. The extruded profiles are produced using a single screw extruder (P.R.T. SERVICE & INNOVATION S.r.l., Sant'Agostino (FE), Italy) with a screw diameter of 50 mm and L/D ratio of 40. The extruder is equipped with a breaker to improve compaction and with a venting zone to help degasification of water vapor. The die is a 50 x 3 mm slit (Fig. 5.1). During extrusion, a uniform temperature distribution of 190°C has been maintained along the barrel, while the die temperature has been set at 180°C and the screw speed at 60 RPM. All samples have been dried at 90°C in a vacuum oven for 12 hours to reduce the moisture content prior to testing.

Tab.5.1 - Mean and standard deviation (in parentheses) of length, diameter and L/D ratio of the fibers.

Length (μm)	Diameter (μm)	L/D
166.1	16.0	10.2
(65.1)	(2.5)	(3.1)

5.4 Degradation of natural fibers

Wood fibers have a low thermal resistance, therefore it is necessary to prevent degradation during measurement. The phenomenon of thermal degradation depends not only on temperature but also on residence time, therefore it is interesting to evaluate the behavior of WPC at a fixed high temperature for a long time. Only the 70% wood flour WPC has been tested because it is the one that would degrade most easily.

A differential scanning calorimeter test using a DSC 823 (Mettler Toledo) under a nitrogen atmosphere has been performed in isothermal conditions to investigate, as a function of time, the degradation of samples obtained from extruded profiles. The temperature has been increased from 25 up to 180°C at a heating rate of 20°C/min, kept at 180°C for 60 minutes and finally decreased down to room temperature at 20°C/min.

A time sweep measurement under a nitrogen atmosphere has been performed using a strain controlled rheometer (ARES, TA Instruments) to evaluate the thermal stability of the samples during the rheological measurements. The temperature has been set at 180°C, the frequency at 3 rad/s and the shear strain at 0.2%. Maintaining these parameters constant, the dynamic shear moduli and the torque have been monitored for 35 minutes.

5.4.1 Thermal characterization

All calorimetry measurements (DSC 823 Mettler Toledo) have been carried out under nitrogen atmosphere. The DSC scans have been performed on 6 - 10 mg samples contained in aluminum sealed pans.
In the ramp test neat PP and WPCs have been analyzed to measure their thermal properties. Compound pellets have been used for the tests. The sample temperature has been increased from 25°C up to 220°C at a heating rate of 10°C/min and held in the molten state for 5 min to erase the thermal history of the specimens and to eliminate residual moisture and voids. After being cooled at 10°C/min down to room temperature, the samples have been reheated to 220°C at 10°C/min. The crystallization temperature, melting temperature, specific heat capacity, melting and crystallization enthalpy have been obtained from the cooling and the second heating scan.

5.5 Rheological characterization

5.5.1 Parallel plate rheometer

The rheological characterization has been performed with a smooth surfaces parallel plate rheometer (ARES, TA Instruments) in dynamic oscillation and strain controlled mode. The samples in the form of 25 mm diameter disks have been cut from extruded profiles using a punch cutter.
The disk specimens have been placed between the parallel plates with a 2.5 mm gap to carry out the rheological measurements. Three types of rheological experiments have been done on WPC specimens: time, strain and frequency sweep, all of them under nitrogen atmosphere at 170°C. For neat PP the strain and frequency sweeps have been performed also at different temperatures, i.e. 170, 180, 190, 200°C.
In the strain sweep test the response of the material to increasing strain amplitudes has been measured at constant frequency and temperature. This experiment allows to determine the linear viscoelastic region (LVR) of the materials, which is important for performing the frequency sweep test correctly. For each material three different frequencies (1, 3, 10 rad/s) have been evaluated and the shear strain has been in the 0.02% – 5% range.
In the frequency sweep test it is possible to observe the response of the material as a function of frequency at constant strain and temperature. The strain value is chosen within the LVR. Different strain values have been chosen for the experiments, i.e. 0.01%, for the WPC 50% wt. and

WPC 70% wt., 0.02%, for the WPC 30% wt. and 5% for neat PP. The frequency has been varied between 0.1 and 100 rad/s. The storage modulus *G′* and the loss modulus *G″* can be measured as a function of frequency. These values are used to calculate the damping factor:

$$\tan\delta = \frac{G''}{G'} \tag{5.1}$$

and the complex viscosity:

$$\eta^* = \sqrt{\left(\frac{G'}{\omega}\right)^2 + \left(\frac{G''}{\omega}\right)^2} \tag{5.2}$$

where ω is frequency.

5.5.2 Capillary rheometry

A capillary rheometer (RHEOTESTER 1500 - GÖTTFERT) has been used to study the shear flow behavior directly. The barrel of the rheometer has a 12 mm diameter reservoir and an effective working length of 200 mm. A mercury-filled pressure transducer of 0.2% precision with a 1000 bar full-scale has been used to measure the pressure drop. The transducer is located above the capillary die entrance. The tests have been set up using different values of the piston velocity in the range 0.01 - 5 mm/s.
Only two materials have been tested, i.e. neat PP and the WPC 30% wt. A smooth tungsten carbide die with 1 mm diameter has been used for neat PP, while for the 30% wt. WPC a rough tungsten carbide die with 2 mm diameter has been used. All measurements have been made at 170°C. Once the pressure drop ΔP is measured, knowing the geometry and the speed of the piston it is possible to calculate the wall shear stress τ_w and the apparent shear rate $\dot{\gamma}_a$as follows:

$$\tau_w = \frac{\Delta P\, R}{2\, L} \tag{5.3}$$

$$\dot{\gamma}_a = \frac{4\, Q_m}{\pi\, R^3} \tag{5.4}$$

where Q_m is the volumetric flow rate, R and L are the radius and length of the die, respectively. Three different capillary lengths (10, 20, 30 mm) have been used in each capillary measurement to correct for entrance effects using the Bagley procedure.

5.6 Scanning Electron Microscopy (SEM)

WPC samples with 30% wt. and 70% wt. wood fiber content have been fractured from an extruded profile. The x - direction corresponds to the extrusion direction while the zy - plane is the cross section (Fig. 5.1). Two fracture surfaces have been observed: one obtained from the xy - plane and the other from the zy – plane.

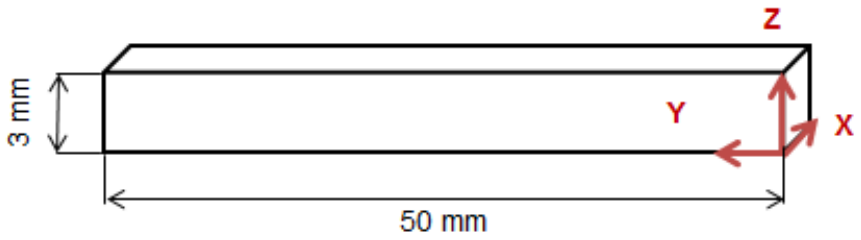

Fig. 5.1 - Extruded profile geometry

The ZEISS EVO MA 15 scanning electron microscope (SEM) has been employed to characterize the morphology of the composites.

5.7 Mechanical characterization

5.7.1 Static mechanical analysis

The mechanical measurements have been performed in tension on a universal testing machine (INSTRON 4467) at room temperature. All samples have been obtained from extruded profiles and have been loaded in the extrusion direction.
The tests have been performed according to the EN ISO 527-1 standard at 2 mm/min crosshead speed and with a 500N load cell. Five dog bone samples have been tested for each material and the average values of the relevant mechanical parameters (Young's modulus and yield strength) and their standard deviations have been reported.

5.7.2 Dynamic mechanical analysis (DMA)

A Dynamic Mechanical Analysis (DMA), is a technique where a small deformation is applied to a sample in a cyclic manner. This allows to study the materials response to stress, temperature and frequency. The term is also used to refer to the analyzer that performs the test. DMA works by applying a sinusoidal deformation to a sample of known geometry. The

sample can be subjected by a controlled stress or a controlled strain. For a known stress, the sample will then deform to a certain amount. In DMA this is done sinusoidally. A motor is used to generate the sinusoidal wave and this is transmitted to the sample via a jaws system that hold the sample.
DMA measures stiffness and damping, these are reported as modulus and tan delta. Since we are applying a sinusoidal force, we can express the modulus as an in-phase component, the storage modulus, and an out of phase component, the loss modulus.
The storage modulus, E', is the measure of the elastic behavior of the sample. The ratio of the loss modulus to the storage modulus is the tan delta and is often called damping factor. It is a measure of the energy dissipation of a material.
While Young's modulus, which is calculated from the slope of the initial part of a stress-strain curve, is similar conceptually to the storage modulus, they are not the same.
Damping is the dissipation of energy in a material under cyclic load. It is a measure of how well a material can get rid of energy and is reported as the tangent of the phase angle. It varies with the state of the material, its temperature, and with the frequency.
Dynamic mechanical analysis has been conducted in simple tension mode using the RSAIII (TA instrument) to carry out the tests. All specimens have been obtained from extruded profiles. Specimens dimensions are 2 x 2.5 x 43 mm and have been determined on the basis of the recommended size range suggested by the instrument manufacturer. Each sample has been clamped at its top and bottom and placed in tension. Dynamic temperature scans have been made from 25°C up to 200°C, with a heating rate of 2°C/min. The frequency used has been 1 Hz. The E' and E'' moduli have been measured as a function of temperature.

5.8 Results

5.8.1 Wood fibers degradation

Tests for evaluating wood fibers degradation have been performed first. In Fig. 5.2 the heat flow is reported as a function of time for the 70% wt. WPC. The thermogram shows an endothermic peak due to melting, after which the heat flow remains constant until the exothermal peak of the cooling phase appears. The constant heat flow during the 60 minutes in which the material is kept at 180°C shows that the material does not degrade in the conditions at which the test was performed.

In Fig. 5.3 the torque and the loss and storage moduli are reported as function of time. It is evident that a stable plateau is reached during the test, thus the 70% wt. WPC does not degrade for the whole duration of the test.

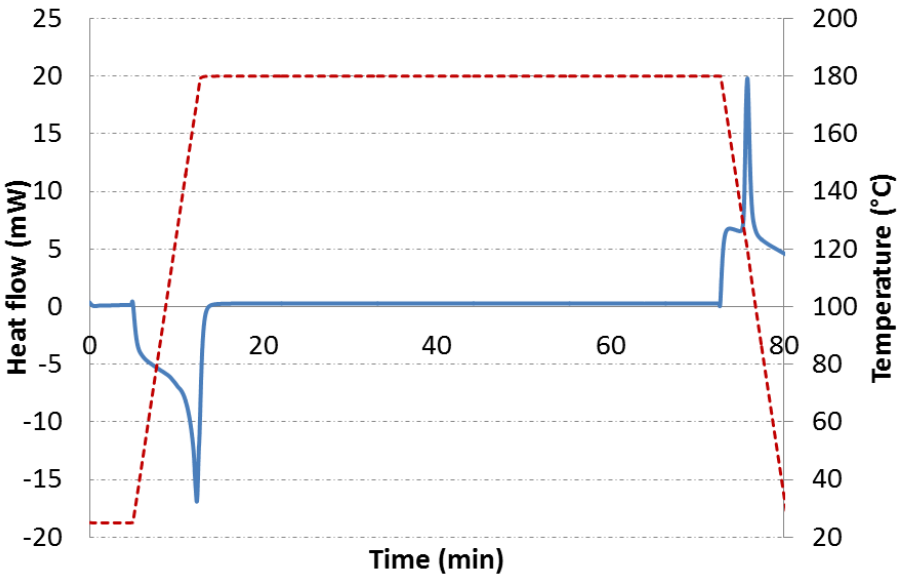

Fig. 5.2 - Heat flow (continuous blue line) and temperature (red dotted line) as a function of time for the 70%wt. WPC

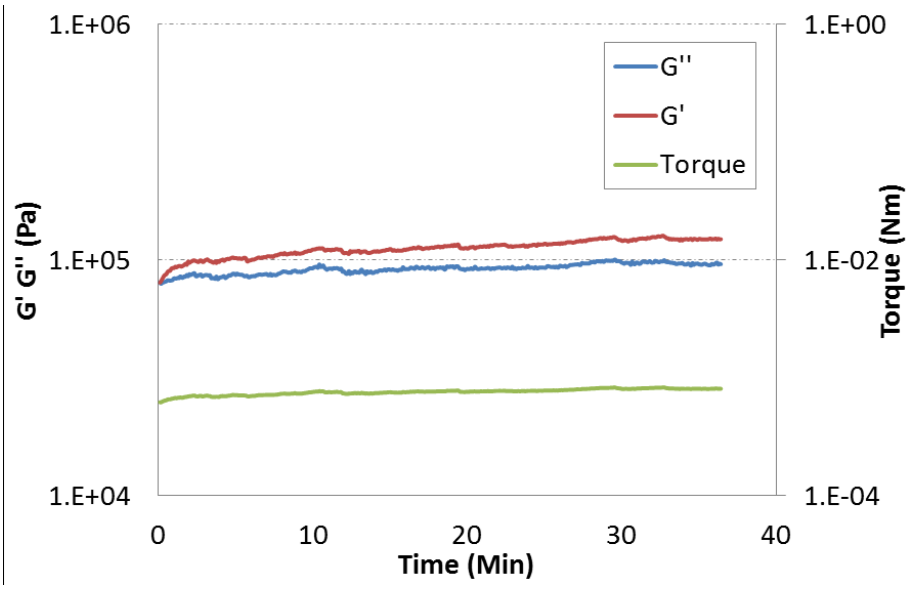

Fig 5.3 - G', G'' and torque vs. time for the 70% wt. WPC at constant strain and frequency

5.8.2 Thermal characterization

The neat PP DSC curves are reported in Fig. 5.4. The melting and crystallization peaks are clearly visible; a second order transition is also present and located at around 110°C in heating (around 80°C in cooling). In Table 5.2 the relevant thermal parameters are listed: solid and liquid specific heat capacity (cp_s and cp_l respectively), crystallization and melting enthalpy (ΔH_c and ΔH_m respectively), crystallization and melting temperature (T_c and T_m respectively), for neat PP and all WPCs.
Cristallinity α_{PP} is obtained as the ratio of the melting enthalpy of the specimen ΔH_m , calculated using only the weight of the PP, and the latent heat of fusion of a pure polypropylene crystal, assumed to be ΔH_0 = 207J/g [Vandewal 1998]:

$$\alpha = \frac{\Delta H_m}{\Delta H_0} \tag{5.5}$$

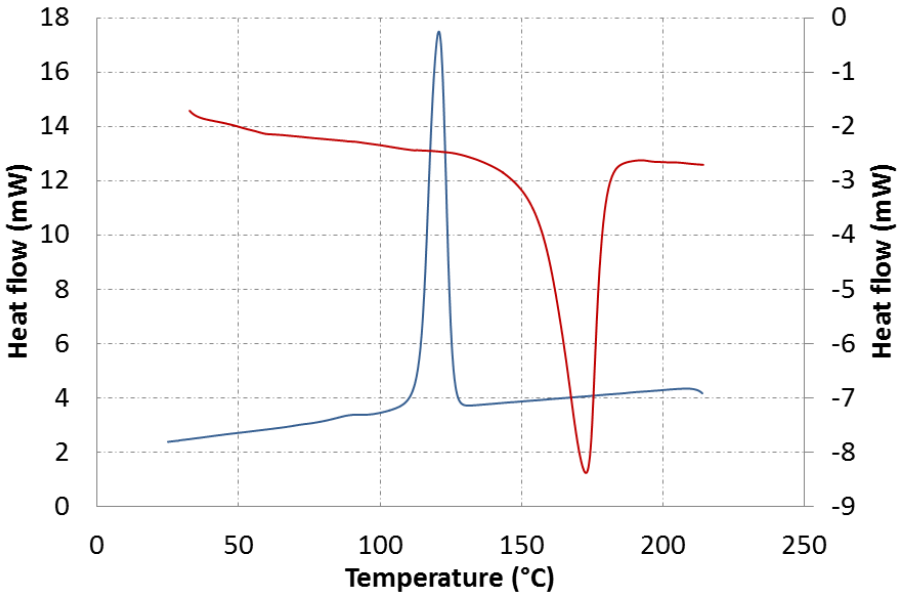

Fig. 5.4 - DSC thermograms of neat PP in the "as received" granule form. Cooling (blue line) and second heating (red line).

Tab. 5.2 - Thermal properties of PP and WPCs measured with the DSC.

Thermal properties	PP	30% wt.	50% wt.	70% wt.
cp_s (J/kg/°C)	1961	1653	1443	1230
cp_l (J/kg/°C)	1924	1727	1516	1354
ΔH_c (kJ/kg)	78	45	35	29
ΔH_m (kJ/kg)	76	36	29	21
α_{PP} (%)	36.7	25.0	27.8	31.0
T_c (°C)	122.5±0.2	124.8±0.2	125.6±0.2	126.1±0.2
T_m (°C)	165.1±0.2	165.8±0.2	165.7±0.2	165.6±0.2
T_g (°C)	- 20.24±0.2	//	//	//

5.8.3 Mechanical characterization

The tensile strength σ_y, stiffness E (Young's modulus) and density ρ for each compound are reported in Tab.5.3. In Fig. 5.5 a representative stress strain curve in tension is shown. All WPCs show brittle behavior.
The storage modulus (E'), loss modulus (E'') and damping factor (tan δ) of WPCs have been measured as a function of temperature (25°C up to 200°C). The moduli precision is ±1%. Fig. 5.6 shows the plot of E' as a function of temperature for each of the WPCs and neat PP. The storage modulus decreases with temperature. The moduli of the WPCs show no important variations with the addition of the fibers, although the 70%wt. has a more stable behavior after melting. The neat PP storage modulus is lower than the WPCs moduli.
In Fig. 5.7 tan (δ) is plotted as a function of temperature. The curves of all materials increase with temperature. A relaxation peak is observed around 70 - 80°C. The increase in the fibers percentage shifts this relaxation peak to higher temperatures.

Tab 5.3. - Mean and standard deviation (in parentheses) of static mechanical properties and density of WPC with different percentages of filler

	Tensile properties		Density[a]
Material	σ_y (MPa)	E (GPa)	ρ (kg/m^3)
70% wt.	16.8 (0.8)	5.6 (0.5)	1183
50% wt.	18.3 (0.9)	4.1 (0.5)	1125
30% wt.	16.6 (0.5)	3.6 (0.7)	1067
0% wt.	19.9 (0.8)	0.9 (0.02)	909

[a] Data supplied by the producer

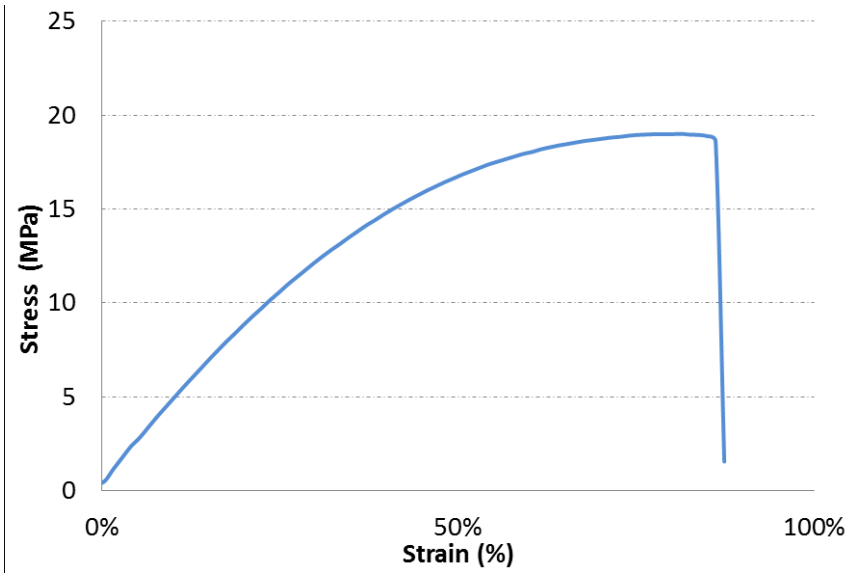

Fig. 5.5 - Typical stress-strain curve for the 50% wt. WPC during tension tests.

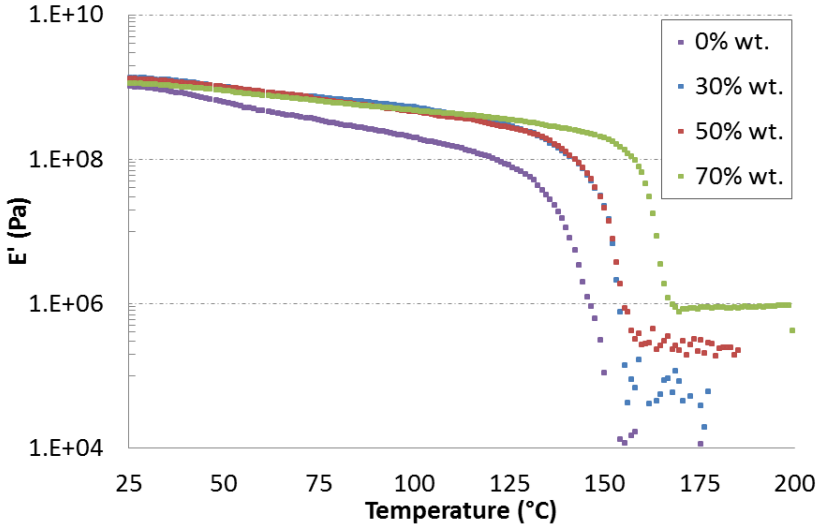

Fig. 5.6 - Storage modulus (E') as a function of temperature for different percentage of fibers WPC and neat PP.

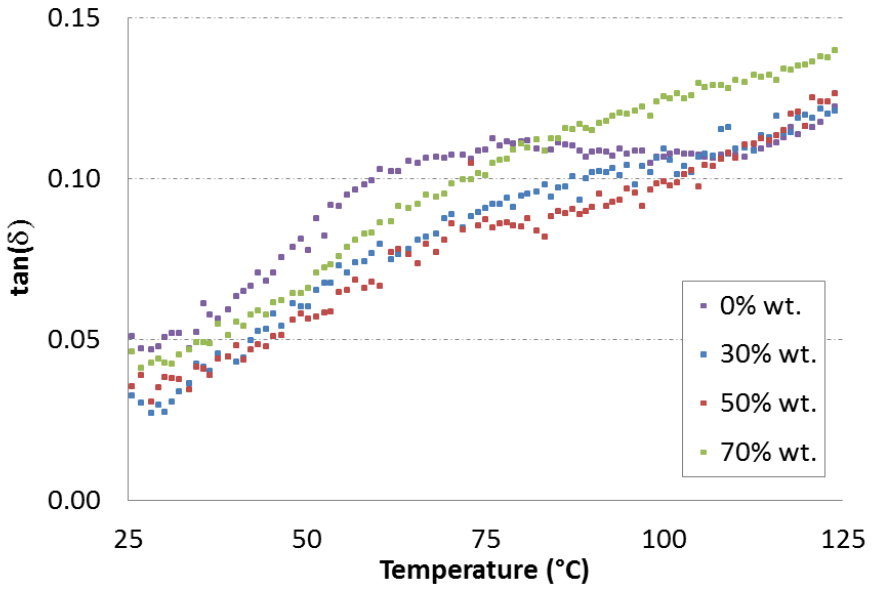

Fig. 5.7 - Mechanical loss factor (tan (δ)) vs temperature (25 – 125 °C) for different WPCs and neat PP.

5.8.4 Scanning Electron Microscopy (SEM)

Fig. 5.8 shows the SEM micrographs of fractured surfaces of (a) 30% wt. and (b) 70% wt. WPC. The x - direction corresponds to the extrusion direction, while the zy - plane is the cross section. The SEM images show a good interfacial bond and compaction between fibers and the PP matrix. There are no voids or pull-out traces within the structure. The 30% wt. WPC shows a relatively smoother surface with respect to the 70% wt. WPC.

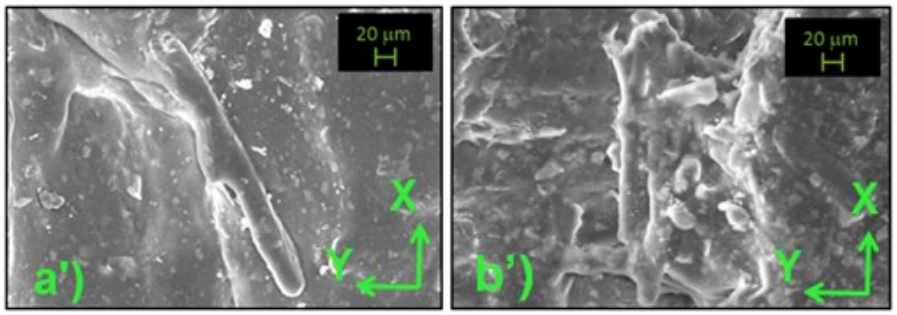

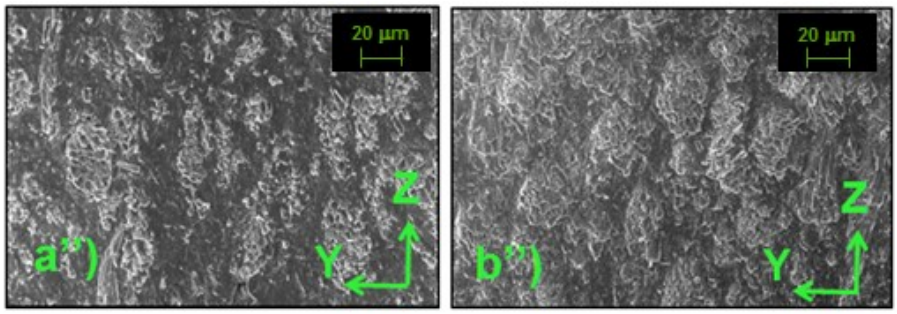

Fig. 5.8 - SEM micrograph of a') 30% wt.in the extrusion direction, a'') 30% wt.in the cross section direction, b') 70% wt. in the extrusion direction and b'') 70% wt. in the cross section direction.

5.8.5 Rotational rheometry

The measurements of the WPC samples have been performed in the linear viscoelasticity region at 170°C. Fig. 5.9 provides the storage and loss moduli as a function of frequency. Both moduli increase with the percentage of fibers and with frequency. At low frequencies neat PP and all WPCs show a liquid viscoelastic behavior ($G'' > G'$), at higher frequencies that of a viscoelastic solid ($G'' < G'$). The crossover between G' and G'' shifts at lower frequencies as the wood fiber percentage increases. Unlike neat PP, the WPCs show storage and loss moduli that are always of the same order of magnitude.
The effect of natural fibers on complex viscosity at 170°C is presented in Fig. 5.10. Complex viscosity increases with the percentage of fibers. All materials show a shear-thinning behavior, but neat PP has a Newtonian plateau at low shear rates. Increasing the temperature the viscosity of neat PP (Fig. 5.11) decreases keeping the same qualitative behavior.

5.8.6 Capillary viscometry

Shear viscosity vs. shear rate at 170°C for neat PP and 30% wt. WPC is presented in Fig. 5.12. The range of apparent shear rate examined is 12 – 3456 s^{-1} for neat PP and 1 - 432 s^{-1} for the 30% wt. WPC. The shear viscosity decreases with shear rate, confirming the shear-thinning behavior. The $\tau(\dot{\gamma}_a)$ data has been treated following the Rabinowitch procedure to obtain the shear viscosity data corrected for shear thinning effects. The shear viscosity range is 10^2 - 10^4 Pa s for neat PP and 10^1 -

10^3 Pa s for the 30% wt. WPC. At low strain rates it is possible to appreciate the beginning of the Newtonian plateau in the neat PP specimen.

The shear viscosity from the capillary rheometer and the complex viscosity from the parallel plate rheometer of neat PP and the 30% wt. WPC are shown together in Figs. 5.13 and 5.14. For neat PP the two viscosities match perfectly in the region were data from both rheometers are available. The 30% wt., shows a shear viscosity from capillary measurements that is consistently lower.

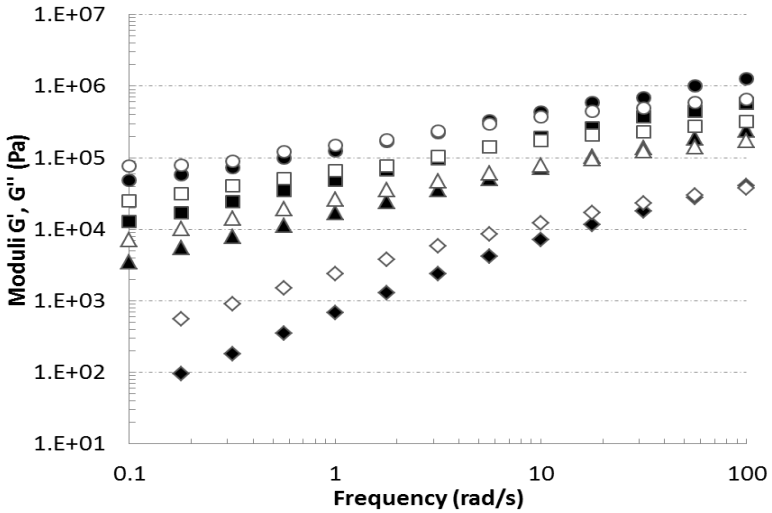

Fig. 5.9 - *G′* (black) and *G″* (white) versus frequency of neat PP (diamond), 30% wt. (triangle), 50% wt. (square) and 70% wt. (circle).

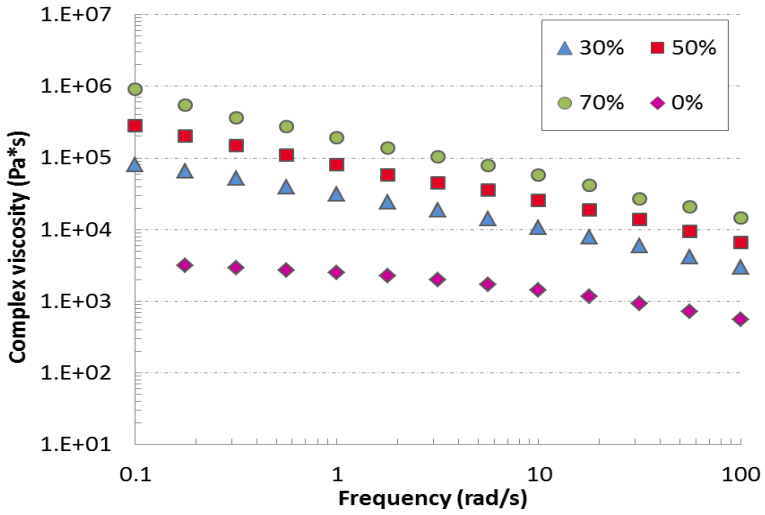

Fig. 5.10 - Complex viscosity as a function of frequency for different percentages of fibers.

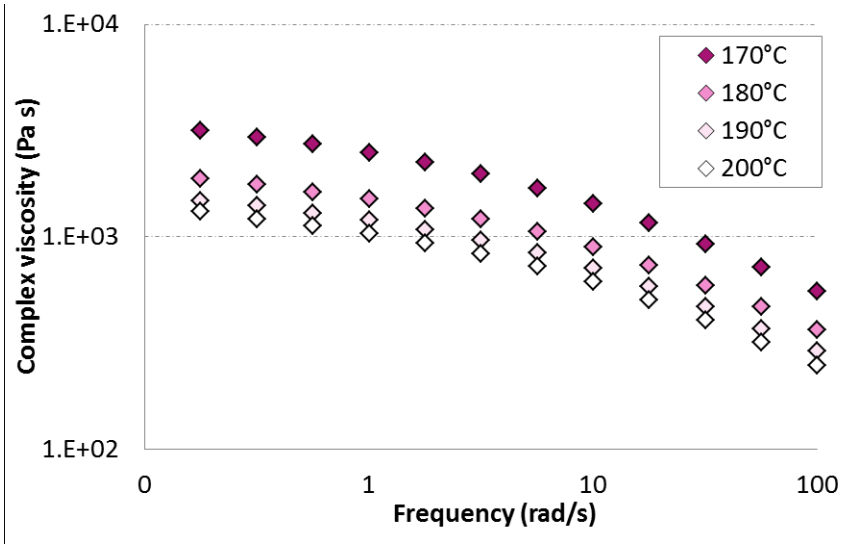

Fig. 5.11 - Complex viscosity of neat PP as a function of frequency at various temperatures.

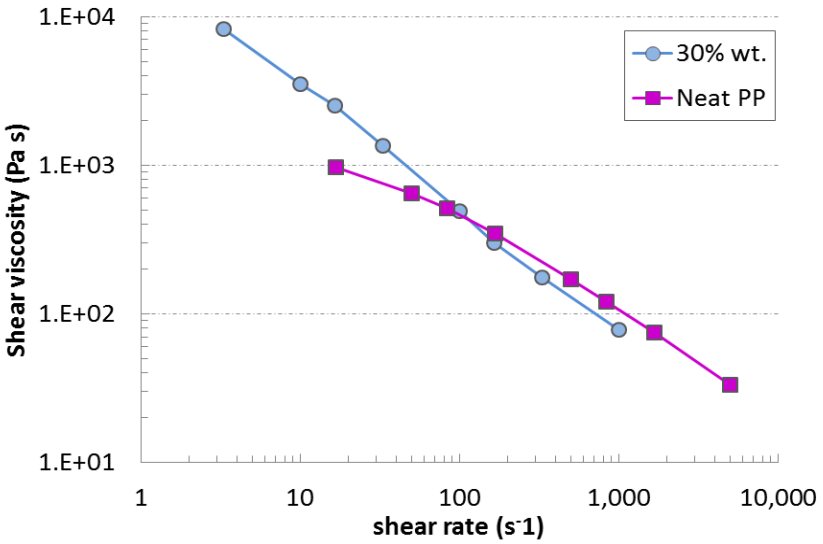

Fig. 5.12 - Shear viscosity as a function of shear rate at 170°C for neat PP and 30% wt. WPC.

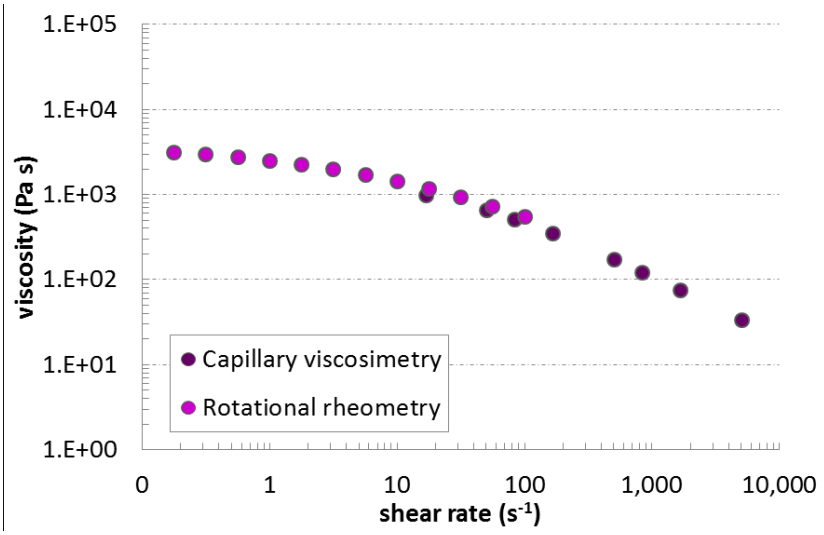

Fig. 5.13 - Complex viscosity rotational rheometry and shear viscosity from capillary measurements for neat PP

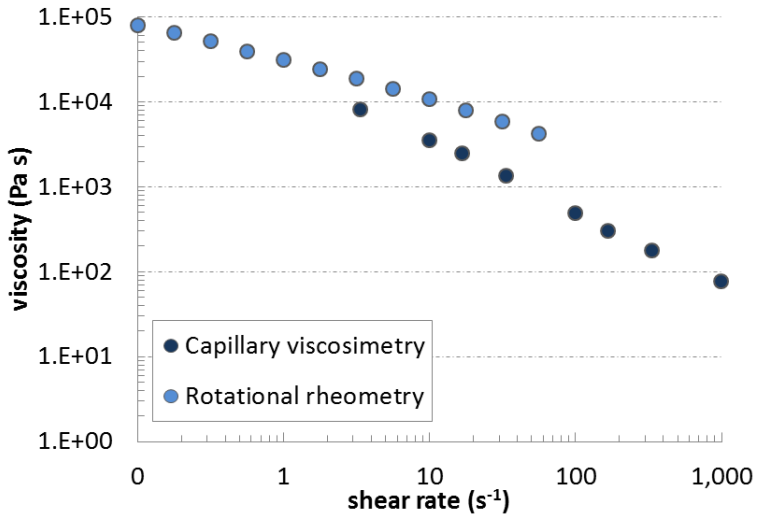

Fig. 5.14 - Complex viscosity from rotational rheometry and shear viscosity from capillary measurements for 30% wt. WPC

5.9 Discussion

An important starting point to study the thermal, mechanical and rheological properties of WPC is to exclude wood degradation during testing. Degradation is a phenomenon that depends on temperature, residence time and presence of oxygen. For this reason a nitrogen atmosphere has been always used, but this may not be sufficient to solve the problem completely: many samples have been prepared using extruded profiles and it is not possible to exclude the presence of oxygen within the samples, for example caught within voids or in areas that were not fully compacted during extrusion.

Neglecting lignin degradation, thermal degradation of natural fibers occurs as a two-stage process at two different temperatures: hemicellulose degradation starts at 195°C while cellulose at 255°C, as reported by Bouafif et al. (2009). The temperature of hemicellulose degradation onset is commonly assumed as the upper limit for WPC processing and has also been chosen as the maximum temperature for testing.

The results presented in Figs. 5.2 and 5.3 confirm the reliability of the tests used to characterize the material. In Fig. 5.2 the constancy of the heat flow is an indication that natural fibers do not degrade at the testing temperature and for the whole duration of the test: exothermal peaks

would be present if degradation occurred. Thermal stability is also clear from Fig. 5.3 where loss and storage moduli and torque as a function of time for the 70% wt. WPC are reported. The values are basically constant during the period of testing. In particular, the time (35 minutes) and temperature (180°C) of the test were greater than those of any subsequent test on WPC samples.

In order to define the test temperature, it is necessary not only to know the upper limit temperature, where the measurements are unaffected by degradation, but also the lower limit, i.e. the melting temperature of the compounds. The DSC tests are used to find the melting temperature, which is the same for all materials (165°C). This value is in agreement with typical values for PP. In the DSC curves of PP it is possible to appreciate two melting and crystallization peaks: these indicate that the PP that is used as the matrix of WPC is a block copolymer; the secondary peak, being centered at around 135°C in heating, probably indicates the presence of ethylene as a co-monomer. Moreover, it is possible to barely appreciate a second order transition around 60 – 80 °C. The thermal properties of the WPCs and neat PP are listed in Tab. 1. The solid and liquid specific heat capacity decrease by increasing the filler content. The specific heat capacity of neat PP at the melting temperature was 1966 J/kg/°C, in general agreement with the theoretical value of 1900 J/kg/°C [Karian 2003]**.** Knowing the specific heat capacity of neat PP ($c_{p,PP}$), of the WPCs ($c_{p,WPC}$) and the mass fractions of fibers (x_f) and matrix (x_{PP}), it is possible to estimate the specific heat capacity of the natural fibers ($c_{p,f}$) using the rule of mixtures as follows:

$$\boldsymbol{c_{p,WPC} = x_f\, c_{p,f} + x_{PP}\, c_{p,PP}} \tag{5.6}$$

The three specific heat capacities of the natural fibers, calculated in this way from each of the WPCs, coincide and are equal to 920 J/kg/°C, in agreement with literature values [Guo 2013]. The WPCs crystallization degree is lower than the neat PP value, although it increases slightly with the wood flour percentage in the composites in agreement with [Ares 2010]. As expected, the melting and crystallization temperatures remain basically constant despite the increase in the filler content since only the polymeric matrix has a melting point.

5.9.1 Mechanical characterization

It is well known that wood fibers and polypropylene are incompatible. Filler - filler interactions are preferred to filler – matrix interactions, especially at high wood fiber contents, and this leads to the formation of wood fibers agglomerates as discussed by Huang and Zhang (2009). The polymer - filler interfacial interaction and its quality are the most important factors that influence the mechanical properties of the composite. A good bond between wood and polymer improves the stress transfer and as a result the mechanical properties, as reported by Shahi et al. (2012), Tasdemir et al. (2009) and Godard et al. (2009).

In Fig. 8 the SEM micrographs of 30% wt. and 70% wt. WPCs are presented. Both compounds show a good fiber dispersion and a satisfactory adhesion between matrix and fibers without voids; this is due to the presence of an appropriate compatibilizer in the composite formulation. The mechanical and physical properties of the WPCs that are listed in Tab. 2 confirm this observation, in particular in the values of the Young's modulus, which increases with the amount of filler and this is explained by the higher stiffness of the filler.

Concerning the strength results, all the composites have a similar value of the yield stress between 17 – 18 MPa, with brittle failure shortly after (Fig. 5.5), while neat PP shows an yield strength of about 19 MPa, slightly greater than WPCs, in agreement with Bouza et al. (2009). In spite of the good adhesion seen in the SEM micrographs, fibers and matrix are anyway incompatible and this prevents a significant improvement in strength with increasing the fibers percentage. Moreover, wood fibers may introduce defects or stress intensity regions that embrittle the material, even if the chemical bonds between the compatibilizer and the filler - polymer interface may be adequate. This results in WPCs displaying a brittle behavior, while neat PP is definitely more ductile.

Among the WPCs, the highest strength is obtained with the 50%wt., although the dispersion of the results does not allow to consider such a result significant from a statistical point of view.

Fig. 5.6 shows the plot of the storage modulus (E') of the WPCs and the neat PP as a function of temperature. As we can see, the storage modulus of each of the WPCs has the same order of magnitude, is higher than the value of neat PP and is a decreasing function of temperature, but as the melting temperature is reached, the storage modulus drops quickly. Interestingly, such a drop occurs for the less filled materials first. This

may be due to the formation of fibers agglomerates at higher filler content.
At higher temperatures, the 70% wt. WPC keeps a minimal mechanical performance. The damping factor (Fig. 5.7) increases with temperature in the 25 – 125 °C range. At higher amounts of filler, the $\tan(\delta)$ value decreases and a relaxation peak between 70°C and 80°C is also visible, although smaller than the one of neat PP. The relaxation peak could be explained by the melting of some PP crystallites as found also by Paul et al. (2010).

5.9.2 Rheological characterization

As previously mentioned, the temperature range in which the parallel plate test can be safely performed on the WPCs is between 165°C and 200°C. The results obtained from the strain sweep test are important to determine the linear viscoelastic region (LVR) and this limits the frequency sweep test temperature: for temperatures above 170°C the WPCs have not shown a sufficiently wide linear viscoelastic domain. Fig. 5.9 presents the storage modulus G' and the loss modulus G'' as a function of frequency for neat PP and the various WPCs. Both moduli increase with frequency and with the filler content and the crossover between G' and G'' shifts at lower frequencies at higher wood fiber percentage. This has been observed also by Godard et al. (2009) for the case of HDPE - based WPC: the transition from fluid - like to solid - like behavior occurring at lower frequencies with increasing the wood fibers percentage indicates that the response of the material tends to become more elastic at higher fiber volume fractions, which is reasonable.
The complex viscosity curves are presented in Fig 10. As expected, complex viscosity increases with the fibers concentration and shows a shear thinning behavior. The neat PP curve displays the transition from a Newtonian plateau to a power law like behavior at 10 rad/s, while the 30% wt. WPC has the same transition at a much lower frequency (less than 1 rad/s). The other composites do not show the Newtonian plateau in the frequency range that has been investigated. Shear thinning is typical of the polymeric matrix, as the polymer chains at high frequencies or shear rates do not have enough time to recreate secondary links for reorganizing the original arrangement. The Newtonian plateau, evident in the neat PP curve, shifts at lower and lower frequencies, as the WPC filler content increases, and eventually disappears from the frequency range

that has been analyzed. This result has been found also by Ares et al. (2010), who ascribe it to the disruption of fiber agglomerates.
For better understanding the shear thinning behavior of the materials, the viscosity curves for neat PP and the WPCs have been fitted with a power law model:

$$\eta = m\,\dot{\gamma}^{n-1}. \tag{5.7}$$

The power law exponent *n* and the consistency index *m* are reported in Tab. 4 for all materials. In the case of neat PP and the 30% wt. WPC, that display the Newtonian plateau in the frequency range considered, curve fitting has been performed for sufficiently high frequencies, in particular between 10 – 100 rad/s for the 30% wt. WPC and 30 – 100 rad/s for neat PP.
Interestingly, *n* basically has the same value irrespective of the wood fiber content, with a very slight decrease. This can be easily explained because the shear thinning behavior depends on the polymeric matrix, not on the filler. The value that is found (around 0.4) is in general agreement with Ares et al. (2010), in the case of high filler volume fractions. The consistency index, on the other hand, increases with the percentage of fibers, as viscosity normally increases with filler quantity.

Tab 5.4 - Power law parameters at 170 °C in a frequency range between 10 – 100 rad/s for the WPCs and 30 – 100 rad/s for PP neat.

Composition	*m* (Pa s^n)	*n*
0% wt	9.00E+03	0.353
30% wt.	3.02E+04	0.444
50% wt.	8.25E+04	0.402
70% wt.	2.06E+05	0.398

Compared to the rotational rheometer, the capillary viscometer is useful for measuring viscosity at higher shear rates. Figs. 13 and 14 show in the same graph the viscosity of neat PP and the 30% wt. WPC obtained both with the rotational rheometer as a function of frequency and with the capillary viscometer as a function of shear rate (the Cox-Merz rule is utilized). The perfect match of the neat PP curve indicates that the results obtained using the Cox-Merz rule are accurate for this material and allow the determination of viscosity in the full range of shear rates between 0.1

– 1000 s^{-1}. In the graph of the 30% wt., on the other hand, the curve from capillary measurements and from the parallel plate rheometer don't match, and moreover, looking at Fig. 5.12, the WPC curve is below the neat PP one, which is unreasonable. This behavior can only be explained with the presence of slip during capillary viscometry measurements, even if rough surface capillaries were used for testing the 30%wt. WPC.

Slip in capillary dies is caused by the lubricating effect given by the alignment of natural fibers along the capillary axis and by the formation of a lubrication layer between the capillary walls and the molten WPC. The natural fibers, in fact, tend to migrate towards the interior of the capillary die, leaving a thin layer of polymer that acts as a "lubricant" that reduces the viscosity at the wall, thus giving rise to an apparent slip phenomenon, which is often observed with filled polymers as reported by Barnes (2003). A similar behavior, specific for natural fibers filled systems, was observed also by Le Moigne et al.(2013) and Hristov et al. (2006).

A single master-curve could be obtained for the viscosity of all WPCs at various fiber percentages and temperatures. This can be very useful for predicting the flow curves of WPCs at temperatures that are more typically in the processing range (180°C - 200°C). Testing at such temperatures is extremely difficult because of slip, degradation and too high viscosity problems when capillary rheometry is used, or the LVR being too small when the parallel plate rheometer is employed.

Let us consider temperature effects on the master-curve first. The viscosity of neat polypropylene has been measured at different temperatures, in particular between 170°C and 200°C, which is a range that is wide enough to contain the usual WPC processing temperatures. Fig. 5.11 shows that the complex viscosity decreases with temperature, which is a well-known effect and can be modeled by shifting the viscosity curves vertically in a log viscosity – log shear rate plot. By doing this, one can obtain the single curve of Fig. 5.15, which represents the viscosity curve of neat PP at 170°C.

The vertical shift factors are listed in Tab. 5 and are also shown as a function of temperature in Fig. 5.16. The temperature shift factors $\log(a_T)$ are fitted using a Williams- Landel-Ferry (WLF) equation:

$$\log(a_T) = -\frac{C_1(T - T_0)}{C_2 + T - T_0} \tag{5.8}$$

in which C_1 and C_2 are fitting parameters and T_0 is the reference temperature, here 170°C. A good fitting can be obtained for the following values: C_1 = 0.57 and C_2 = 16°C .

Concerning the influence of the filler content, as introduced by Highgate and Whorlow (1970) and reported also by Barnes (2003), a single master curve can be obtained by shifting the viscosity curves vertically in a viscosity – shear stress bilogarithmic plot. It is possible to show (it will be shown in Section 5.10) that such a procedure is equivalent also to shifting the flow curves in a log viscosity - log shear rate plot, but in a 45° diagonal direction, in which an horizontal shear rate shift is superimposed onto the vertical shift. The two shifts would have the same value but opposite sign. Notice that this procedure is the same as the one used by Trappe and Weitz (2000) and, in the case of natural fiber filled composites, also by Marcovich et al. (2004) and by Godard et al. (2009).
The 170°C flow curves of neat PP and all WPCs (Fig. 5.10) have been shifted diagonally until they matched the curve for neat PP (Fig. 5.17), thus this master-curve is really relative to the viscosity of the unfilled system at 170°C and will be denoted by $\eta_{PP,170°}$. This curve has been fitted with a Carreau – Yasuda model:

$$\boldsymbol{\eta_{PP,170°}} = \frac{\boldsymbol{\eta_0}}{(\mathbf{1} + (\boldsymbol{\lambda}\,\boldsymbol{\omega})^{c})^{\frac{\mathbf{1}-\boldsymbol{n}}{\boldsymbol{c}}}} \tag{5.9}$$

where ω is frequency, η_0 is the viscosity value at the Newtonian plateau for neat PP at 170°C, *n* is related to the slope of the shear thinning portion of the curve in a log-log plot and λ and *c* are fitting parameters.

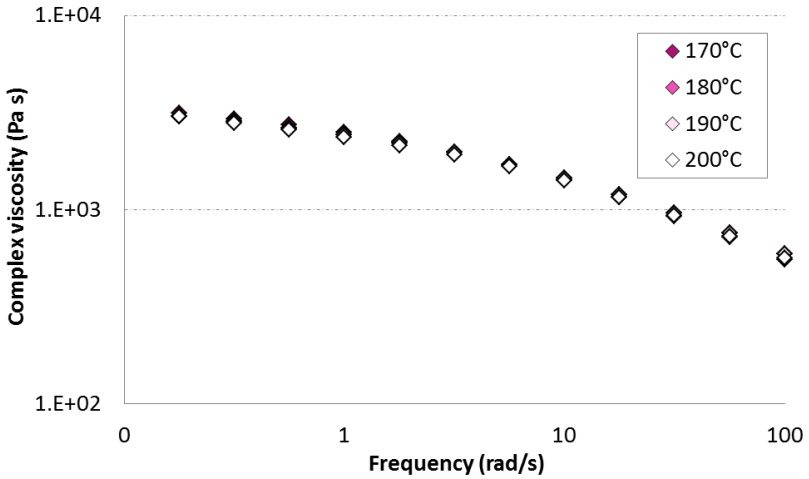

Fig. 5.15 - Complex viscosity master - curve at different temperature for neat PP

Tab. 5.5 - Vertical shift factor as a function of temperature

Temperature (°C)	Vertical Shift factor $\log(a_T)$
170	0
180	0.21
190	0.31
200	0.36

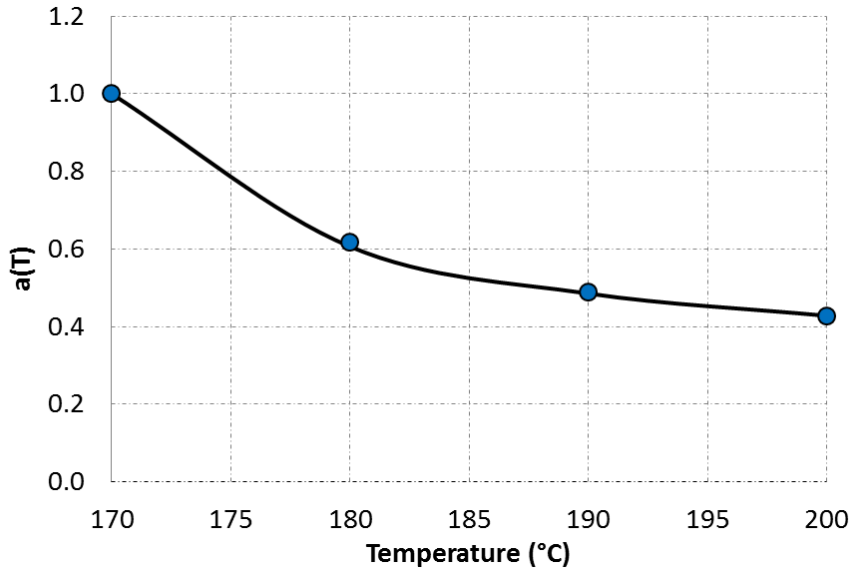

Fig. 5.16 - Function $a(T)$ vs. temperature T and curve fitting using Eq. 5.8.

The constants used in the Carreau - Yasuda model are listed in Tab. 5.6. The values used for the diagonal shift factor, that will be indicated with $\log(b_\phi(\phi))$, are listed in Tab. 5.7. The function $b_\phi(\phi)$ is the ratio of the viscosity of the WPC with filler volume fraction ϕ and that of neat PP at constant shear stress, thus it represents a sort of relative viscosity at 170°C, keeping the shear stress constant. In Fig. 5.18 $b_\phi(\phi)$ is plotted as a function of the filler volume fraction ϕ and fitted using a modified Eilers model [Ferrini 1979]:

$$b_{\phi}(\phi) = \left[1 + \xi \frac{\phi}{1 - \frac{\phi}{\phi_{max}}}\right]^2 \quad (5.10)$$

where the model parameters are ϕ_{max}= 0.79 and ξ= 14.55. The ϕ_{max} parameter is the maximum possible volumetric loading of wood fibers in the PP matrix and the ξ parameter should be half of the intrinsic viscosity of the wood fiber - PP mixture, according to [Ferrini 1979]. In the case of rigid spheres in a dilute solution such a value is 2.5 according to the well-known Einstein relation, in the present case this value is much higher due to the non-spherical shape and deformability of the particles.

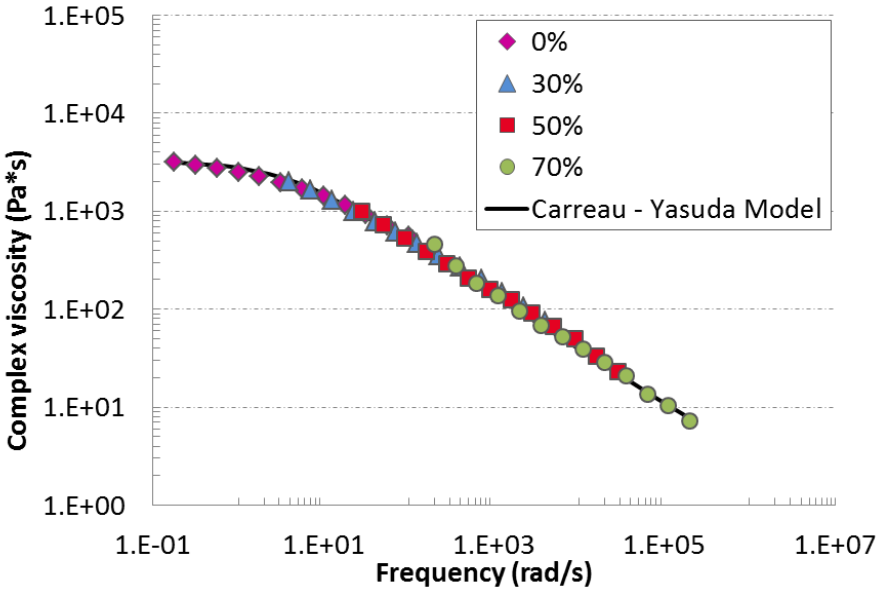

Fig. 5.17 - Complex viscosity master-curve at 170°C for neat PP and all WPCs fitted with a Carreau - Yasuda model

Tab. 5.6 - Fitting parameters used in the Carreau – Yasuda model

Fitting Parameters	
λ (s)	0.3
c	1
n	0.45
η_0(Pa s)	3200

Tab. 5.7 – Diagonal shift parameter as a function of the filler volume fraction

WF mass fraction % wt.	ϕ WF volume fraction % vol.	Diagonal shift factor log(b_ϕ)	Relative viscosity b_ϕ
0	0	0	1
30	27	1.60	40
50	44	2.45	251
70	61	3.20	1585

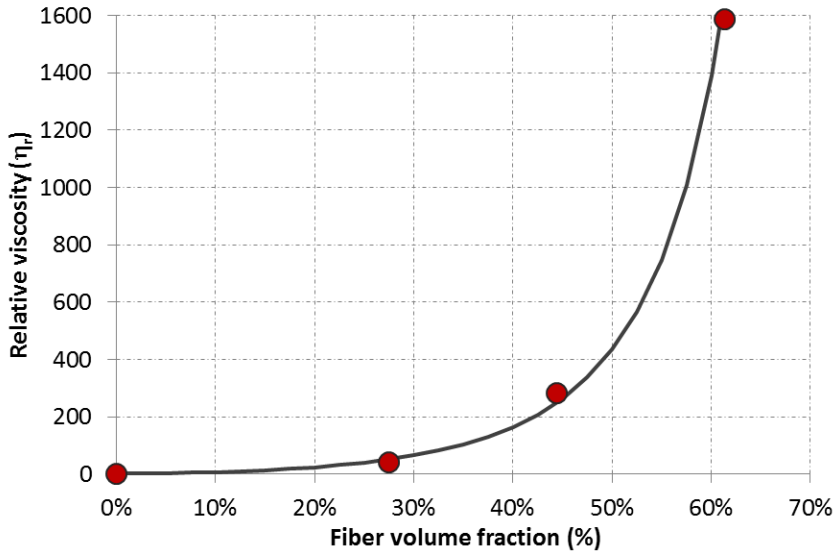

Fig. 5.18 – Relative viscosity $b_\phi(\phi)$ as function of fiber volume fraction $\boldsymbol{\phi}$ and curve fitting using Eq. 5.10

Now, considering both shifts, i.e. the vertical thermal shift and the diagonal volume fraction shift, the master curve that is proposed takes the following form:

$$\boldsymbol{\eta(T,\phi,\dot{\gamma}) = a_T(T) b_\phi(\phi) \eta_{PP,170^\circ}\left(\frac{\dot{\gamma}}{b_\phi(\phi)}\right)} \quad (5.11)$$

in which the functions a_T, b_ϕ and $\eta_{PP,170^\circ}$ have been introduced in Eq. 5.8, 5.9 and 5.10.

Despite Eq. 5.11 has been obtained only for neat PP at various temperatures and only at 170°C for the various filler volume fractions, we propose that such a curve may be used in general to estimate the viscosity of PP - WPC in the whole range of temperatures and filler volume fractions. For such an hypothesis to hold, it must be assumed that the net response on viscosity of temperature and filler volume fraction is the sum of the effects which would have been caused by each of these variables individually. This is reasonable if the influence of temperature on filler – filler and filler – polymer interactions is negligible, thus the most significant effect of temperature is only on the PP viscosity.

The other models for natural fiber filled polymeric composites that have been proposed in the recent literature [Godard 2009, Azizi 2009] have also been able to construct a single master curve that is valid for a wide range of filler volume fractions. Such models are constructed in the same way as the one which is proposed in the present article, concerning the filler volume fraction dependence. To our knowledge, though, the model that is presently proposed is the first one that takes into account both, temperature and natural fibers percentage. The interest in combining temperature and filler fraction effects in a single model stems from the possibility of producing the flow curve of the materials by running tests at lower temperatures, where degradation problems are less relevant and also the linearity in the viscoelastic response is guaranteed.

5.10 Equivalence of shifts directions in $\eta - \tau$ and $\eta - \dot{\gamma}$ plots

In this appendix it will be shown that a vertical shift in a log viscosity – log shear stress diagram corresponds to a 45° shift in a log viscosity – log shear rate diagram. To this end, consider the two curves (τ_1, η_1) and (τ_2, η_2) in the viscosity shear stress diagram of Fig. 5.19.

As can be seen, the two curves differ by a vertical shift factor, thus:

$$\forall\, \boldsymbol{\tau_1 = \tau_2} : \boldsymbol{log}\,(\boldsymbol{\eta_1}) = \boldsymbol{log}\,(\boldsymbol{\eta_2}) - \boldsymbol{log}(k) \quad (5.12)$$

From the definition of viscosity, i.e. $\tau = \eta\dot{\gamma}$, we have:

$$\mathbf{log}(\boldsymbol{\tau_i}) = \mathbf{log}(\boldsymbol{\eta_i}) + \mathbf{log}(\dot{\boldsymbol{\gamma}}_{\boldsymbol{i}}), \quad \boldsymbol{i} = \mathbf{1}, \mathbf{2} \tag{5.13}$$

so that, if $\log(\tau_1) = \log(\tau_2)$, then using Eq. 5.12:

$$\begin{aligned} &\mathbf{log}(\boldsymbol{\eta_1}) + \mathbf{log}(\dot{\boldsymbol{\gamma}}_{\mathbf{1}}) = \\ &= \mathbf{log}(\boldsymbol{\eta_2}) - \mathbf{log}(\mathrm{k}) + \mathbf{log}(\dot{\boldsymbol{\gamma}}_{\mathbf{1}}) = \\ &= \mathbf{log}(\boldsymbol{\eta_2}) + \mathbf{log}(\dot{\boldsymbol{\gamma}}_{\mathbf{2}}) \end{aligned} \tag{5.14}$$

and therefore:

$$\mathbf{log}(\dot{\boldsymbol{\gamma}}_{\mathbf{1}}) = \mathbf{log}(\dot{\boldsymbol{\gamma}}_{\mathbf{2}}) + \mathbf{log}(\mathrm{k}) \tag{5.15}$$

Now, considering Eqs. 5.12 and 5.15, one obtains that if two flow curves differ by a positive vertical shift in a viscosity – shear stress bilogarithmic diagram, then in a viscosity – shear rate bilogarithmic diagram the two curves are shifted both vertically by the same amount and horizontally by the opposite of the vertical shift Fig. 5.20.
Without using logarithms and defining b = 1/k we would have:

$$\dot{\boldsymbol{\gamma}}_{\mathbf{1}} = \frac{\dot{\boldsymbol{\gamma}}_{\mathbf{2}}}{\boldsymbol{b}}, \qquad \boldsymbol{\eta_1} = \boldsymbol{b}\,\boldsymbol{\eta_2} \tag{5.16}$$

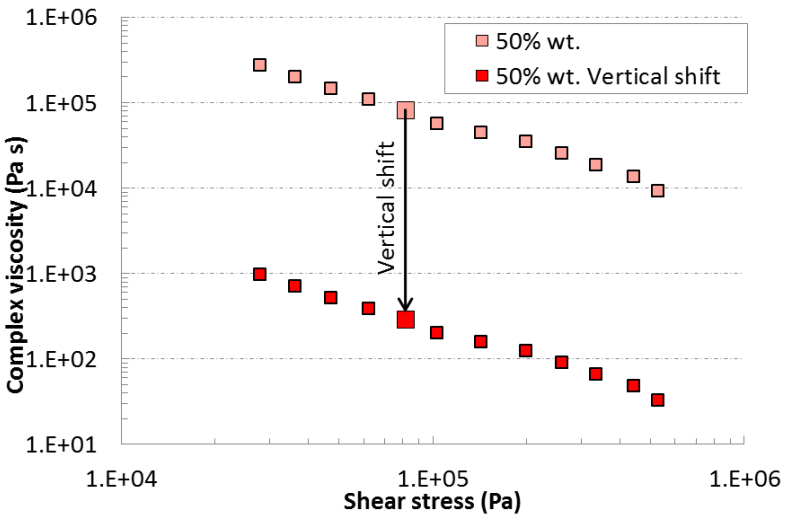

Fig. 5.19 - Vertical shift in the viscosity vs. shear stress curve. η_1 (red squares), η_2(pink squares). The vertical shift is equal to log(k)

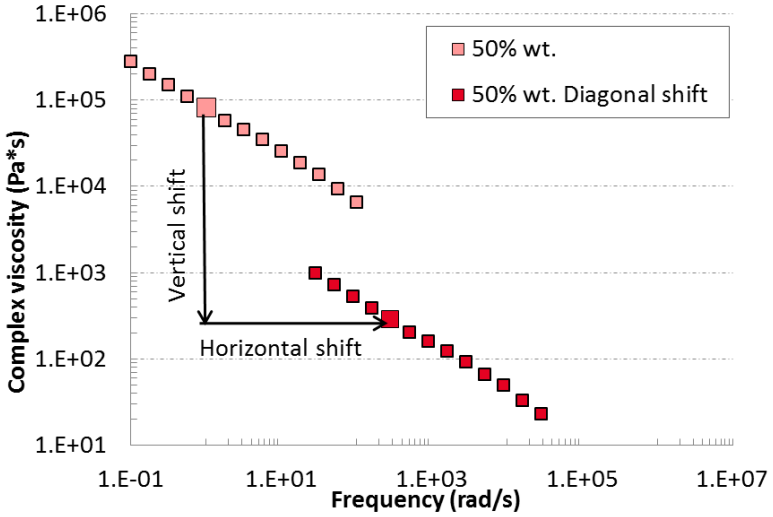

Fig. 5.20 - Diagonal shift in the viscosity vs. shear rate curve. η_1 (red squares), η_2 (pink squares). The vertical and horizontal shifts are log(k).

CHAPTER 6

IN – LINE RHEOMETRY

6.1 Introduction

As noted in chapter 5, for Wood Polymer Composites (WPC) in particular at high temperature and high percentages of filler, the rheological properties may be very challenging to obtain with standard off – line rheological techniques. Several different problems affect the typical instruments used for the rheological characterization of the WPC. As an example, using the parallel plate rheometer in oscillation mode, the main problem is due to the reduced linear viscoelastic region at high temperature. This problem did not allow to perform rheological measurements at temperatures higher than 170°C, which is quite below the typical processing temperatures of WPCs - PP based. Using the capillary rheometer, the problem of linear viscoelastic region is solved, but the high viscosity makes it impossible to test highly filled WPC (more than 50%wt.). For low filled WPC (30%wt.), the viscosity is lower, yet the results that would be obtained might be unreliable due to the following issues. First, the presence of the orifice would "sieve" the WPC melt in such a way that the filler fraction that is extruded through the capillary is smaller than the nominal fraction, while a greater filler fraction remains inside the reservoir. Secondly, the high shear rates that are involved in the measurements procedure have the effect of orienting the wood fibers along the capillary axis and this in turn reduces the apparent viscosity.
Another difficulty that affects all off – line tests at high temperature and at high percentage of filler is the problem, well described in chapter 1, of wood degradation. This phenomenon changes the properties of the material and makes the measurement unreliable if not carried out in a controlled atmosphere. Another disadvantage in the use of the off – line rheometers is that it is not possible to monitor the rheological characteristics of the composite using the specific conditions set during the extrusion process, in fact samples prepared for the off - line rheological measurements do not come directly from extrusion, but rather from pellets or disks produced by injection molding.
In order to eliminate several drawbacks a process rheometer has been developed. In the specific case of the WPCs the major advantages are that the measurements are made in real extrusion conditions and with a

limited presence of oxygen inside the extruder barrel, which reduces the risk of degradation. Using a process rheometer it is also possible to consider if the samples preparation influences the rheological measurements, in particular for a material that is non – homogenous and easily degradable like the WPCs. This type of instrument is a convenient way to eliminate the problems presented by off – line rheometers and it is very useful to obtain real-time data for study the real conditions of the fluid during processing.

In the past different process rheometers have been developed to monitor rheological properties of flowing polymer melts for quality control or process control purposes [Dumoulin 1996]. Usually two categories of rheometers are used in the process: on - line and in - line types. On – line rheometers (Fig. 6.1) take a side stream of melt from the main process flow, usually by the action of a by – pass and a gear pump to the rheometer. After rheological measurement, the sample is returned to the process or more usually discarded as waste. Rheometers are generally capillary or slit with a pressure drop being measured over a range of processing rates.

In – line rheometers are installed directly into the process stream as shown in Fig. 6.2. and the flow does not have abrupt changes of direction. Samples are directly generated by the process flow. Processing rate is dependent only on the extruder flow rate. The slit is usually the geometry of the rheometer with two or more pressure transducers to measure the pressure drop.

For unfilled material, the use of in – line and on – line rheological dies have been widely reported in the literature. Lodge and de Vargas have constructed a slit die to measure the properties of viscous polymers at low shear rate using two pressure transducers flush mounted at the die wall and a third mounted in a transverse slot opposite the flush mounted transducer. Using a gear pump the volumetric flow rate was controlled. The study has been carried out on two low – density polyethylenes (LDPE) at shear rate in a range between 0.1 – 8 s-1. The result obtained has been that the pressure data agreed with off – line measurements.

Rauwendaal and Fernandez carried out a similar study using a slit viscometer inserting four pressure transducers flush mounted. A Brabender extruder fed the die through a gear pump. The viscosity values of an high –density polyethylene (HDPE) measured on the slit die viscometer showed a good reproducibility but tended to be lower than

those measured on capillary rheometer. A possible explanation is the shear modification of the polymer melt in the plasticating extruder.

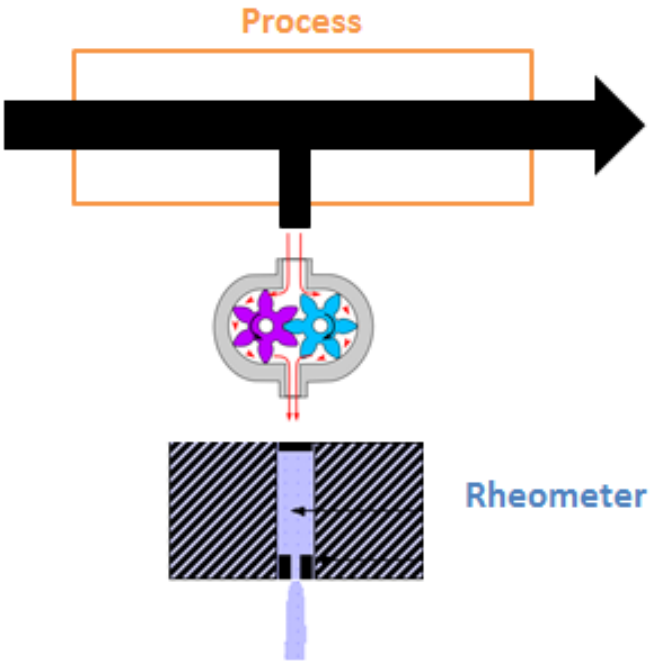

Fig. 6.1 - Schematic On – line rheometer

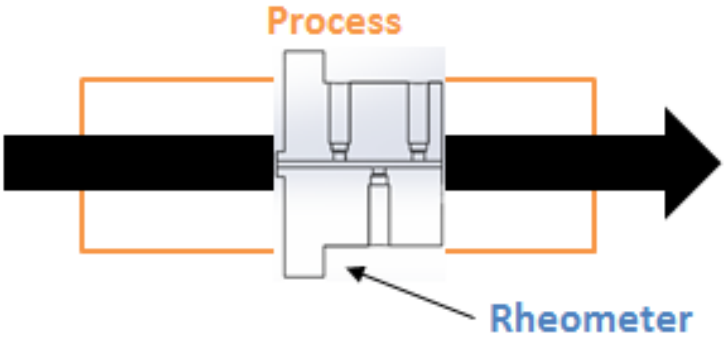

Fig. 6.2 - Schematic in – line rheometer

Pabedinskas et al. present a development of an in – line extrusion rheometer based on the flow of polymer through a wedge (vertically tapered slit). This had the effect of increasing the shear rate along the length of the slit without the need to change the polymer flow rate. A series of polypropylenes prepared via reactive extrusion were studied. Three pressure transducers were flush mounted to the slit wall. The range of shear rates measured was 100 – 1000s^{-1} Experimental results showed very good agreement with the off - line rheometer for low viscosity material but for higher viscosities the values were significantly lower.

Padmanabhan and Battacharya developed a slit and capillary in – line rheometer to measure exit, hole, and entry pressure simultaneously. This apparatus allows to measure simultaneously viscosity, first normal stress difference and extensional viscosity under processing conditions using a Brabender single screw extruder. Two LDPE are used measuring the mass flow rate by weighing the throughput. Experimental results showed that the estimation of shear viscosity was lower when compared with the measurements with a rotational rheometer. As in other studies this phenomenon is explained with a shear modification.

Coates et al. used an in – line rheometer to monitor and control the gelation levels in UPVC compounding. Two flush mounted pressure transducers were used to monitor the pressure drop in a constant flow cross section. It was observed that in – process results can predict accurately the gelation level.

Lodge describes the design of an on – line slit die rheometer with two transverse slots located in one die wall and a third flush mounted transducer at a location opposite the center in the other die wall. A Zenith gear pump is used to control the flow rate. A polystyrene was tested and the values are compared with a cone – plate and capillary rheometer with good results.

Kelly et al. studied a LDPE compound during extrusion with three in – process rheometer: a capillary on – line rheometer, a four sensor slit die in – line rheometer and a six sensor slit die. The in – process devices exhibit a very good agreement with measurement made off – line. A really interesting work has been developed by Glomsaker et al. using different formulations of PVC, in which they were shown a wall slip behavior. Four dies with nominal slit heights were used to study the slip with the Mooney procedure. Many aspects and sources of uncertainties were taken into account like the true heights of the die and the position of the transducers. The in – line measurements showed significant geometry

effect and the data did not fit into the Mooney pattern. The authors state that the mechanisms that produce the peculiar effects are not fully understood. However the flow in the die was basically plug flow and this result is mostly related to the interface between the polymer and the wall and not due to the polymer bulk. Another study with the aim to design an instrumented slit die for PVC has been performed by Thorsteinsen et al. The instrument was composed with a dual slit adapted to a twin screw extruder. The system contains a regulating piston that can block off a variable part of the melt channel in order to adjust the screw tip pressure independently of the melt flow out of the slit die. The second part of the system splits the flow into two separate channel controlled by the regulating pistons. Each die has four flush mounted pressure transducers. The geometry of each slit has two different slit heights, but authors wish to emphasize that a Mooney analysis based on only two slit heights is subject to uncertainties, thus more heights are needed in order to verify the results.

Teixeira et al. extend the design of a slit die in - line rheometer to perform the measurements of the first and second normal – stress differences in shear flow at shear rates typical of LDPE and polystyrene (PS) processing. The results show that the method can be used to measure the viscosity and the first normal stress - difference but not the second normal stress – difference which is zero within the experimental uncertainties.

Most of the in – process rheometers have been developed in conjunction with an extruder, but there is another branch of study that could be interesting to review: the study of the in – process rheometry using an injection molding machine.

Bariani et al. try to increase the reliability of numerical simulation of the injection molding process by measuring the rheological properties of polycarbonate (PC) using an in - line slit die rheometer witch has been mounted, as a mold, onto an injection molding machine validating the data with an off – line capillary rheometer. A similar approach has been proposed by Aho et al. studying the rheological properties of PP and PS using a slit die attached to an injection molding machine. The modular design allows variable slit heights for evaluating the presence of wall slip. The slit height adjustment was accomplished by means of three exchangeable inserts. The superposition of the shear stress vs. shear rate curves verifies the absence of wall slip. The trend observed for in – line experiments compared to capillary rheometer is slightly lower. This

phenomenon is attributed in literature to stronger preshearing by plasticizing screw.
Gou et al. have developed a different system to obtain PP rheological properties under injection molding processing condition to use for numerical simulation. The apparatus forces the plastic melt from the injection of the screw, in a cylindrical barrel where it passed through two capillaries with the same diameter but different length. The measurement data were correlated by the Cross - WLF model. Numerical simulation were carried out by Moldflow software with the rheological data measured to analyze the shrinkage and warpage of the sample.
Zhang and Gilchrist present another measurement system to evaluate the rheological behavior of Pebax® (polyether block amides) molten under a micro injection molding process. The originality of the system is the dumbbell shape of the mold that allows to use the sample for mechanical testing after rheological measurement. Another non - conventional features for an in – process rheometer used during the injection molding process has been developed by Fernandez et al. The device is attached directly to the nozzle of the plasticizing unit allowing in – line measurements of the pressure drop and temperature that are necessary to calculate the apparent viscosity at different shear rates. The results have been used to characterize a mineral filled PP and its recycled form to obtain the constants of its Carreau – WLF rheological model.
The objective of this work is to describe a device that enables to characterize a temperature sensitive and high viscous WPCs directly during processing. This apparatus permits to carry out the measurements at the processing temperature and for three different amount of filler present in the compound (30 – 50 – 70 %wt.) and compare the viscosity values obtained with those measured with standard techniques.

6.2 In – line rheometer design

The first step in the design of the rheometer has been to choose the process rheometer type. In the specific case of the WPCs an in – line rheometer, respect an on – line one, has several positive aspects. The flow does not have abrupt changes of direction with respect to the direction of the process, this reduces the time to reach steady state and therefore the time of test. Decreases the possibility of instability formation in the melt that make the measure unreliable and eliminates a source of pressure drop that could produce overpressure. Another positive aspect of an in - line rheometer is that it is not necessary to use the gear pump to

control the flow rate, this reduces a possible cause of degradation for the natural fiber that could stick between gears and a possible material separation between the polymer and natural fibers if the light between the gears is too small compared to the size of the fibers.
The geometry chosen for the design of the in - line rheometer has been the slit die. This selection is motivated by several aspects. First, the focus was to study the condition of the material during processing and not to explore the complete viscosity curve of the WPC, thus it was not necessary to test the material at really high and really low shear rates obtainable only with capillary and parallel plate rheometer respectively. Moreover, the use of the capillary was excluded due to the high viscosity of the WPC with a content of filler higher than 50% wt. The most significant advantage of the slit is that the die allows flush mounting of the pressure transducer. In the slit die the transducer is perfectly flat with respect to the die surface. This geometry facilitates a more accurate measurement of the melt pressure, in particular when evaluating a fluid that is highly filled such as the WPCs. In fact the influence of some flow disturbance due to the presence of gap or edge caused by a non-perfect adhesion between the transducers and the surface of the die could give unreliable measurements. Asperities along the material flow tend to produce burned inclusions that grow with time as the thermally sensitive natural fibers degrade and thus should be avoided. The effect of pressure drop that converges into capillary entrance is not present and thus is not necessary to perform the Bagley correction. Another advantage of this type of geometry is the large exit opening of the slit die geometry that reduces some of the particle size problems and does not limit the analysis to small particle sizing. It is possible to assume that the slit is infinitely wide and to ignore the edge effects with good accuracy if the width is more than 10 times the height [Han 1971]. This condition satisfies the assumption that flow in the slit is acting between infinite parallel plates, thus allowing that the edge effects are negligible. If the height-to-width is less than 1:10 it is possible to introduce a shape factor to reduce the effect of the wall on flow rate between infinite parallel plate. This correction has been presented by [Berker 1963] for a Newtonian fluid and by [Son 2006] for a Non-Newtonian fluid.
Another important aspect in the design of the slit die is the location of the pressure transducers. In particular, the first transducer must provide sufficient distance from the die entrance to assure a fully developed flow. A minimum of 3 - 4 times the slit height is needed for this length. As an

example for a 6 mm slit height, a 25 mm minimum distance between the end of the transition and the first transducer was required.
According to the directions described an in – line slit die rheometer at variable height has been developed. Fig. 6.3 gives a schematic drawing of the apparatus and the comprehensive 2D plans are in Appendix A.

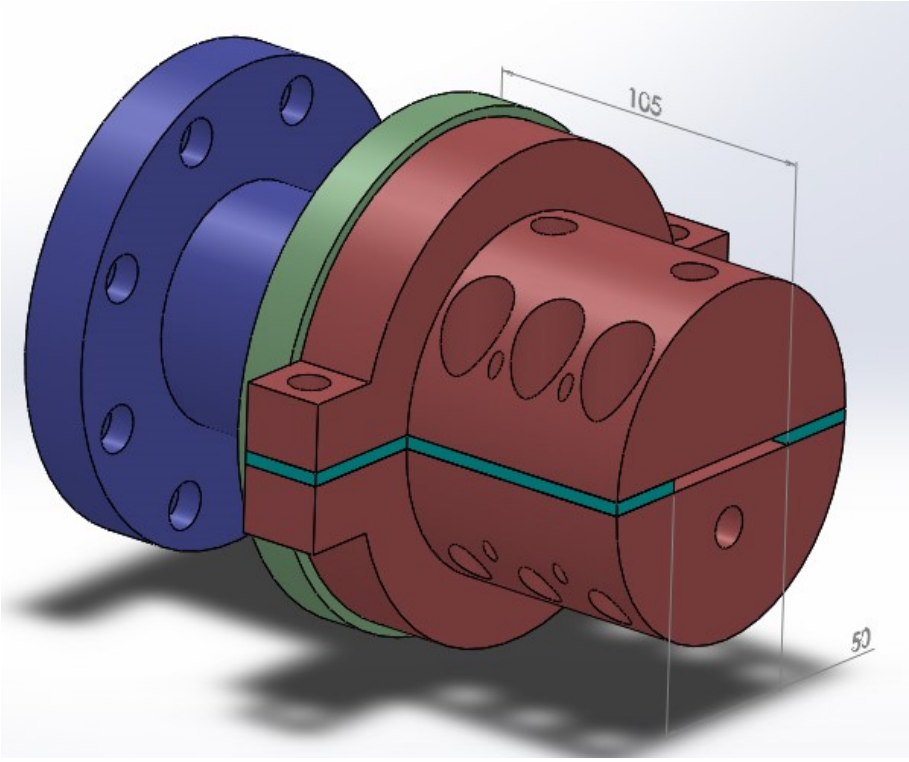

Fig. 6.3 – Schematic diagram of the apparatus

The apparatus is composed of six parts: an extruder die (blue component), an adapter (green component), two separators (light blue components) and upper and lower halves that create the main body of the slit die (red components). A picture of the system is shown in Fig. 6.4. The two halves of the rheometer body (Fig. 6.5), bolted together with eight M10 screws, constitute the top surface and bottom of the slit. The heights, used for the Mooney procedure are 1.3, 2, 4, 6 mm. The heights are obtained using the separators of adequate height (Fig. 6.6).

These separators create also the lateral wall of the die channel that is 50 mm wide and 105 mm long. The slit die is connected with the single screw extruder by an adapter (Fig. 6.7). This part provides a convergent flow path for polymer leaving from 50 x 8 mm rectangular channel of the die extruder to the profile required to create a flow regime in the slit die at different heights. The die adapter is connected to the extruder and to rheometer body by a bolted connection.

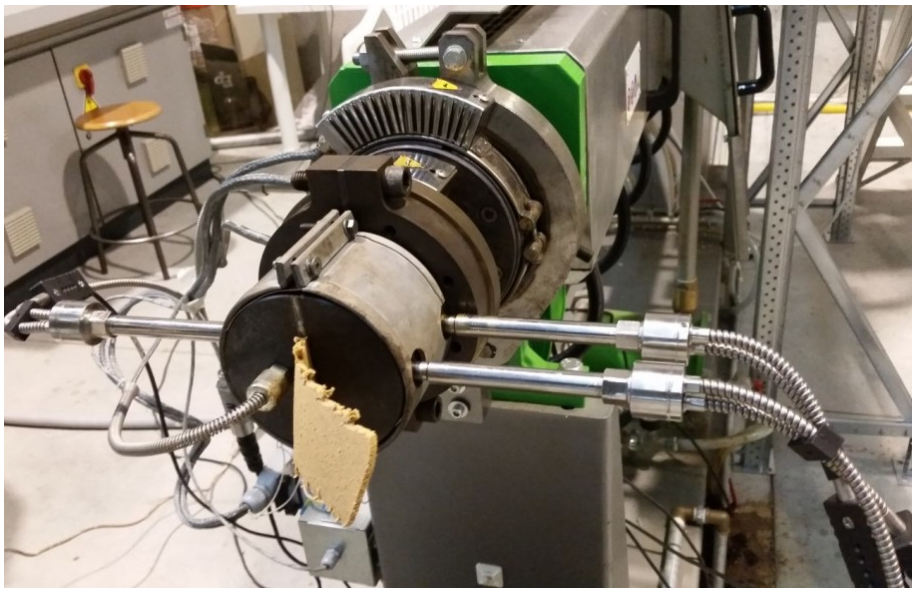

Fig. 6.4 – Picture of the apparatus

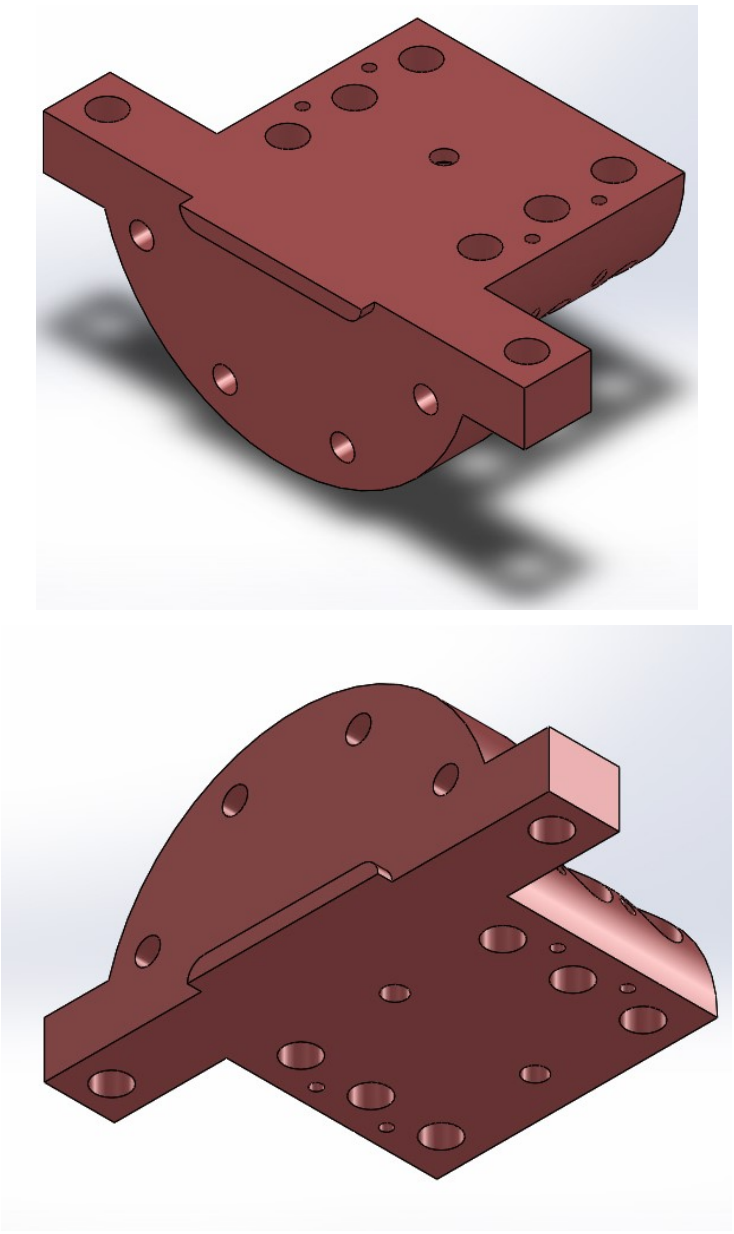

Fig. 6.5 - Upper and lower halves of the slit die rheometer

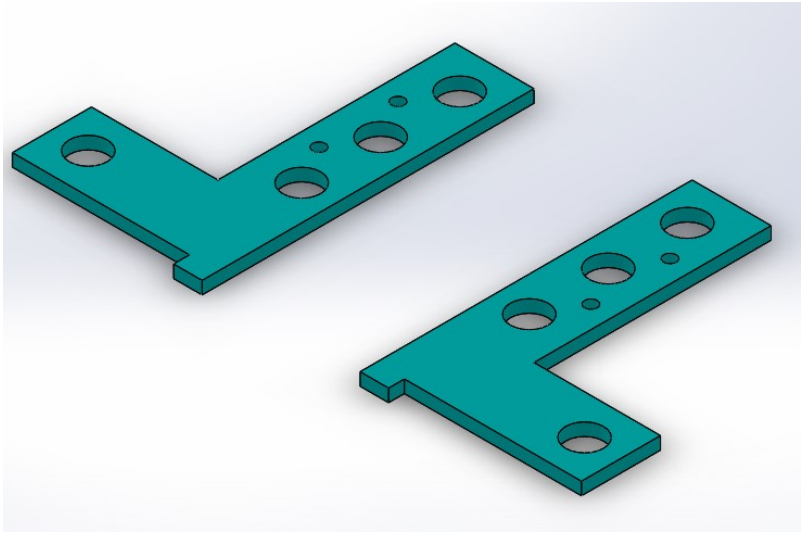

Fig. 6.6 – Separators for the construction of the die channel

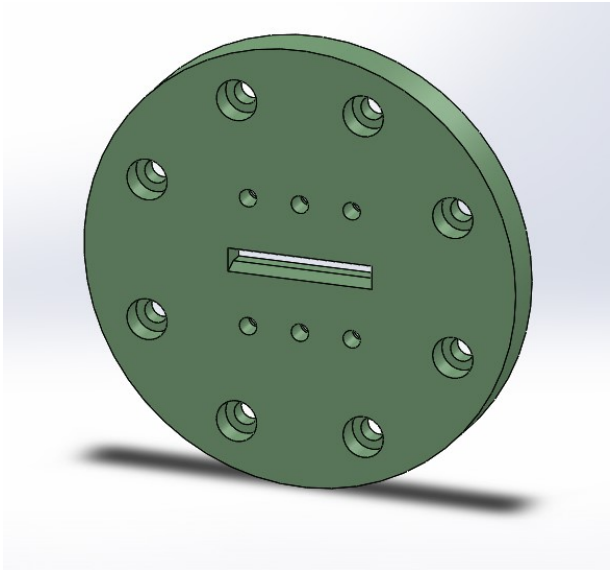

Fig. 6.7 - Adapter for the connection between extruder and the slit die

Heating is achieved by three external resistance heaters with two control thermocouples located in the metal of the body close to the melt. The apparatus temperature is controlled by using two controllers in the extruder panel. To make the rheological measurements reliable it is necessary not only to check the temperature in the metal body of the system but also to check the temperature of the polymer on the surface of the slit die. However, due to the in – process nature of the system, accurate temperature control is difficult during extrusion, and shear heating generally leads to increased melt temperature. Three pressure transducers are flush mounted along the slit length allowing pressure drop along the die and the melt temperature to be measured (Fig 6.8). To ensure a fully developed flow of the highly filled melt, the first pressure transducer was placed 40 mm from the entrance of the slit. The remaining two transducers were located at 65 and 90 mm.
The modularity of this apparatus allows the complete dismantling of each component and the complete cleaning of the system.

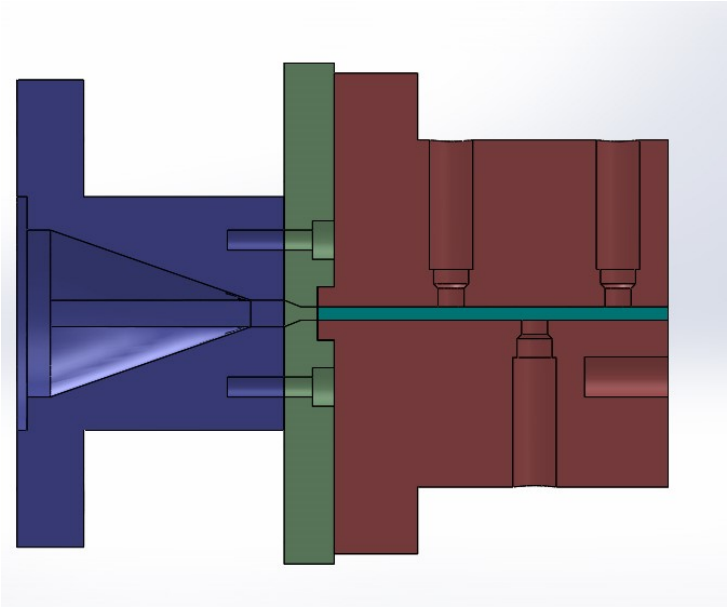

Fig. 6.8 – Section of the instrumented die with the three pressure transducers along the slit

6.3 Instrumentation

An important part of any process measurement is the instrumentation used to carry out the tests. The in – line rheometer used in this study needs melt pressure transducers to measure the pressure drop, temperature thermocouples to control the process and an acquisition system to acquire and save the rheological data. Accuracy and repeatability of each sensor are important for the quality of the results.

6.3.1 Melt pressure measurement

In all melt pressure measurements made, GEFRAN mercury – filled transducers were used. The transducers used are M32 series, with a flexible connection between the transducer body and the stem. The transducers have a maximum operating temperature of 400°C with a overpressure without degradation of the double of the full scale. The transducers range used varied from 0 – 100 bar and 0 – 500bar, depending to the particular application. The accuracy is $\pm$0.25% FS.
By analyzing the construction of a filled sensor, it is evident that the structure is designed to transfer media pressure to the transduction part and keep it as far as possible from heat source.
The hydraulic circuit is composed of a tip with 0.1 mm internal diameter, at the end of which the contact diaphragm and extensimetric diaphragm are welded.
Inside the sensor, a filling fluid (mercury) with low compression coefficient transfers the pressure . The fluid quantity is 40 mm^3.
Diaphragm geometries are designed on the basis of the volumes and pressures that come into contact during measurement; the pressure that the medium exerts on the contact diaphragm must create a precise deformation of the measurement diaphragm.
The measurement element, called extensimeter, is glued to the measurement diaphragm, and converts the physical pressure quantity into an electrical signal. An extensimeter consists of a thin metal wire that is bent and inserted in a flexible insulating material according to a specific geometry. The metal wire (measurement element) is an extra-thin leaf of a metal alloy formed by means of chemical engraving. This special engraving process produces metal grills with specific geometries that have maximum ability to modify their characteristics as they change shape.

6.3.2 Temperature measurement

J- type thermocouples (GEFRAN) were used, in the slit die, to monitor temperature for control purposes. Three are located adjacent to polymer, in coincidence with the pressure transducer and two are located in the die metal close to the melt flow. These thermocouples have an accuracy of ±0.1°C

6.3.3 Data acquisition system

A diagram of the acquisition system is shown in Fig. 6.9. Analogue signals from process instrumentation are conditioned and interfaced to a PC using a NI CompactDAQ 9178 (National Instrument) modular interface unit.

Fig. 6.9 – Acquisition system

This unit consists in eight interchangeable slots where it is possible to insert acquisition modules. Two modules have been used for acquiring and converting the pressure and temperature analogic signals to digital signals then transmitted to the PC. Pressure transducer outputs have been conditioned with a NI 9923 (National Instrument) and temperature outputs with a NI 9211 (National Instrument). Labview 2013 software has been used to collect and display data.

6.3.4 Single screw extrusion line

In – process rheological measurements are performed on a single screw extruder (P.R.T. SERVICE & INNOVATION S.r.l., Sant'Agostino (FE), Italy). The extrusion line is shown in Fig. 6.10 and Fig. 6.11. The machine is driven by a motor which provides power to a speed reduction gearbox. The drive motor allows a screw speed range of 0 – 110 RPM. The extruder barrel, with a maximum pressure rating of 300 bar, consists of six individual thermal section. Each section has a heater element and a fan. The barrel heaters can operate up to a maximum temperature of 300°C and are controlled by Gefran 600 temperature controllers. Controlling thermocouples are located in the body of each barrel section, the barrel has also been modified to include ports for pressure transducers along the length of the barrel. The extruder screw is 50 mm in diameter, has a length to diameter ratio of 40 and a compression ratio of 1.23. In Tab. 6.1 the different zones of the screw are presented and the detailed diagram is in Appendix B. The extruder is equipped with a breaker to improve compaction and with a venting zone to help degasification of water vapor.
The extruder is run by a control system which allows temperature, screw speed setting and monitoring the pressure die and the current absorption of the motor. The extruder has been starve fed using a controlled volumetric feeder using a volumetric feeder (Fig.6.12). The polymer has been stored in the hopper and the mass flow rate was determined by the velocity of the feeder screw which has the function of delivery the polymer to the extruder at the base of the hopper.
With only a few exceptions, neat polymer, practically do not adsorb water. Incorporating natural fiber into polymer increases the water adsorption [Klyosov]. This hydrophilicity causes many problems during process. The water contained inside the pellets, during extrusion, vaporizes creating voids and defects in the material. This problem makes the final product imperfect and moreover with the presence of bubbles or voids makes the flow of the material not homogenous and the measurement non reliable. To reduce the moisture content (less than 2 – 3%) before processing, a drying system has been designed. This apparatus (Fig. 6.13) consists in a hopper, an infrared lamp and a handling system that by the presence of two motors keep the pellets moving during the drying.

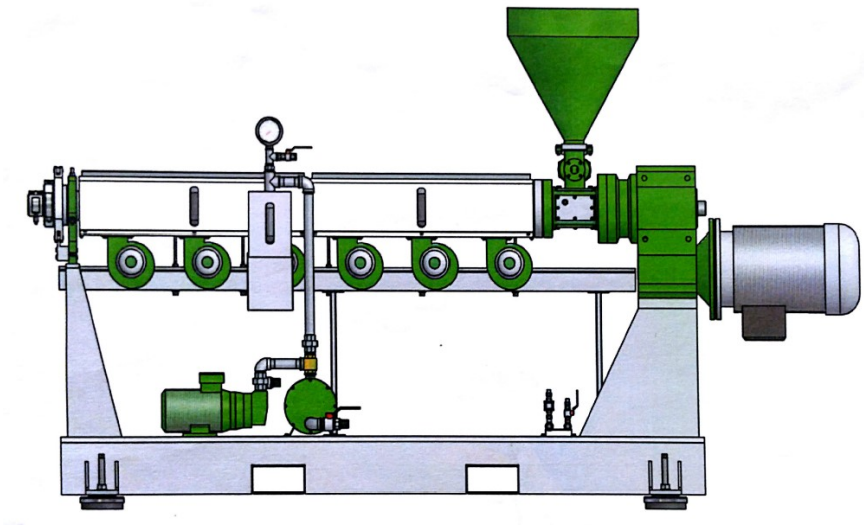

Fig. 6.10 Schematic representation of the single screw extruder line

Fig. 6.11 the single screw extruder line

Tab 6.1 – Screw zones

Zone	Length	N° of turns	Screw diameter
Solid Conveyed zone	400 mm	8	35 mm
Melting zone I	250 mm	5	variable
Metering zone I	450 mm	9	43 mm
Venting zone	250 mm	4	30 mm
Melting zone II	200 mm	4	variable
Metering zone II	400 mm	8	42 mm

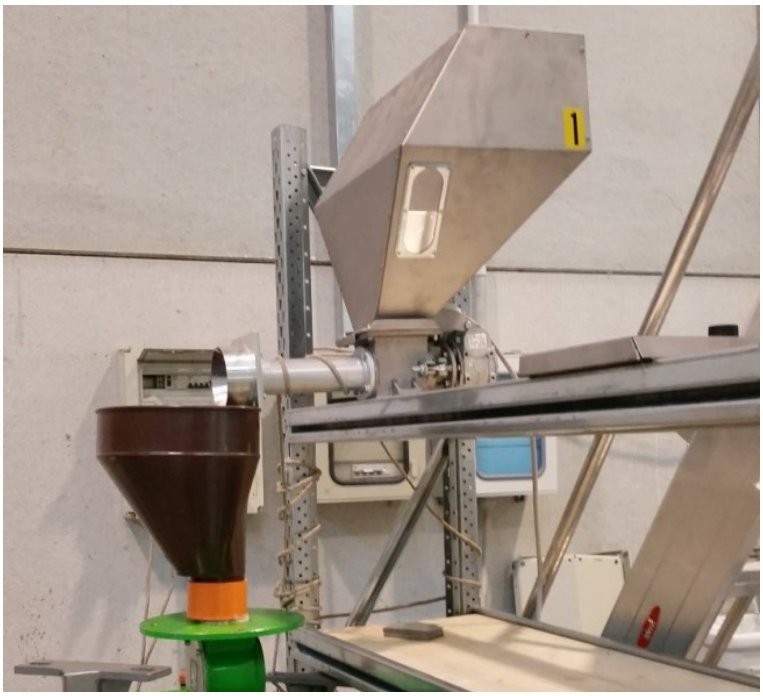

Fig. 6.12 - Feeding system

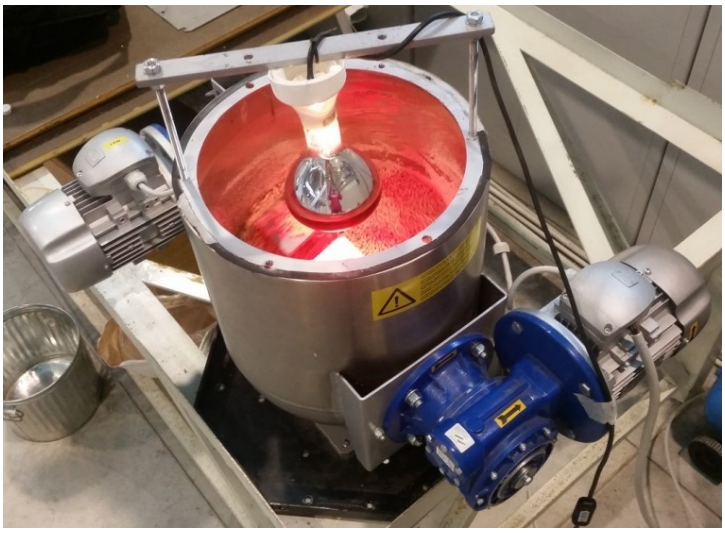

Fig. 6.13 - Infrared drying system

6.4 Experimental procedures

Prior to performing the extrusion and the rheological tests, the WPCs (30% wt. and 70% wt.) have been dried at 95 °C in the drying system for 12 hours to reduce the moisture content.
Following thorough cleaning, to remove remains of material, the slit die was mounted to the single screw extruder Each transducer is calibrated and data are digitally acquired in the course of the test.
During extrusion, a uniform temperature distribution of 195°C± 2.0 °C has been maintained along the barrel and the die using separate band heaters and type J thermocouples that were attached to the control system of the extruder. In the slit, wall shear strain rates are calculated from extruder volumetric throughput and slit dimensions. These shear rates can be changed during the experiments by varying the extruder throughput.
In a flood fed plasticating extruder, the machine works at full capacity and the flow rate depends on the speed imposed on the screw only. As a result in a flood fed extruder it is possible to change the shear rate by varying the screw velocity. The use of a single extruder in flooded conditions is usually preferable because the risk of fluctuations is reduced. The use of starve fed conditions could introduce several advantages, in particular in cases of material with thermal sensitivity like WPCs. It is extremely

convenient to produce with a starved single screw extruder because the risk of degradation due to a too high viscous heating is reduced and the kinetics of melting is controlled better. In starved conditions, the throughput becomes another degree of freedom to be controlled in the process. Thus, the flow rate depends especially by the velocity imposed by the feeder. During the rheological measurements both type of feeding conditions have been used, thus the shear rate has been varied by controlling the volumetric feeder screw and the extruder screw.

6.5 Results from in – line measurements for 70%wt. PP - WPC

The wall shear stress is calculated from the pressure drop measurements along the die length as

$$\tau_w = \frac{h}{2}\frac{\Delta P}{L} \tag{6.1}$$

where *L* is the length of the slit, ΔP is the pressure drop along the slit and h is the slit height.
The pressure profiles obtained from the flush mounted transducers, measured to calculate the shear stress, must be linear. Fig. 6.14 shows some typical pressure profiles inside the slit die for different mass flow rates. The linear fit approximation of the pressure is good with a coefficient of determination (R^2) of 0.99 at least.
The apparent shear rate $\dot{\gamma}_a$ in a rectangular slit is

$$\dot{\gamma}_a = \frac{6Q}{wh^2} \tag{6.2}$$

where *w* is the width of the slit, Q is the flow rate and h is the slit height. The flow rate was determined by weighing with a laboratory scale the extruder throughput and dividing by the known density of the fluid at the testing temperature.
Fig. 6.15 shows the shear stress versus apparent shear rate for the three different heights (1.95, 4.1 , 6 mm) used for the 70% wt. WPC processing. This plot is useful in order to detect possible wall slip. The curves are fitted with a power law model and fitting parameters are listed in Tab 6.2. From the plot it is evident that the curves are not coincident. There is more flow, corresponding to an higher apparent rate, in small heights at a given shear stress. This effect corresponds to a slip influenced flow phenomenon. The slip velocity is obtained by using a

traditional Mooney analysis. In Fig. 6.16 the Mooney plot is presented. The linear fit shows a good agreement with a coefficient of determination not less than 0.98, thus it is possible to apply the standard Mooney procedure. From the slope of the Mooney curves, it is possible to find the slip velocity and the apparent shear rate without the slip velocity contribution.

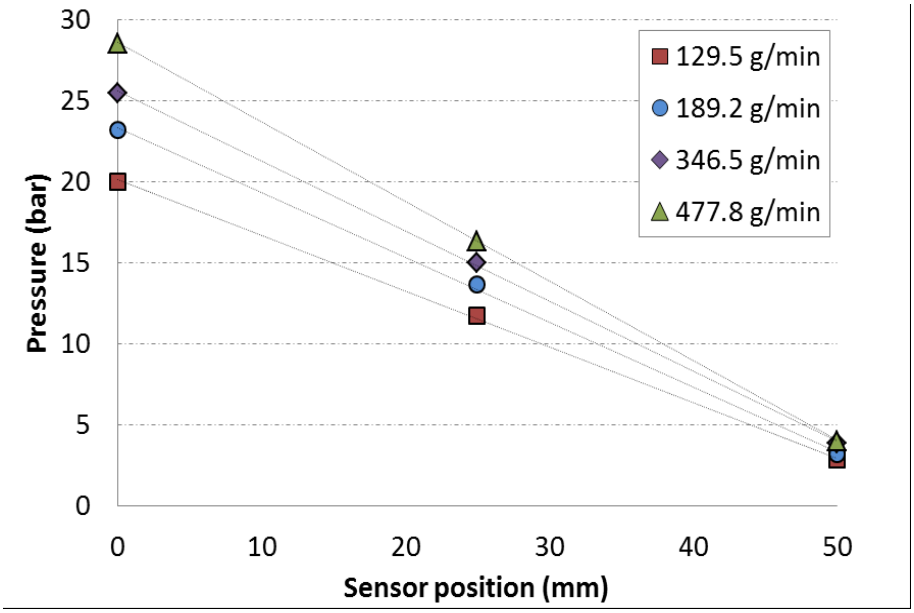

Fig. 6.14 – Pressure profile versus the sensor position for 70% wt. WPC at different mass flow rate at 195°C. The corresponding linear fits are indicated with lines.

Tab 6.2 - Power law parameters for the shear stress versus apparent shear rate curves at 195 °C for the 70% wt. at different slit heights.

Slit heights (mm)	m (Pa s^n)	n	R^2
2	41.17	0.328	0.98
4	58.03	0.445	0.98
6	63.23	0.281	0.99

In Fig. 6.17 a plot of slip velocity as function of shear stress is presented. The slip velocity increases rapidly with the shear stress. The slip velocity

values are between 4.87 – 16.73 mm/s. It is possible to expect that at slip velocities equal to zero does not correspond a zero value for the shear stress. Thus, the curve can be fitted with an equation such as

$$\boldsymbol{v_s = k(\tau - \tau_0)^n} \tag{6.3}$$

where v_s is the slip velocity, τ_0 = 71 kPa is the critical shear stress below which slip does not appear, k = 0.075 mm/s and n = 1.2 are fitting parameters.
After the Mooney procedure, using Rabinowitsch correction, it is possible to obtain the shear viscosity as function of the true shear rate (Fig. 6.18). The 70%wt. WPC viscosity decreases with the shear rate showing a shear thinning behavior. The viscosity curve has been fitted with a power law model

$$\boldsymbol{\eta = m\,\dot{\gamma}^{n-1}.} \tag{6.4}$$

where n = 0.15 is the power law exponent and m =93058 Pa s^n is the consistency index.

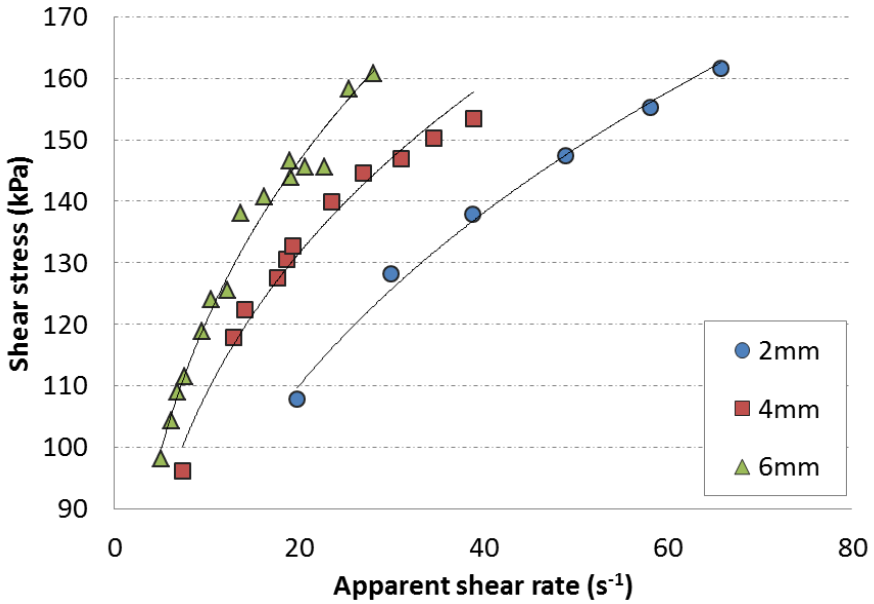

Fig. 6.15 - Shear stress versus apparent shear rate on 70% wt. WPC at 195°C. Data are fitted with power law model (lines).

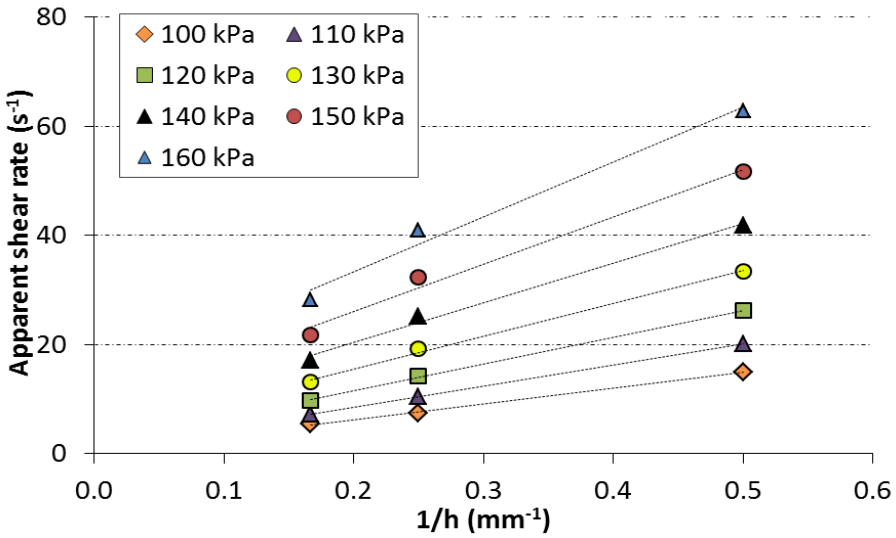

Fig. 6.16 – Standard Mooney plot for in – line measurements on 70% wt. WPC at 195°C based on the fitted curves in Fig. 6.15

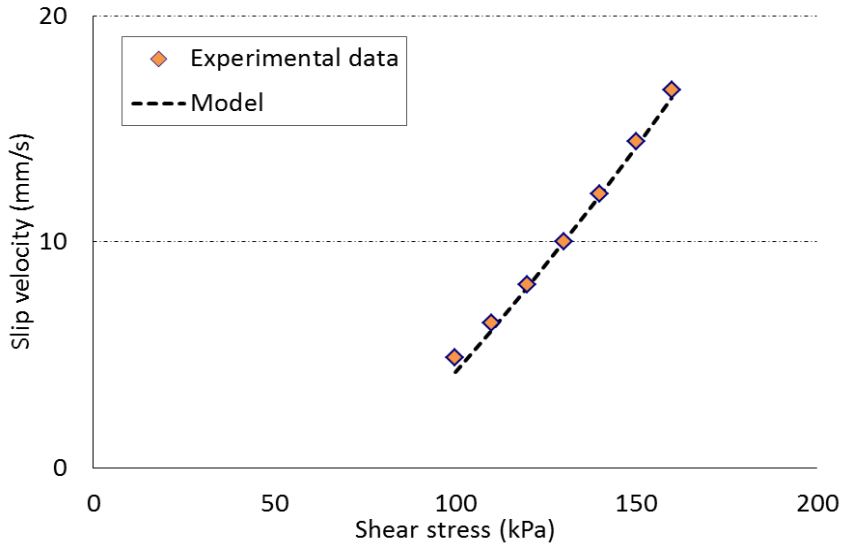

Fig. 6.17 – In line slip velocities for 70% wt. obtained from the slopes of the Mooney plot lines

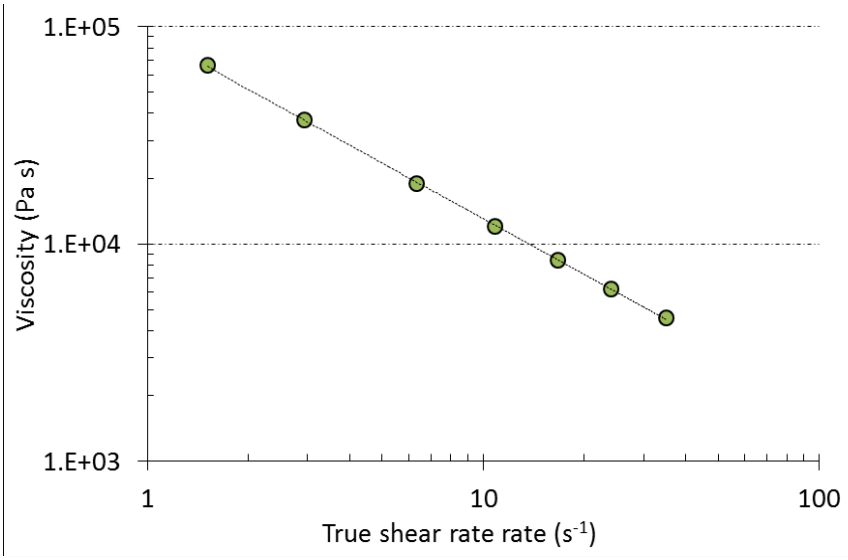

Fig. 6.18 – Shear viscosity versus true shear rate for 70% wt. WPC at 195°C. Data are fitted with power law model (line)

6.7 Results from in – line measurements for 30%wt. PP-WPC

The determination of the shear viscosity curve has been carried out with the same procedure for the 30% wt. WPC.
As for the 70% wt. WPC, also the pressure profiles along the slit of the 30% wt. WPC are linear with a good approximation and the mass flow rate was determined by weighing the extruder throughput.
Using Eq. 6.1 and Eq. 6.2, the shear stress and the apparent shear rate were calculated.
In Fig 6.19 the shear stress versus the apparent shear rate curves is pictured for the three different slit heights (1.3, 1.95, 4.1 mm) used for the 30% wt. WPC. Although also the 30% wt. WPC curves are not coincident, the difference is less pronounced. This effect corresponds to a smaller amount of slip.
The slip correction is obtained with the Mooney procedure. In Fig. 6.20 the Mooney plot is shown. The fit shows a quite good agreement with a coefficient of determination better than 0.97. Using the Mooney curves slope, it is possible to determine the slip velocity.
In Fig. 6.21 the slip velocity is shown as a function of shear stress. The slip velocity increases with the shear stress. The slip velocity values are

between 1.76 – 12.22 mm/s. The curve is fitted with Eq. 6.3. The fitting parameters are τ_0 = 1.2 kPa i.e. the shear stress below which no slip appear, k = 0.001 mm/s and n = 2.15.
Using the Rabinowitsch procedure, it is possible to correct the apparent shear rate. In Fig. 6.22 the plot of the shear viscosity versus the true shear rate is presented. The 30%wt. WPC shows the same trend of the 70% wt. WPC. The viscosity decreases with the shear rate showing a shear thinning behavior. The viscosity curve has been fitted with Eq. 6.4 and the fitting parameters are n = 0.36 and m =17140 Pa s^n.

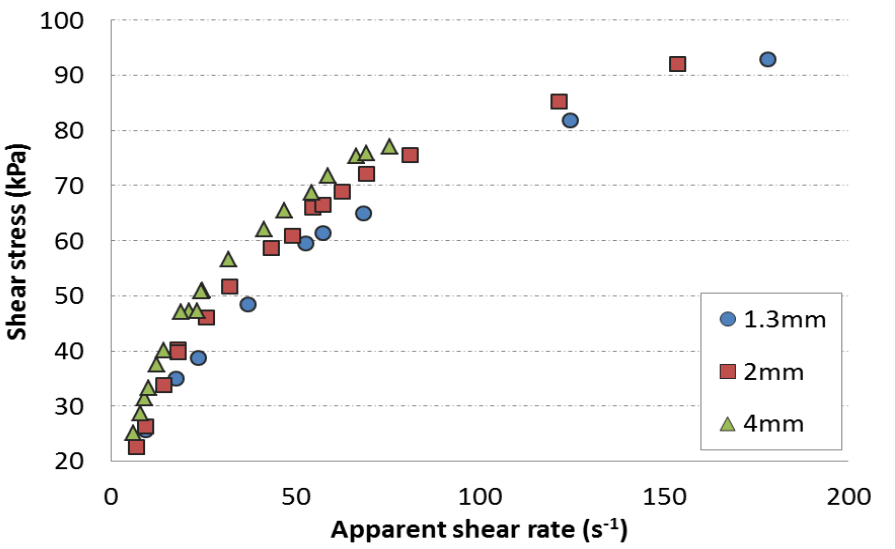

Fig. 6.19 - Shear stress versus apparent shear rate on 30% wt. WPC at 195°C.

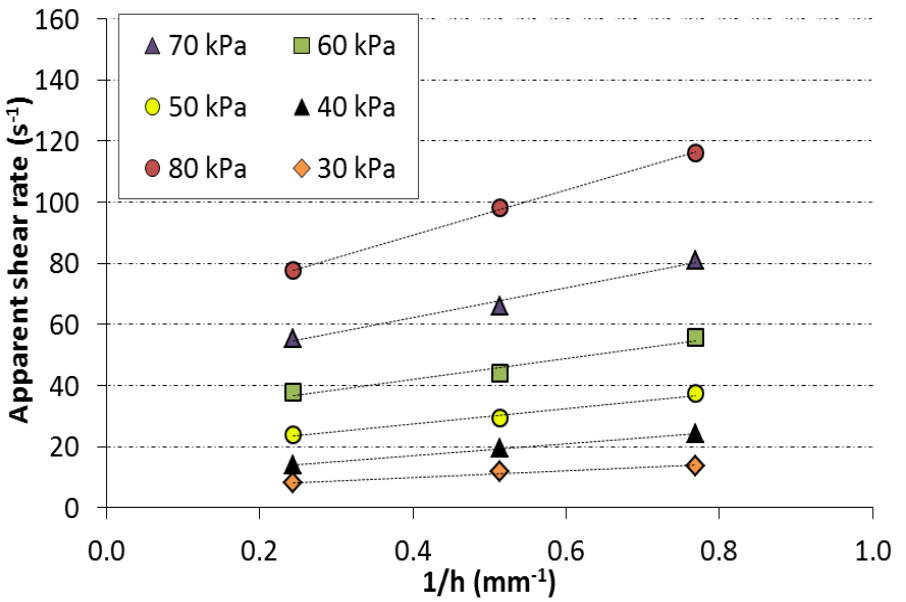

Fig. 6.20 –Mooney plot on 30% wt. WPC at 195°C

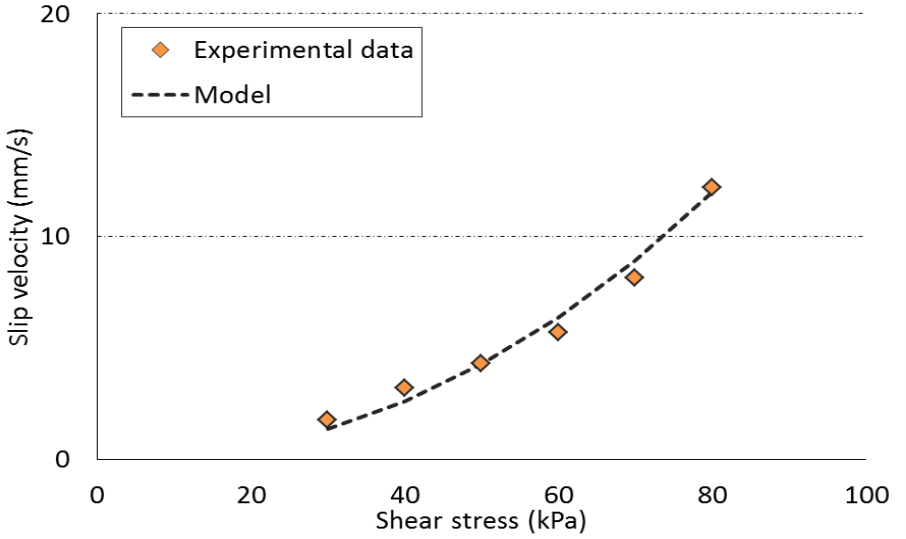

Fig. 6.21 – In line slip velocities for 30% wt. obtained from the slopes of the Mooney plot lines.

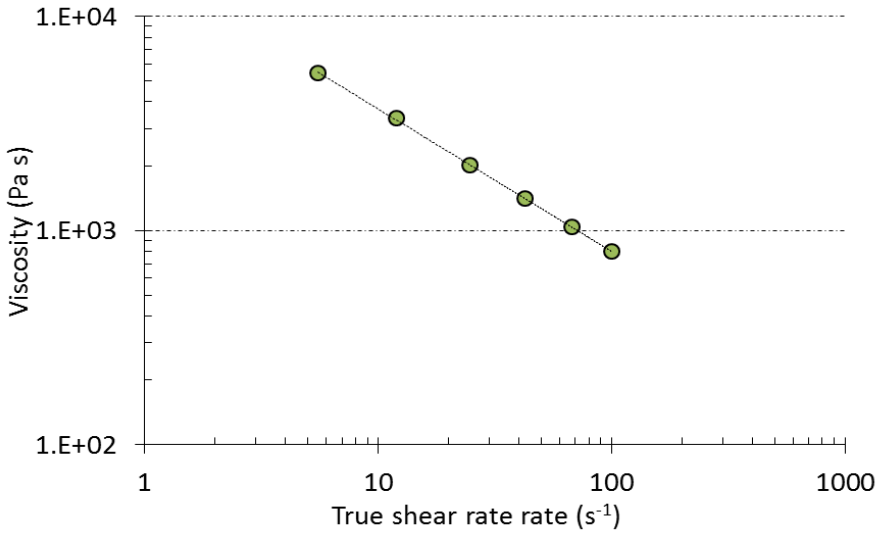

Fig. 6.22 – Shear viscosity vs. true shear rate for 30% wt. WPC at 195°C. Data are fitted with power law model (line).

6.7 Comparison between 70% wt. and 30% wt. WPCs

In Fig. 6.23 the slip velocity is presented, calculated with the Mooney procedure, versus shear stress plot for different percentage of natural filler (30%wt. and the 70% wt.). WPC. From the plot, it is well evident that both materials show a slip velocity that increases with the shear stress. The 30%wt. WPC shows a greater slip velocity than the 70% wt. WPC while the critical stress, defined as the stress at which the slip appears, is greater for the 70%wt. than the 30%wt.

Fig.6.24 provides the slip velocity as a function of true shear rate. The slip velocity increases with true shear rate and both materials show the same qualitative behavior. From this plot is evident that the 70%wt. WPC is the material more affected by the slip phenomenon.

The effect of natural fibers on shear viscosity at 195°C is presented in Fig. 6.25. Shear viscosity increases with the percentage of fibers. Both materials show a shear-thinning behavior, but the slope of the curves appear slightly different. In particular the slope of the 70% wt. is greater than the 30%wt.

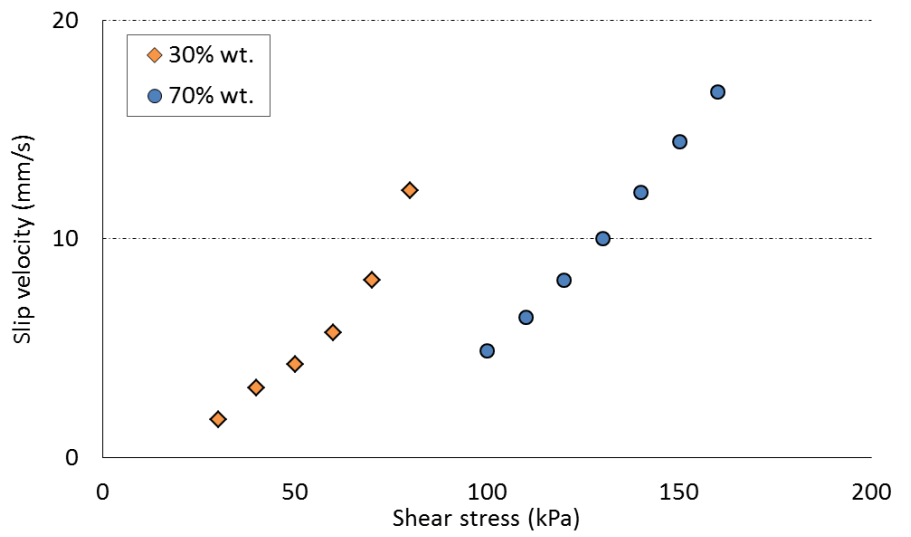

Fig. 6.23 – Slip velocity versus shear stress for 30%wt. and 70% wt.

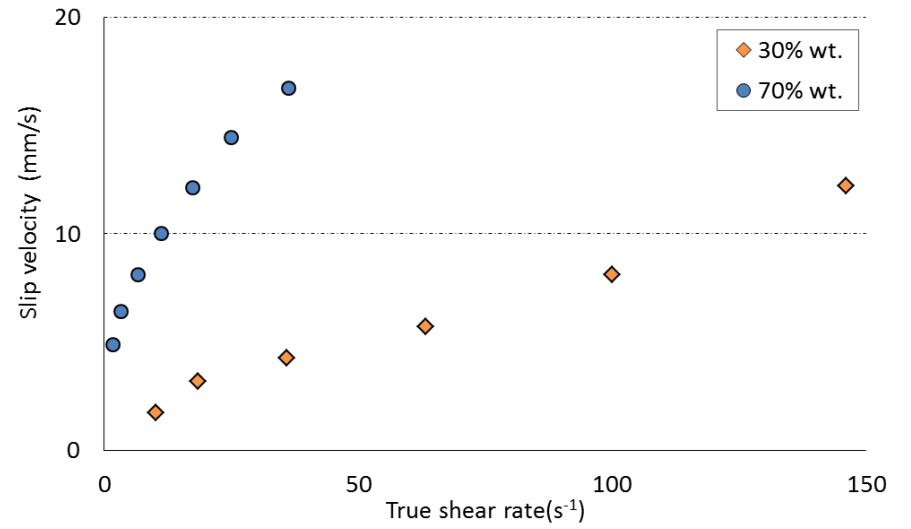

Fig. 6.24 – Slip velocity vs. true shear rate for 30%wt. and 70% wt.

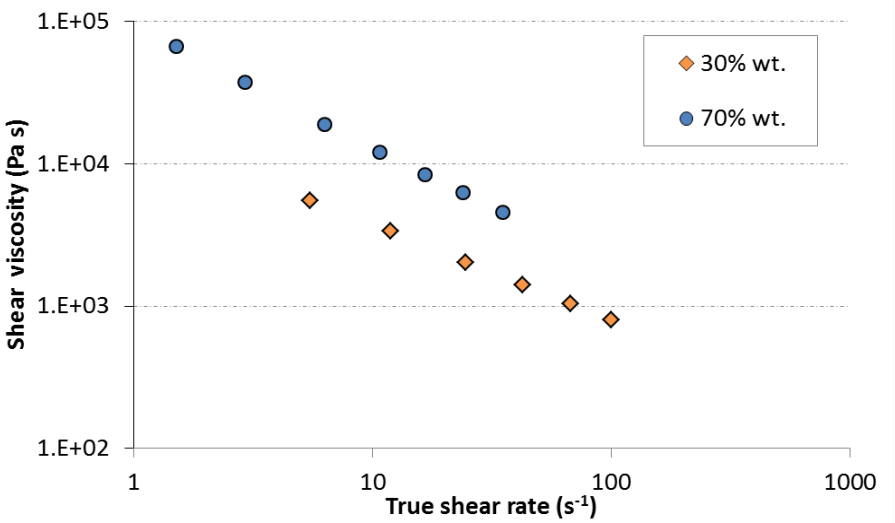

Fig. 6.25 - Shear viscosity vs. true shear rate for 30%wt. and 70% wt

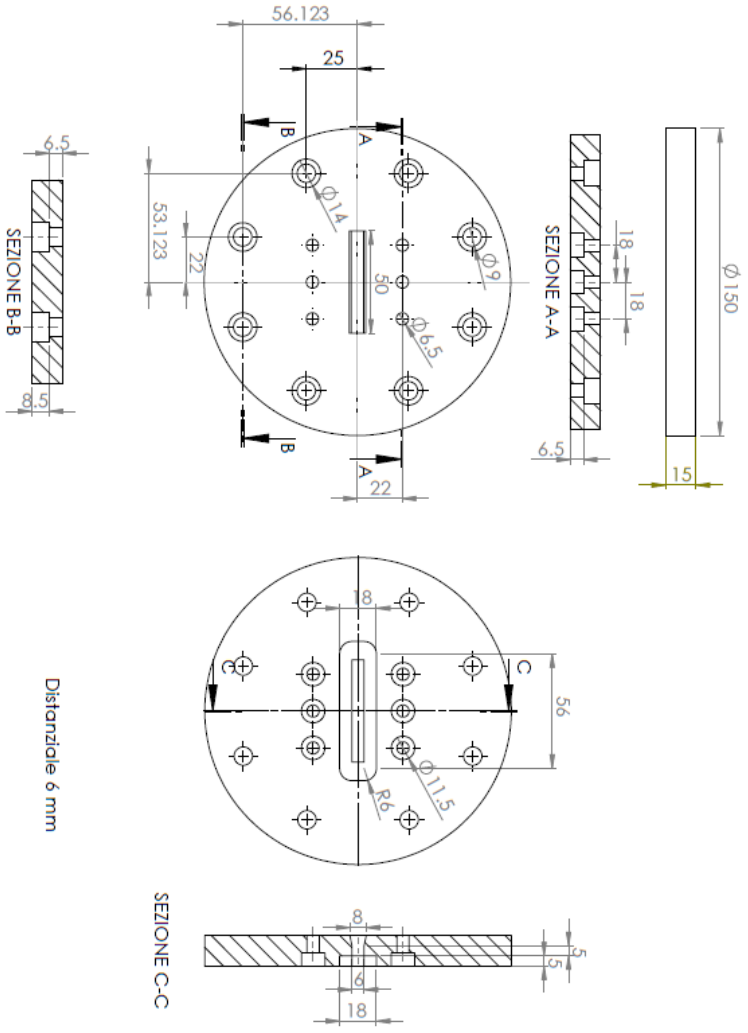
56.123
25
6.5
SEZIONE B-B
8.5
53.123
22
Ø14
Ø9
50
Ø6.5
B
A
22
SEZIONE A-A
18
18
6.5
Ø150
15
Distanziale 6 mm
18
C
C
56
Ø11.5
R6
SEZIONE C-C
8
5
5
6
18

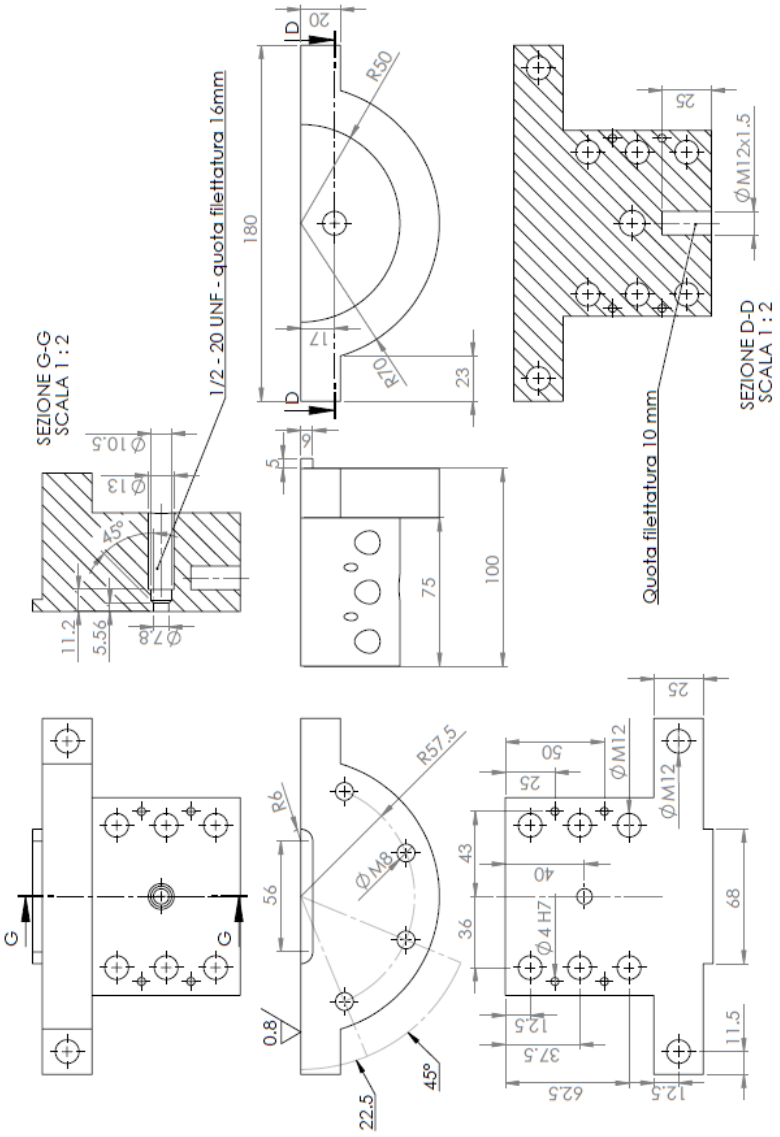
SEZIONE G-G
SCALA 1 : 2
1/2 - 20 UNF - quota filettatura 16mm
Ø10.5
Ø13
45°
11.2
5.56
Ø7.8
D
20
R50
180
17
R10
23
5
6
75
100
Quota filettatura 10 mm
SEZIONE D-D
SCALA 1 : 2
25
ØM12x1.5
G
G
R6
56
R57.5
ØM8
0.8
22.5
45°
25
50
25
ØM12
ØM12
43
40
36
Ø4 H7
68
12.5
37.5
62.5
12.5
11.5

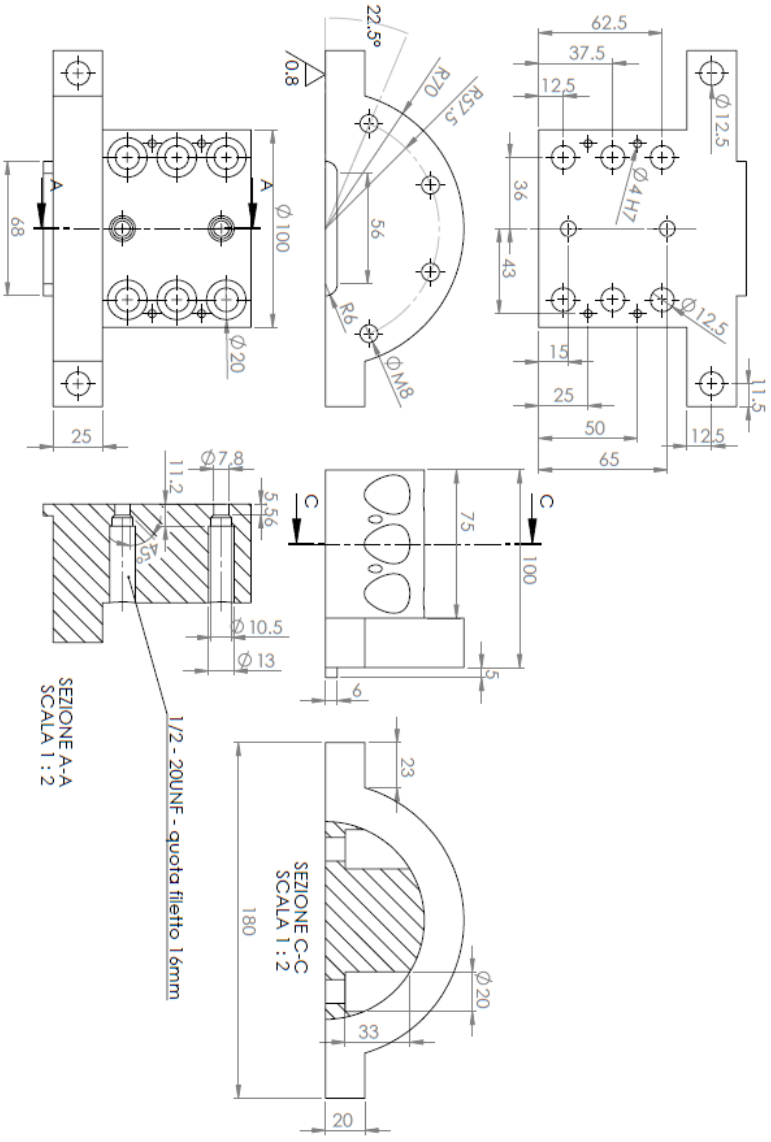
22.5°
0.8
R70
R57.5
62.5
37.5
12.5
Ø 12.5
Ø 4 H7
36
43
Ø 12.5
15
25
50
65
12.5
11.5
A
A
68
Ø 100
Ø 20
56
R6
ØM8
25
Ø 7.8
11.2
5.56
15°
Ø 10.5
Ø 13
C
C
75
100
5
6
SEZIONE A-A
SCALA 1 : 2
1/2 - 20UNF - quota filetto 16mm
23
180
SEZIONE C-C
SCALA 1 : 2
Ø 20
33
20

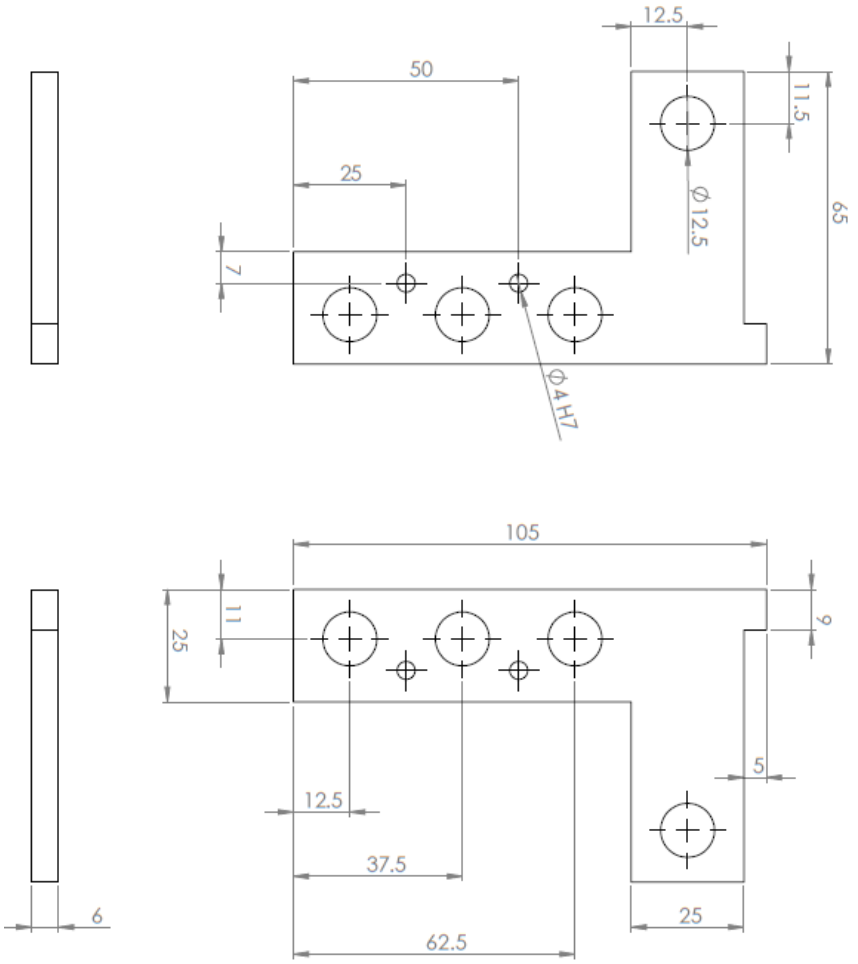
12.5
50
11.5
25
Φ12.5
65
7
ΦA H7
105
11
25
9
5
12.5
37.5
25
6
62.5

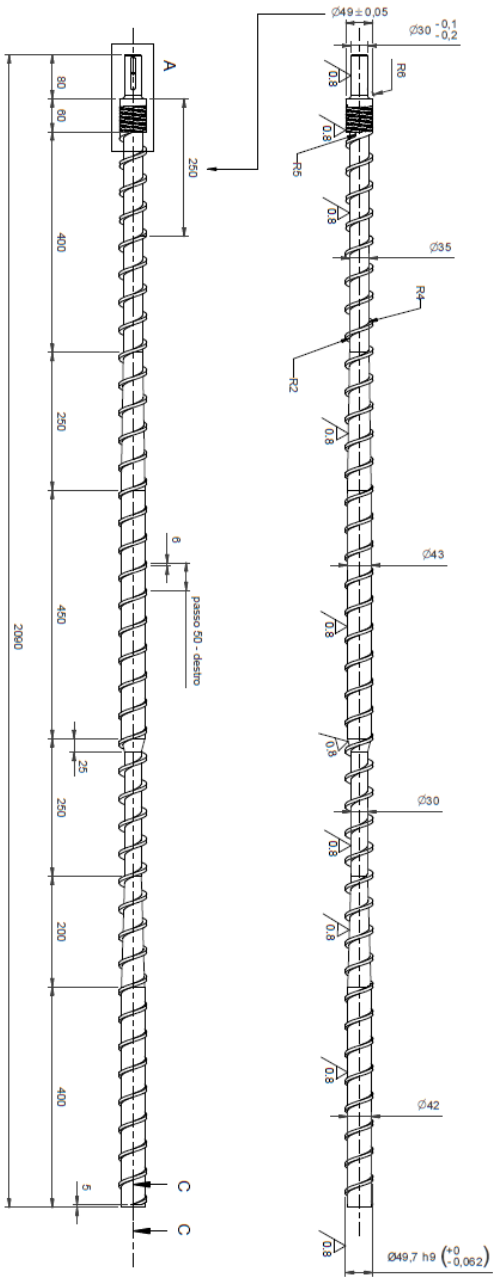
Ø49 ± 0,05
Ø30 -0,1 -0,2
R6
R5
R4
R2
Ø35
Ø43
Ø30
Ø42
Ø49,7 h9 (+0 -0,062)
0,8
A
C
C
80
60
250
400
250
450
250
200
400
2090
6
passo 50 - destro
25
5

CHAPTER 7

CONCLUDING REMARKS

The aim of this thesis has been to investigate the mechanical and rheological properties of PP based Wood Polymer Composites.
The work has been developed in several phases. At the first step, PP – WPC, at various wood fiber percentages, has been characterized from the mechanical, thermal and rheological point of view. The mechanical characterization has shown that wood fibers make the composite stiffer without lowering strength values too much, while thermal properties have confirmed that the processing window for this material is rather narrow, being limited upwards by wood fiber degradation and downwards by the melting temperature, which is around 165°C.
Classical off – line rheological measurements on WPCs have been performed both with parallel plate and capillary rheometer at 170°C. Complex viscosity increases with the percentage of fibers. All materials show a shear-thinning behavior with similar slopes of the flow curves and neat PP also displays a Newtonian plateau at low shear rates. The testing temperature is imposed by the possibility of performing the parallel plate testing within the linear viscoelasticity region, but the data that are measured are not directly useful for processing, as a convenient processing temperature should be around 185°C – 195°C.
In order to obtain the WPC viscosity at such temperatures, the model presented in Chapter 5 (Eq. 11) has been proposed. This model uses the WPC viscosity measured at 170°C at various wood quantities and of neat PP viscosity measured at various temperatures in the 170°C – 200°C range. These measurements have been used to create shift factors that allow to estimate the WPC viscosity on the basis of neat PP viscosity, temperature and wood fibers content.
In order to validate the model, it is necessary to evaluate the flow curve of PP - WPC material at a temperature other than 170°C. This has been possible using an instrumented extruder slit die. This instrument allows the determination of the flow characteristics of the material in a condition that is very similar to the actual processing conditions.
In Fig. 7.1 shear viscosity versus shear rate, obtained with the in – line rheometer, for 30%wt. and 70%wt. WPCs are presented (orange and blue curves). In the plot these curves are compared with complex viscosity versus frequency for both materials (black curves), but measured with

standard off line viscosimetry (Ares TA Instruments) and shifted using the model of Chapter 5.

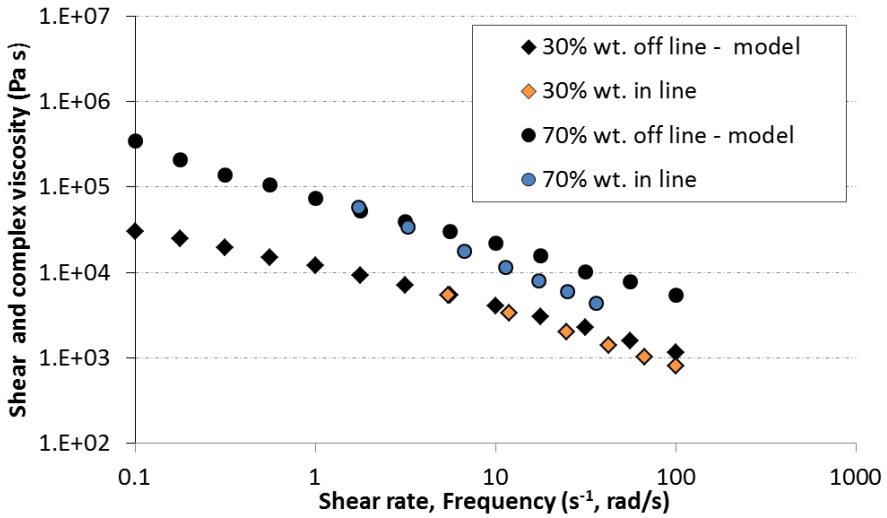

Fig. 7.1 - True shear viscosity vs. shear rate for 30% wt. and 70% wt. calculated with in – line rheometer. For comparison complex viscosity vs. frequency for 30% wt. and 70% measured with standard off line rheometer (Ares TA Instruments) and using the model described in Chapter 5 are presented.

The results from in – line and off – line viscometry are in reasonably good quantitative agreement, in particular for the 30% wt. WPC. Nevertheless, the curves do not match perfectly, in particular for the 70% wt. WPC. Here, the viscosity curve obtained with the in – line rheometer appears with a slope that is greater than the one performed with the off – line rheometer and shifted using the model.
Rauwendaal and Fernandez (1989) gave a possible reason for the non-complete agreement between in - line and off –line rheological measurements. The authors observed that, for a non-filled material (HDPE), the in - line measurements are underestimated compared with capillary measurements. This behavior can be explained because a substantial amount of shearing deformation prior to measurement, caused by the single screw extruder on the polymer, reduces viscosity by shear thinning and viscoelastic effect. The state in which the WPC melt reaches the channel is affected by a strong shear history. The amount of shear

effect depends on the environment, the shear rate and the time elapsed between the preshearing and the measurement. This reason, despite being non completely exhaustive for such a difference in slope for the 70%wt. WPC, is anyway very relevant.
Another reason of a non-perfect match between the two curves, might be related to the presence of uncertainties during the measurements of shear stress Eq. 6.1 and apparent shear rate in the presence of slip Eq. 6.2 and the procedures for obtaining the viscosity with the slit rheometer, i.e. the Mooney and Rabinowitsch procedures. These uncertainties are due to the complexity of the rheological experimentation and could make the measure not reliable.
In order to quantify these contributions, the analysis of the uncertainties has been performed in agreement with ISO/IEC Guide 98 (1995).
The total uncertainties on τ and $\dot{\gamma}_{app}$ are around 8.6% and 10.8%, respectively. These values are relatively very high, but one has to consider that they have been calculated for the condition of greater uncertainty.
In Tab. 7.1 the uncertainty contributions for each of the parameters involved in the calculations are listed. If the aim is to minimize the total uncertainties, the parameter that must be measured with greatest accuracy is the slit height.

Tab. 7.1 – Shear stress and apparent shear rate in presence of slip parameters and corresponding relative uncertainties.

Shear stress parameters	Relative uncertainties
h	5%
L	0.076%
P_1 and P_2	5%
Apparent shear rate parameters	**Relative uncertainties**
m	2%
W	0.1%
h	10%
ρ	2%
t	3%

Moreover, although the measurements made using the in - line rheometer are apparently direct measurements, they require the correction for slip (Mooney procedure) and for the non – Newtonian behavior (Rabinowitch correction). Both are well-known and necessary but render the measurements indirect and affected by additional uncertainties related to

the fitting that is involved in the procedure. In spite of this, the measurement uncertainties, though not negligible, still do not completely explain the differences between the slope of the 30% wt. and the 70% wt. WPC.
In Tab. 7.2 the power law fitting parameters, for all curves (Fig. 7.1), are presented. Observing the pseudoplastic index (i.e. the slope of the viscosity curve in the log-log plot), the 70%wt. has an extremely low value.
Comparing the pseudoplastic index values for the 30% wt. and the 70% wt. in – line measures, there is a large difference between the two WPCs, while the off – line measures are much closer.

Tab. 7.2 – Power law parameters for the shear viscosity versus true shear rate curves at 195 °C for 30% wt. and 70% wt. WPC and for the complex viscosity versus frequency for 30% wt. and 70% WPC measured with standard off line rheometer (Ares TA Instruments) and shifted with the model described in Chapter 5.

WPC	m (kPa s^n)	n
30% wt. in - line	17.5	0.33
30% wt. off - line	15.0	0.44
70% wt. in - line	91.0	0.15
70% wt. off - line	78.12	0.40

This extremely shear thinning behavior could be investigated by observing the evolution of the shear stress as a function of the true shear rate. In Fig. 7.2, shear stress versus true shear rate for the 70%wt. and 30% wt. WPC are presented. From this plot, a non-Newtonian behavior is confirmed. Both materials show the same qualitative trend with a shear stress that increases with true shear rate and with the percentage of fibers. The range of shear rates that are measured is rather limited. The values are between 1.51 – 35.1 $s^{-1}$for the 70% wt. and 5.50 – 42.04 s^{-1} for the 30% wt.
The trend of the curves, in particular for the 70%wt. WPC, suggests the presence of an yield stress. This could explain the particular low pseudoplastic index value for the highly filled material. In order to take this into account, a model that includes the yield stress, such as the Herschel – Bulkley equation (Eq. 2.14), can be used.
In Tab. 7.3, the Herschel Bulkley fitting parameters are presented. Using this model, the pseudoplastic index for the 70% wt., increases up to a

reasonable value and both WPCs thus show similar values of pseudoplastic index.
Observing the 70% wt. fitting values, the relatively high τ_0 value confirms the presence of yield, while the 30% wt. shows a τ_0 that is almost negligible, thus the presence of yield stress is not so evident.

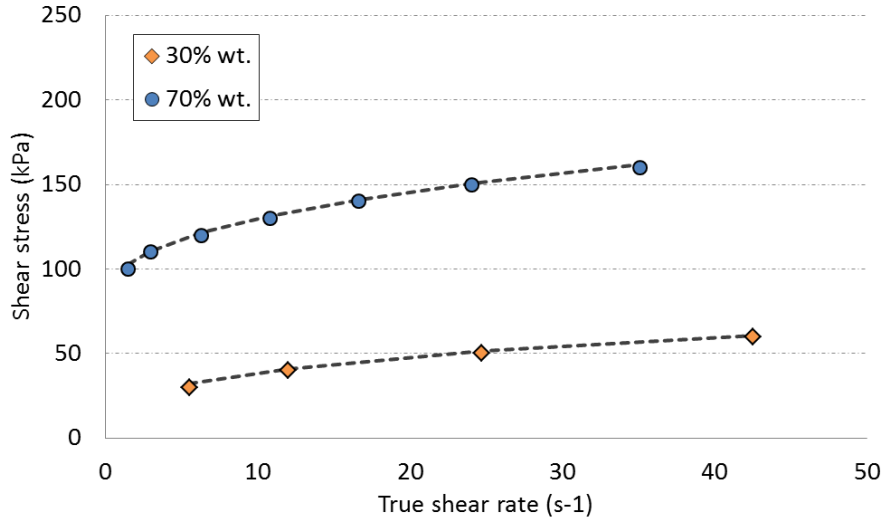

Fig. 7.2 – Shear stress vs. shear rate for 30% wt. and 70% wt. Data are fitted with Herschel–Bulkley model (dotted line)

Tab. 7.3 - Herschel–Bulkley parameters for the shear stress versus true shear rate curves at 195 °C for 30% wt. and 70% wt. WPCs.

WPC	m (kPa s^n)	n	τ_0(kPa)
30% wt.	16	0.35	1
70% wt.	25	0.34	76

The off-line measurements also need to be discussed concerning their reliability. The off – line viscosity curves at 170°C have been obtained by assuming that the WPCs obey the Cox Mertz rule. This assumption sometimes is not true for filled materials: in fact, the Cox - Merz rule is known not to work in two main cases, i.e. fibers alignment and presence of an yield stress.
The validity of the Cox Mertz rule is linked to the structure formed by natural fibers and how this changes during the rheological test. As an

example, in an oscillation mode rheometer, the fibers usually are randomly oriented [Ausias (1992)] while in a capillary/slit rheometer they align along the flow direction [Barbosa (2000)]. As a result, data obtained with capillary rheometer are much lower than the ones obtained with oscillation measurements [Le Moigne].
In the case of the present work, this potential source of uncertainty cannot be completely eliminated. In fact, although the samples used for oscillation tests were obtained from an extruded profile and the fibers were aligned along the extrusion direction, they were not oriented along the shear stress direction.
The other case in which the Cox - Mertz rule is not reliable is the presence of an yield stress. Since the 70%wt. shows the presence of an yield stress, the reliability of the data using the Cox – Mertz rule for the highly filled material is questionable. The behavior of 30% wt., however, does not show the presence of the yield stress and thus confirms the validity of the Cox – Mertz rule and the reliability of the tests.
The comparison between the off - line and the in – line data at 195°C, is not direct but is obtained using the model proposed in Chapter 5. In order to verify the reliability of the off – line curves at 195°C it is necessary to discuss the hypothesis involved in the realization of such a model. The main simplifying hypothesis, in addition to the validity of the Cox – Mertz rule, was that the effects of temperature and filler content on the composite viscosity are assumed to be disjoint.
The meaning of this hypothesis is that the effects of temperature variation and concentration of filler on the rheological properties of the WPC must superpose without interference.
Observing Figs. 7.3 and 7.4, it is evident that the viscosity increases with decreasing temperature and increases with the percentage of fibers. Moreover, the viscosity curves at different percentage of fibers and the neat PP at different temperatures show quite similar slopes, while the consistency indices are different. This means that both temperature and percentage of fibers do not affect the pseudoplastic character of the material, but act only in the sense of increasing or decreasing the viscosity.
At the microscopic level, an increase in temperature increases the mobility of the chains and reduces the entanglement forces that are present between the macromolecular chains and hence reduces the viscosity [Birley 1991].

On the other hand, an increase in the percentage of fibers has the effect of reducing the room available for the polymeric matrix flow and this produces an increase in the viscosity.
In the light of the foregoing considerations, the viscosity is only influenced by the steric impediment due to the structure formed by the natural fibers and by the mobility of the polypropylene chains.
The temperature and the fibers concentration variations may thus be considered disjoint: a viscosity increase due to a temperature decrease is not influenced by an increase in the fibers concentration, in that this effect occurs at the scale of the macromolecules dimension, i.e. of sub micrometer order, while the fibers are of hundreds of micrometers (Tab.5.1), thus the mobility of the PP chains due to a temperature effect will not be affected by an increase in the percentage of fibers.
On the other hand, excluding the phenomenon of degradation, the increase of viscosity due to the steric impediment of the fibers is not affected by temperature: the temperature range is not sufficient to increase the volume occupied by the fibers by thermal expansion of wood and to reduce the voids in which the matrix flows.
On the basis of the findings of this work, the viscosity curve for the 30% wt. WPC validates the model presented with a reasonably good agreement. Since the agreement for the 70% wt. is less justified and such a material displays a marked yield stress, we can conclude that it is the yield stress that is probably the single issue that makes the present model questionable.
In this regard, a future work that we propose is to modify the model by selecting a Carreau-Yasuda model with a yield stress to account for the increase in the viscosity at low shear rates. Thus, an important development will be to measure the values of the yield stress at different fiber concentrations and temperatures and to evaluate the minimum value of fiber percentage for which it appears. A method to measure yield stress is to use a rheometer in stress control mode. This type of test provides a shear stress ramp and measures the stress in correspondence of the viscosity peak. Prior to this viscosity peak, the material is undergoing elastic deformation and hence the strain rate is almost constant even though the stress is increasing linearly. This peak in viscosity represents the point at which the elastic structure breaks down (yield) and the material begins to flow. This coincides with a rapid increase in shear rate and a consequent reduction in viscosity.

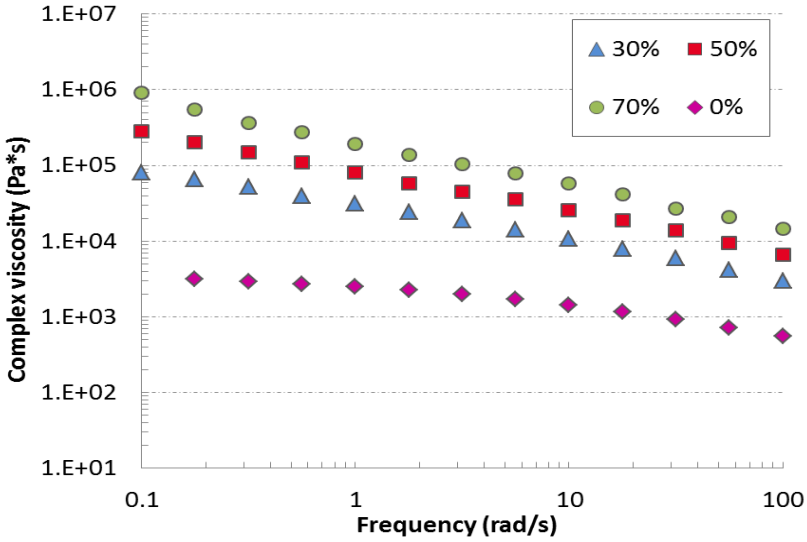

Fig. 7.3 - Complex viscosity as a function of frequency for different percentages of fibers using off – line rheometer.

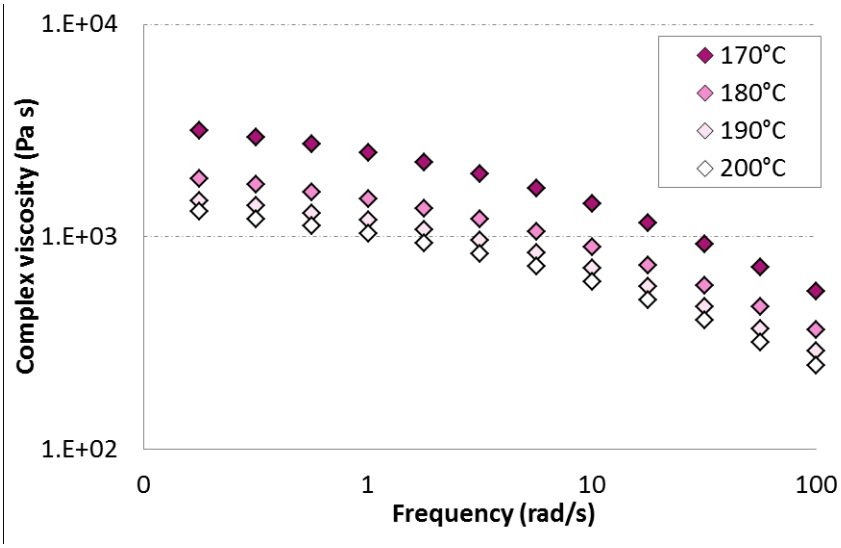

Fig. 7.4 - Complex viscosity of neat PP as a function of frequency at various temperatures using off – line rheometer.

REFERENCES

Adhikary K. B., Park C. B., J. of Thermoplastic Composite Materials, 24, 155-171 (2011)

Aho J., Syrjala S., Polym testing, 30, 595 – 601 (2011)

Alimkaynak A., Crabtree S.L., Intern Polymer Processing XXVI 2 (2011)

Ares A., R. Bouza, S. G. Pardo, M. J. Abad, L. Barral, J. Polymer Environ, 18, 318-325 (2010)

Ashori A., Biosurce technology, 99, 4661 – 4667 (2008)

Ashori A., Nourbakhsh A., Waste Managment, 30, 680 – 684 (2010)

Ausias, G.; Agassant, J. F.; Vincent, M.; Lafleur, P. G.; Lavoie, P. A.; Carreau, P. J. J.of Rheology, 36,525 - 542 (1992)

Azizi H., I. Ghasemi, Polym. Compos., 30, 429-435(2009)

Bagley E. B., J. Appl. Phys. 28, 624 (1957)

Barbosa, S.E., Kenny J.M., Polym Engin Sci 40, 11-22. (2000)

Bariani P.F., Salvador M., Lucchetta G., J. Mat. Process Tech, 191, 119 – 122 (2007)

Barnes H. A., Rheology Review, 1-36 (2003)

Beckermann G. W., Pickering K. L., Composites: Part A, 40, 210-217 (2009)

Berker, R., Handbuch der Physik, 2, 1–384 (1963)

Birley A. W., Haworth B., and Batchelor J., Physics of plastics Hanser Publishers, Munich, (1991)

Bismarck A., Baltazar Y Jimenez, Sarlakakis K., Development and Sustainability. 8, 445-463 (2006)

Bledzki A., Faruk O., J. Composite Materials., 10, 365-379 (2003)

Bledzky A. K., Gassan J., Theis S. Machanic Composite Materials, 34, 563 – 568 (1998)

Bouafif H., Koubaa A., Perré P., Cloutier A., Riedl B., J. App. Polym. Sci., 113, 593-600 (2009)

Bouza R., S. G. Pardo, L. Barral, M. J. Abad, Polym. Compos., 30, 880-886 (2009)

Broyer E. and Tadmor Z., Polym.Eng.Sci.,12,1,12-24 (1972)

Brydson J. A. Plastics Materials, seventh edition, Butterworth Heinemann (1999)

Carreau J.P. DeKee D. Chhabra R.P. Rheology of polymeric systems principles and applications, Hanser/Gardner Publications, Cincinnati, OH (1997)

Carrino L., S. Ciliberto, G. Giorleo, U. Prisco, Polym. Compos., 32, 796-809 (2011)

Cheung H., Ho M., Lau K., Cardona F., Hui D. Composites: Part B, 40, 655 – 663 (2009)

Cheung Hoy-Yan, Ho Mei-po, Lau Kin-tak, Cardona F.,Hui D., Composites Part B, 40, 655-663 (2009)

Chiu Hsien-Tang, Chiu Wei-Ming, Materials Chemistry and Physics 56, 108-115 (1998)

Clemons, C. Forest Products Journal, 52, 10 -18 (2002)

Coates P.D., Rose R.M., Wilkinson B., Plast. Rubb. Compo. Process. App. 23, 295 – 303 (1995)

Cox W.P. and Merz E.H., Journal of Polymer Science, 28, 619 (1958)

Cross M. M., Rheology of non-Newtonian fluids- A new flow equation for pseudoplastic systems, J. Colloid. Sci., 20(5) (1965)
Cui Y, Lee S., Noruziaan B. Cheung M., Tao J. Composites: Part A, 39, 655 – 661 (2008)

Darnell W. H. and Mol. A. E. J., Soc.Plast.Engs.J.,12,20-28(1956)

Das. S., Saha A. K., Choundhury P. K., Basak R. K., Mitra B.C., Todd T., Lang S., Rowell R.M., J. App. Polym. Sci., 76, 1652 – 1661 (1999)

Englund K., V. Villechevrolle, J. App. Polym. Sci., 120, 1034-1039 (2011)

Fernandez A., Muniesa M., Javierre C., Polym testing, 33, 107 - 115 (2014)

Ferrini F., D. Ercolani, B. de Cindio, L. Nicodemo, L. Nicolais, S. Ramaudo, Rheol. Acta, 18, 289-296 (1979)

Gao H., Song Y. M., Wang M., J. of Forestry Research, 19, 315 – 318 (2008)

Glomsaker T., Hinrichsen E. L., Thorsteinsen P., Polym Eng. Sci, 41, 2231 - 2248 (2001)

Godard F., M. Vincent, J. F. Agassant, B. Vergnes, J. App. Polym. Sci., 112, 2559-2566 (2009)

Gonzàlez-Sànchez C., C. Fonseca-Valero, A. Ochoa-Mendoza,A. Garriga-Meco, E. Rodriguez-Hurtado, Composites: Part A, 42, 1075-1083 (2011)

Gou G., Xie P., Yang W., Ding Y., Polym testing, 31, 826 – 832 (2011)

Guo W., C. J. Lim, X. Bi, S. Sokhansanj,S. Melin, Fuel, 103, 347-355 (2013)

Herschel, W.H.; Bulkley, R., Kolloid Zeitschrift 39, 291–300 (1926)

Highgate D. J., R. W. Whorlow, Rheol. Acta, 9, 569 – 576 (1970)

Hosseinaei O., Wang S., Enayati A. A., Rials T. G., Comp. Part A, 43, 686 – 694 (2012)

Hristov V., E. Takàcs, J. Vlachopoulos, Polym. Eng. Sci., 46, 1204-1214 (2006)

Hristov V., J. Vlachopoulos, Rheolo. Acta, 46, 773-783 (2007)
Huang H. X., J. J. Zhang, J. App. Polym. Sci., 111, 2806-2812 (2009)

Hugot F., G. Cazaurang, J. Of Wood Chemistry and Technology, 28, 283-295 (2008)
Hugot F., G. Cazaurang, Mécanique & Industries, 10, 519-524 (2009)

Ichazo M. N., Albano C., Gonzàles J., Perera R., Candal M. V., Composites Structures, 54, 207-214 (2001)

ISO/IEC Guide 98 *(*1995*)* A Guide to Expression of Uncertainty in Measurement*.*

Jeske H., Schirp A., Cornelius F., Termochim. Acta, 543, 165-171 (2012)

Kacir L. and Tadmor Z., Polym. Eng.Sci.,12,5,387-395 (1972)

Karian H. G., Handbook of Polypropylene and Polypropylene Composites, Revised and Expanded, CRC Press (2003)

Kelly A.L., Woodhead M., Coates P.D., Barnwell D., Martin K. Intern. Polymer Processing, 4, 355 – 360 (2000)

Kim J. K., Pal K. Recent Advances in the Processing of Wood – Plastic Composites, Springer (2010)

Klyosov A. A. Wood Plastic Composites Wiley (2007)

Kumari R., Ito H., Yakanani M, Uchiyama M., Okamoto T., J. Wood Sci., 53, 470 – 480 (2007)
Kuruvilla J., Sabu T., Pavithran C., Polymer, 37, 5139-5149 (1996)

Le Mogne N., M van den Oever, T. Budtova, Polym. Eng. Sci., 53, 2582–2593 (2013)

Leu Shao-Yuan, Tsu-Hsien Yang, Sheng-Fong Lo, Te-Hsin Yang, Construction and Building Materials, 29, 120-127 (2012)

Li T. Q., M. P. Wolcott, Composites: Part A, 35, 303-311 (2004)

Li T. Q., M. P. Wolcott, Polym. Eng. Sci., 45, 549-559 (2005)

Li T. Q., Wolcott M. P., Polym. Eng. Sci., 46, 464-473 (2006)
Lodge A. S., Rheol Acta, 35, 110 – 116 (1996)

Lodge A.S., Vargas L., Rheol Acta 22,151 – 170 (1983)

Lu J. Z., Wu Q., Negulesco I. I., J. App. Polym. Sci., 96, 93-102 (2005)

Maddock B. H., A visual analysis of flow an d mixing in extruder screws, SPE ANTEC Proceedings, New York , NY, Jan., (1959)

Maiti S. N., R. Subbarao, M. N. Ibrahim, J. App. Polym. Sci., 91, 644-650 (2004)

Maldas D., Kokta B. V., Polym. Eng. Sci., 31, 1351–1357 (1991)

Maldas D., Kokta B.V., Raj R., Deneault C., Polymer, 29, 1255-1265 (1988)

Marcovich N. E., M. M. Reboredo, J. Kenny, M. I. Aranguren, Rheol Acta, 43, 293-303 (2004)

Marcovich N.E., Aranguren M. i., Reboredo M.M., Polymer, 42, 815-825 (2001)

Markarian J., Plastics, Additives and Compounding, 4, 20–25 (2008)

Markarian J., Plastics, Additives and Compounding, 7, 20–26 (2005)

Migneault S., Koubaa A., Erchiqui F., Chaala A., Englund K., Krause C., Wolcott M., J. App. Polym. Sci., 110, 1085-1092 (2008)

Mohanty A. K., Misra M., Polym. Plast Technol Eng, 34, 729 - 792 (1995)

Mooney M., J. Rheol. 2, 210-222(1931)

Morrison F. A An Introduction to Fluid Mechanics (Cambridge University Press, 2013)

Nabi Saheb D. and Jog J. P., Adv. Polym. Technology, 18, 351 – 363 (1999)

Nabi Saheb D., Jog J.P., Adv. Polym. Tech, 18, 351 – 363 (1999)

Ndiaye D., Matuana L. M., Morlat-Therias S., Vidal L., Tidjani A., Gardette J. L., J. App. Polym. Sci., 119, 3321-3328 (2011)

Pabedinskas A., Cluett W. R., Balke S. T., Polym. Eng. Sci., 31, 365 – 375 (1991)

Padmanabhan M., Bhattacharya M., Rheol Acta, 33, 71 – 87 (1994)

Paul S.A., C. Sinturel, K. Joseph, G. D. Gem Mathew, L. A. Pothan, S. Thomas, Polym. Eng. Sci., 50, 384-395 (2010)

Polec I., Hine P.J., Bonner M. J., Ward I. M., Barton D. C., Comp. Sci. and Tech., 70, 45 – 52 (2010)

Pritchard G. Reinforced plastics, 48, 26–29 (2004)

Raj R. G., Kokta B. V., Polym. Eng. Sci., 31, 1358–1362 (1991)
Ramamurthy AV, J Rheology 30, 337-357(1986)

Ramiah M. V., J. App. Polym. Sci., 14, 1323-1337 (1970)

Rauwendaal C., Fernandez F., 25, 765 – 771 (1985)

Rauwendaal C., Polymer Extrusion, Cincinnati, Hanser Gardner Publications, Inc. (1985)

Sabaa M. W. Polym Degrad Stab, 32, 209 – 217 (1991)

Schirp A., Stender J., Eur. J. Wood Prod, 68, 219-231 (2010)

Scott Blair G., Hening W., , Wagstaff J.C., J. Phys. Chem., 43, 853–864(1939)

Shahi P., Behravesh A. H., , Daryabari S. Y, Lotfi M., Polym. Compos., 33, 753-763 (2012)

Son Y, Polymer, 48, 632–637 (2007)

Soury E., A. H. Behravesh, G. M. Rizvi, N. J. Jam, J. Polymer Environ, 20, 998-1006 (2012)

Street L. F., Int Plast. Eng., 12-89 (1961)

Sundstrom D.H. and Lo J. R., Polym. Eng. Sci. 18,422 (1978)

Tadmor Z. and Gogos C.G., Principles of polymer processing, United States, John Wiley & Sons Inc. (1979)

Tadmor Z. and Klein I., Engineering principles of plasticating extrusion, New York, Van Nostrand Reinhold Book Co. (1970)
Tadmor Z., and. Broyer, Polym.Eng.Sci.,12,5,378-386 (1972)

Tadmor Z., Polym.Eng.Sci.,6,3,185-190 (1966)

Tanner I. R., Engineering rheology, Oxford Engineering science series 52 (2002)

Tasdemir M., Biltekin H., Caneba G.T., J. App. Polym. Sci., 112, 3095 – 3102 (2009)

Tasdemir M., H. Biltekin, G. T. Caneba, J. App. Polym. Sci., 112, 3095-3102 (2009)

Teixeira P.F., Hilliou L., Covas J., Maia J.M., Rheol Acta, 52, 661 – 672 (2013)

Thibault F., Blouin D., Polym.Eng.Sci, 34,18,1377-1386, (1994)
Thorsteinsen P, Hinrichsen E. L., Glomsaker T., J vinyl & additive tech., 9, 188 - 197 (2003)

Trappe V., D. A. Weitz, Phys. Rev. Lett., 85, 449-452 (2000)

Tserki V., Zafeiropoulos N. E., Simon F., Panayiotou C., Comp. Part A, 36, 1110 – 1118 (2005)

Vanderwal A., J. J. Mulder, R. J. Gaymans,Polymer, 39, 5477-5481, (1998)

Viksne A., Rence L., Progress in Rubber and Recycling Technology, 24, 153- 169(2008)

Wales J.L.S., den Otter J.L.. Janeschitz-Kriegl H., Rheol Acta 13, 471-484 (1964)

Wiedenhoeft A. Wood Handbook, Wood as an Engineering Material, Chapter 3, USDA (2010)

Wilczynski K., Journal Proc. Tech, 109, 303-313 (2001)

Wilczynski K., Polym. Plast. Technol. Eng. 35,3,449-477 (1996)

Wilczynski K., Polym. Plast. Technol. Eng. 38,4,581-608 (1999)

Winter HH, Adv Heat Transfer 13, 205 - 267(1977)

Xiong C., Qi R., Wang Y., J. App. Polym. Sci., 114, 1160-1168 (2009)

Yam K. L., Gogol B. K., Lai C. C., Selke S. E., Polym. Eng. Sci., 30, 693–699 (1990)

Zhang N., Gilchrist M. D., Polym testing, 31, 748 - 758 (2011)

Zhang Y., Zhang S. Y., Choi P., Holz Roh Werkst, 66, 267-274 (2008)

Zhang Zhen Xiu, Jin Zhang, Bing-Xue Lu, Zhen Xiang Xin, Chang Ki Kang, Jin Kuk Kim, Composites: Part B, 43, 150-158 (2012)

Zini E., Scandola M. Polym Comp, 32, 1905–1915 (2011)